



MINISTÉRIO DA EDUCAÇÃO
UNIVERSIDADE FEDERAL DO TRIÂNGULO MINEIRO
PROGRAMA DE PÓS-GRADUAÇÃO EM CIÊNCIAS FISIOLÓGICAS

Rhéltheer de Paula Martins

**DESENVOLVIMENTO DE IMUNOSSENSORES ELETROQUÍMICOS BASEADO EM
NANOCRISTAIS DE ÓXIDO DE ZINCO DOPADOS COM COBRE OU ESTRUTURA
METAL-ORGÂNICA (MOF) PARA DETECÇÃO DE
ALFA-AMILASE SALIVAR HUMANA**

Uberaba
2024

Rhéltheer de Paula Martins

**DESENVOLVIMENTO DE IMUNOSSENSORES ELETROQUÍMICOS BASEADO EM
NANOCRISTAIS DE ÓXIDO DE ZINCO DOPADOS COM COBRE OU ESTRUTURA
METAL-ORGÂNICA (MOF) PARA DETECÇÃO DE
ALFA-AMILASE SALIVAR HUMANA**

Tese apresentada ao Programa de Pós- Graduação em Ciências Fisiológicas, área de concentração I: Bioquímica, Fisiologia e Farmacologia, da Universidade Federal do Triângulo Mineiro, como requisito parcial para obtenção do título de doutor em Ciências Fisiológicas.

Orientadora: Renata Pereira Alves

Coorientador: Robson T. S. De Oliveira Jr.

Catálogo na fonte:

Biblioteca da Universidade Federal do Triângulo Mineiro

M345d Martins, Rhéltheer de Paula
Desenvolvimento de imunossensores eletroquímicos baseado em nanocristais de óxido de zinco dopados com cobre ou estrutura metal-orgânica (MOF) para detecção de alfa-amilase salivar humana / Rhéltheer de Paula Martins. -- 2024.
100 p.: il., fig., graf., tab.

Tese (Doutorado em Ciências Fisiológicas) -- Universidade Federal do Triângulo Mineiro, Uberaba, MG, 2024

Orientadora: Profa. Dra. Renata Pereira Alves

Coorientador: Prof. Dr. Robson Tadeu Soares de Oliveira Júnior

1. Eletroquímica. 2. Técnicas biossensoriais. 3. Materiais nanoestruturados. 4. alfa-amilases salivares I. Alves, Renata Pereira. II. Universidade Federal do Triângulo Mineiro. III. Título.

CDU 544.6

RHÉLTHEER DE PAULA MARTINS

**DESENVOLVIMENTO DE IMUNOSSENSORES ELETROQUÍMICOS BASEADO EM
NANOCRISTAIS DE ÓXIDO DE ZINCO DOPADOS COM COBRE OU ESTRUTURA
METAL-ORGÂNICA (MOF) PARA DETECÇÃO DE
ALFA-AMILASE SALIVAR HUMANA**

Tese apresentada ao Programa de Pós- Graduação em Ciências Fisiológicas, área de concentração I: Bioquímica, Fisiologia e Farmacologia, da Universidade Federal do Triângulo Mineiro, como requisito parcial para obtenção do título de doutor em Ciências Fisiológicas.

Orientadora: Renata Pereira Alves

Coorientador: Robson T. S. De Oliveira Jr.

Aprovado em 22 de Outubro de 2004.

DEDICATÓRIA

Dedico esta tese, primeiramente, aos meus pais, Marilena e Ricardo. Duas pessoas extraordinárias que moldaram meu caráter, meus valores e meu senso de responsabilidade. Eles me ensinaram a ser resiliente, a buscar o conhecimento incessantemente e a lutar pelos meus objetivos com garra e determinação. Esta jornada não seria possível sem o apoio, compreensão e incentivo dos meus pais. Ao meu companheiro de vida, Marlon, que me encorajou todos os dias a me levantar para lutar pelo que acredito.

Em segundo, e não menos importante, dedico esta tese à minha orientadora, Professora Renata Pereira Alves, que me possibilitou adentrar e conhecer este imenso mundo de sensores. E através deste novo mundo vivenciar novas tecnologias e vislumbrar novas metodologias diagnósticas. Obrigado por todas as orientações e lembre-se de que todas as etapas deste doutorado foram com muita emoção.

AGRADECIMENTOS

Em um primeiro momento, agradeço a Deus pelo dom da vida e por cada pessoa iluminada que Ele permitiu cruzar meu caminho, semeando ensinamentos valiosos e guiando meus passos. Agradeço por cada oportunidade de crescimento, por cada desafio superado (e foram muitos) e por cada triunfo conquistado. Agradeço ainda, porque tenho a certeza de que até aqui o Senhor tem nos ajudado. Agradeço aos meus pais, Marilena e Ricardo, por serem meus alicerces. Agradeço ao meu companheiro de vida, Marlon, por toda paciência e dedicação ao longo destes anos. Agradeço a Deus pela benção de me presentear com essa família tão especial.

Minha jornada acadêmica não seria a mesma sem o apoio, a amizade e a dedicação de pessoas incríveis que cruzaram meu caminho, em especial, agradeço à Beatriz Rodrigues Martins, minha mais sincera gratidão. Você foi uma das gigantes a quem me apoiei para chegar até aqui. À minha orientadora, Renata Pereira Alves, que ao longo desses anos, me ensinou tudo que eu sei e me possibilitou viver os biossensores eletroquímicos.

A todos, meu muito obrigado!

“Ensinar não é transferir conhecimento, mas
criar as possibilidades para a sua própria
produção ou a sua construção.”

Paulo Freire

RESUMO

Este trabalho descreve a importância dos biossensores eletroquímicos para a detecção de Alfa-amilase salivar humana (HSA). O tema central da tese de doutorado apresentada baseia-se na descrição de uma metodologia de detecção que refere-se ao desenvolvimento de um imunossensor eletroquímico decorado com nanomateriais para a detecção de HSA em saliva. Foram utilizados nanomateriais de ZnO, CuO e ZnO x Cu (0.1, 0.4, 1.0, 4.0 e 12.0) nanocristais (Ncs) e estrutura metal-orgânica (MOF).. A Incorporação do Cu^{2+} na estrutura do ZnO e a formação de nanocompósito foram demonstradas nas caracterizações químicas. Foram utilizados eletrodos de grafite que apresentaram aumento de 40% no sinal eletroquímico ao utilizar ZnO:1.0Cu e 4.0Cu (0.25mg/mL^{-1}), em imunossensor (0.372mg/mL^{-1} anti-HSA e caseína 1%). Foram observadas diferentes interações entre as biomoléculas e os NCs antes e depois da adição da saliva ($4\mu\text{L}$). O imunossensor mudou a especificidade devido à interação do cobre. As amostras de ZnO:1Cu e ZnO:4Cu apresentaram 50% de interferência na detecção quando usadas antes da adição de saliva. As propriedades eletroquímicas foram avaliadas por voltametria cíclica (VC) ($0,1\text{V}\cdot\text{s}^{-1}$). O par redox Ferri/Ferrocianeto de Potássio, possibilitaram a análise dos picos de corrente anódicas e catódicas. Os resultados foram obtidos pelo potenciostato EmStat1/software PsTrace8. O imunossensor apresentou especificidade de 100% e sensibilidade de $0,00196\text{U/mL}^{-1}$. Os resultados apresentaram que a ordem de adição de NCs nos sensores deve ser testada e avaliada a fim de evitar interpretações equivocadas. Portanto, este sensor pode ser apresentado como um dispositivo promissor para detecção de HSA, presentes na saliva. No decorrer da construção da tese de doutorado, outros trabalhos envolvendo a temática dos biossensores eletroquímicos também foram desenvolvidos e constam neste material.

Palavras-chave: Eletroquímica, Nanomateriais, Biossensores, alfa-Amilase Salivar

ABSTRACT

This work describes the importance of electrochemical biosensors for the detection of human salivary alpha-amylase (HSA). The central theme of the presented doctoral thesis is based on the description of a detection methodology that refers to the development of an electrochemical immunosensor decorated with nanomaterials for the detection of HSA in saliva. ZnO, CuO and ZnO x Cu (0.1, 0.4, 1.0, 4.0 and 12.0) nanocrystals (Ncs) metal-organic framework (MOF) nanomaterials were used. The incorporation of Cu²⁺ into the ZnO structure and the formation of nanocomposite were demonstrated in the chemical characterizations. Graphite electrodes were used, which showed a 40% increase in the electrochemical signal when using ZnO: 1.0Cu and 4.0Cu (0.25mg/mL⁻¹), in immunosensor (0.372mg/mL⁻¹ anti-HSA and 1% casein). Different interactions between biomolecules and NCs were observed before and after the addition of saliva (4 µL). The immunosensor changed its specificity due to the interaction of copper. The ZnO:1Cu and ZnO:4Cu samples received 50% interference in detection when used before the addition of saliva. The electrochemical properties were evaluated by cyclic voltammetry (CV) (0.1 V.s⁻¹). The redox couple Ferri/Potassium Ferrocyanide allowed the analysis of anodic and cathodic current peaks. The results were obtained by the EmStat1 potentiostat/PsTrace8 software. The immunosensor showed 100% specificity and 0.00196U/mL⁻¹ sensitivity. The results showed that the order of addition of NCs in the sensors should be tested and evaluated in order to avoid misinterpretations. Therefore, this sensor can be presented as a promising device for the detection of HSA, present in saliva. During the construction of the doctoral thesis, other works involving the theme of electrochemical biosensors were also developed and will be included in this material.

Keywords: Electrochemistry, Nanomaterials, Biosensors, Salivary alpha-Amylase

LISTA DE ILUSTRAÇÕES

Figura 1: Representação esquemática dos componentes de um sensor	18
Figura 2: Representação esquemática dos componentes de um biossensor eletroquímico	21
Figura 3: Número de publicações por ano sobre detecção eletroquímica na saliva (2017 a 2022).	
.	22

LISTA DE ABREVIATURAS E SIGLAS

Ac – Anticorpo

Ag – Antígeno

Cu – Cobre

CuO – Óxido de cobre

α -HA – α -amilases humanas

α -HPA – amilase

pancreática

humana μ -HSA – amilase salivar

humana

$K_3[Fe(CN)_6]$ / $K_4[Fe(CN)_6] \cdot 3H_2O$ – Ferri/Ferrocianeto de potássio

KCl – Cloreto de Potássio

mL – Mililitro

mg – Miligrama

μ L – Microlitro

NCs – Nanocristais

OMS – Organização Mundial de Saúde

VC – Voltametria Cíclica

ZnO – Óxido de zinco

SCREEN-PRINTED – Eletrodo impresso

SUMÁRIO

1.	REVISÃO DE LITERATURA	13
2.	INTRODUÇÃO	13
2.1	Nanomateriais	13
2.2	Alfa amilase salivar humana.....	14
2.3	Eletroquímica.....	15
2.4	Sensores Eletroquímicos.....	17
2.5	Biossensores Eletroquímicos	20
3.	REFERÊNCIAS	24
4.	APÊNDICE A – ARTIGO PUBLICADO NA TEMÁTICA DA TESE	32
5.	APÊNDICE B – SÍNTESE E CARACTERIZAÇÃO DE ESTRUTURA METAL-ORGÂNICA (MOF) E PROVA DE CONCEITO NO DESENVOLVIMENTO DE BIOSSENSOR PARA DETECÇÃO DE ALFA-AMILASE SALIVAR HUMANA	48
6.	ANEXO A – Demais trabalhos publicados durante o doutorado	67

1. REVISÃO DE LITERATURA

Este capítulo apresenta uma abrangente revisão da literatura sobre a utilização de nanomateriais em biossensores eletroquímicos, com foco na detecção da alfa amilase salivar humana (HSA) por meio de um imunossensor eletroquímico. Esta enzima humana, utilizada como marcador para algumas patologias humanas, tem relação direta com a ingestão de carboidratos e o aumento deste marcador tem correlação com estresse cotidiano. Já na área industrial, a monitoração auxilia na produção e no controle de qualidade de diferentes processos tecnológicos. A detecção precisa, sensível e específica é crucial para o sucesso do acompanhamento e tratamento de doenças, além do controle de qualidade em processos industriais.

2. INTRODUÇÃO

2.1 NANOMATERIAIS

Desde a década de 60, as pesquisas utilizando nanopartículas estão em andamento. O primeiro estudo com aplicação biológica foi na década de 1980 (Kreuter, 2006). Esta ciência, que erroneamente se relacionava exclusivamente com o tamanho, começa a diferenciar-se descobrindo as propriedades únicas que surgem neste design nanométrico. Sendo assim, as nanopartículas apresentam um universo com infinitas possibilidades e enorme potencial tecnológico, principalmente no desenvolvimento de biossensores.

Na literatura, observa-se que pesquisadores independentes trabalham em pesquisas desenvolvendo plataformas e aplicação de técnicas objetivando rotas de síntese controláveis, usando mais ferramentas de caracterização sensíveis e, finalmente, modelos e teorias convergentes como observações experimentais. (HEILIGTAG, NIEDERBERGER, 2013; SABIR, ARSHAD, CHAUDHARI, 2014; ELFEKY, MAHMOUD, YOUSSEF, 2017; KHAN, SAEED, KHAN., 2017).

Nas últimas décadas, materiais de tamanho nanométricos têm atraído a atenção devido às suas propriedades interessantes e potencial aplicação em muitos campos importantes. As propriedades desses materiais são muito afetadas por seu tamanho e forma que geram interesse na síntese de nanopartículas semicondutoras exibindo diferentes formatos, como nanotubos, nanofios, nanoesferas, nanoplacas e nanoflores entre outros.

Analisando diferentes tipos de nanopartículas, o óxido de zinco (ZnO), atraiu maior

atenção por suas extraordinárias propriedades e características químicas, além de ser um produto de baixo custo, já está no mercado como agente para bioimagem e um excelente dispositivo elétrico (II-VI semiconductor com energia, ou seja, 3,3 eV, e alta energia de excitação, ou seja, 60 eV) (ROMEIRO, *et al.*, 2015). ZnO em sua forma mais simples mostra a geometria do tetraedro em que cada íon é cercado por quatro íons apontando para os cantos de um tetraedro. Esta configuração tetraédrica é responsável pela piezoelectricidade e piroelectricidade. (VANMAEKELBERGH E VAN VUGT, 2011; BAI *et al.*, 2015).

Com o desenvolvimento de nanopartículas bimetálicas e seus compósitos, ambos têm atraído mais atenção em comparação com as nanopartículas monometálicas, tanto em termos tecnológicos como visão científica, pois apresentam melhores propriedades. São muitas vezes utilizados como catalisadores com redução no tamanho e aumento da área superficial. (SILVA *et al.*, 2017; REGO-FILHO *et al.*, 2017).

As nanopartículas de ZnO dopadas com outros metais (Cu, Cr, Ni, Au, Ag, Al, Sn, Ga, Fe, Mn e Co) auxilia na fabricação de novos materiais tendo propriedades desejadas que não podem ser alcançadas por um único átomo de metal. (PHOOHINKONG, FOOPHOW, PECHARAPA, 2017).

Além disso, percebe-se que a forma e a morfologia dos produtos são fortemente dependentes da razão Cu:Zn durante a síntese. Por mais de quatro décadas, as nanopartículas e outras nanoestruturas têm sido utilizadas em diagnóstico molecular, um campo que pertence à ciência (PHOOHINKONG, FOOPHOW, PECHARAPA, 2017).

2.2 ALFA AMILASE SALIVAR HUMANA

As alfa-amilases humanas (α -HAs) são um grupo de isoenzimas distintas, elas são produzidas e liberadas principalmente nas glândulas salivares e no pâncreas, sendo respectivamente, alfa-amilase salivar humana (α -HSA) e alfa-amilase pancreática humana (α -HPA). Os genes da α -amilase estão localizados em um cluster no cromossomo que inclui os genes da α -amilase salivar (AMY1), dois genes da α -amilase pancreática (AMY2A e AMY2B) e um pseudogene relacionado (SANTOS *et al.*, 2012).

A α -HA é constituída por duas famílias de isoenzimas, que catalisam a hidrólise das ligações α -1,4, em glicose e em maltose, sendo a principal enzima na digestão do amido e dos carboidratos na cavidade oral. A massa molecular da α -HSA varia entre 55 a 67kDa. As concentrações e atividades desta enzima são variáveis devido a diversos fatores tais como a idade, o sexo, hábitos tabágicos, exercício físico, dieta, hidratação e fatores

psicológicos (SEQUEIRA, 2013). Seres humanos saudáveis são normalmente capazes de produzir de 500 a

1.500 mL de saliva por dia a uma taxa de 0,5mL/min (CARDOSO, *et al.*, 2023).

As α -HAs são responsáveis pela hidrólise de polissacarídeos provenientes dos alimentos. Estas enzimas são encontradas em diversos fluídos corpóreos e em diferentes concentrações, tendo na saliva uma concentração de 3.09 a 47.08U/mL de α -HSA, representando cerca de 50- 60% do total de proteínas presentes na saliva (REBELO *et al.*, 2021). A secreção da α -HSA é influenciada pela regulação adrenérgica do sistema nervoso simpático e pelo eixo hipotálamo- pituitária-adrenal (GRANGER *et al.*, 2007).

Os níveis de concentração da α -HSA tem correlação com algumas patologias humanas, como por exemplo: esquizofrenia, depressão, algumas doenças bucais e insuficiência cardíaca, e, portanto pode ser utilizada como um biomarcador para doenças que atingem o sistema nervoso simpático. Concentrações elevadas de α -HSA foram correlacionadas com estresse fisiológico e psicológico (DEUTSCH *et al.*, 2008), com alcoolismo crônico, parotidite e caxumba, já os níveis reduzidos indicam mau funcionamento renal.

Estudos recentes relatam a α -HSA como um possível biomarcador para a mais prevalente das doenças bucais infecciosas, a cárie dentária. A Organização Mundial de Saúde (OMS) reconhece esta doença como a principal razão da perda irreversível dos dentes (HIRA *et al.*, 2024).

As metodologias mais utilizadas para quantificação de α -amilase são eletroforese, cromatografia, teste de Phadebas ou ensaios imunológicos (REBELO *et al.*, 2021).

Na rotina do laboratório clínico as α -HAs não são diferenciadas, geralmente dosa-se a atividade da α -HPA no soro ou no plasma como marcador de acometimentos pancreáticos e na urina para confirmar ou descartar casos de macroamilasemia. Dado este fato, a diferenciação entre α -HPA e α -HSA é importante, uma vez que, norteiam para o diagnóstico de diferentes patologias.

2.3 ELETROQUÍMICA

Como campo científico, a eletroquímica contou com experimentos e descobertas de físicos, químicos e outros pesquisadores, que ajudaram a chegarmos ao que hoje compreendemos entre a relação de reações químicas e eletricidade. As observações e os experimentos realizados por William Gilbert, Benjamin Franklin, Luigi Galvani, Michael Faraday, Alessandro Volta, William Nicholson, Anthony Carlisle, Svante Arrhenius, John

Frederic Daniell, entre outros estudiosos, marcaram as descobertas dos princípios fundamentais para o desenvolvimento da eletroquímica (ALVAREZ, 2007; BOULABIAR *et al.*, 2004; BRESADOLA, 1998; BURNS *et al.*, 1993; COTTI, 1995; FARA, 2009; FERREIRA, 1978; GUEDES, 1999; KNIGHT, 2000; PICCOLINO, 2006, 1997; ROSS, 2002).

Apartir das observações na fisiologia com a contração muscular em resposta a estímulos de eletricidade levaram com que Galvani pudesse observar a eletricidade animal (CAJAVILCA *et al.*, 2009; PICCOLINO, 1998). Assim, a eletroquímica começava a se apresentar como área da ciência capaz de investigar as relações existentes entre os fenômenos elétricos e as reações químicas.

Algumas técnicas analíticas foram desenvolvidas no século XX, pelos pesquisadores Jaroslav Heyrovsky; William Grove e outros cientistas que conseguiram aperfeiçoar os estudos eletroquímicos, tendo a voltametria cíclica (VC) como exemplo (PETROVIC, 2021). Desse modo, a literatura científica desenvolvida por vários pesquisadores, foi responsável por estabelecer o início dos avanços que resultaram nas aplicações atualmente visualizadas nas mais diversas áreas que envolvem a eletroquímica, como sensores eletroquímicos, desenvolvimento de dispositivos médicos e o desenvolvimento de baterias recarregáveis (BREITKOPF; SWIDER- LYONS, 2017; LUBERT; KALCHER, 2010). Sendo subárea da química, a eletroquímica permite explorar a relação entre eletricidade e interações químicas, possibilitando o desenvolvimento de tecnologias inovadoras que impactam diversos setores da sociedade (BURNS *et al.*, 1993).

A partir dos avanços significativos alcançados no desenvolvimento e fabricação de eletrodos, os desenvolvimentos de métodos de medições ficaram mais confiáveis e precisos (SHUKLA; KUMAR, 2008). Surgiram diferentes tipos de eletrodos, como por exemplo, eletrodos de disco de platina e eletrodos de vidro, inventado por Max Cremer, estes contribuíram de maneira significativa para a evolução dos sensores eletroquímicos. (KORYTA, 1990).

Com esses avanços, em 1930, houve o desenvolvimento dos primeiros sensores de pH baseados em medições eletroquímicas, com eletrodos de vidro. (SZABADVÁRY; BELCHER; GORDON, 2016).

Nos anos 1960, os pesquisadores começaram a trabalhar com a leitura de biomoléculas como incumbência dos sensores eletroquímicos. Neste sentido, o caminho dos biossensores eletroquímicos estava começando a ser inserido na área da eletroquímica (GUERRA, 2018). Com a descoberta da enzima glicose oxidase, bem como a sua aplicação como molécula alvo para detecção de patologias. Este marco possibilitou

avanços, deste modo, ambas as ciências foram integradas e a aplicação dessa biomolécula nos sensores eletroquímicos deu origem aos sensores de glicose, conhecidos atualmente como glicosímetro (CLARK; CLARK, 1973).

Visto que, estes sensores apresentam alta sensibilidade e seletividade têm ampliado os interesses de pesquisas voltadas para esta área de monitoramento e diagnóstico de doenças complexas, controle de qualidade alimentar, vigilância ambiental, controle de qualidade da produção industrial, dentre outros.

As microtecnologias e nanotecnologias têm contribuído com algumas características importantes desta técnica, assim, torna-se possível a fabricação de sensores portáteis, baratos e com alta sensibilidade e especificidade para as diversas aplicações possíveis (PAROLO; MERKOI, 2010; FAUSTINO *et al.*, 2022).

Para que as reações eletroquímicas ocorram, é necessário um impulso que oriente o fluxo de elétrons. Essa força motriz é representada pelo potencial eletroquímico, uma grandeza termodinâmica que mede a tendência de uma espécie química de doar ou receber elétrons. A diferença de potencial eletroquímico entre duas espécies determina a viabilidade e a espontaneidade da reação eletroquímica. Essas reações ocorrem nas células eletroquímicas, fundamentalmente, compostas por dois eletrodos (cátodo e ânodo) imersos em um eletrólito, as células eletroquímicas fornecem o ambiente ideal para a transferência de elétrons e a geração de corrente elétrica.

As reações eletroquímicas envolvem a transferência de elétrons entre espécies químicas, gerando corrente elétrica ou consumindo-a. Essa transferência de elétrons é conhecida como processo redox (oxirredução), onde uma espécie química perde elétrons (oxidação) enquanto outra os ganha (redução) (LIMA *et al.*, 2018).

Assim, em um mundo em constante transformação, a eletroquímica, apresenta-se como um campo dinâmico e em constante evolução que contribui para o enfrentamento de diversos

desafios do século XXI. Compreendendo seus princípios fundamentais, aliados à sua alta sensibilidade e versatilidade, podemos solucionar problemas e impulsionar o desenvolvimento tecnológico em diversos setores.

2.4 SENSORES ELETROQUÍMICOS

Os sensores eletroquímicos (Figura 1) se destacam como ferramentas úteis para

desvendar as composições químicas de diversos materiais. Mais do que simples dispositivos, eles representam uma associação entre o mundo molecular e o macroscópico, convertendo informações químicas em sinais elétricos mensuráveis. Uma resposta eletroquímica é desencadeada pela interação entre uma espécie química alvo e a superfície do sensor (FREIRE; PESSOA; KUBOTA, 2003). Essa resposta, na forma de corrente ou potencial elétrico, é proporcional à concentração da espécie alvo, permitindo a quantificação e qualificação precisa da substância alvo.



Fonte: Trevisan; Poppi, 2006.

Figura 1: Representação esquemática dos componentes de um sensor.

Um sensor, por meio do transdutor, é capaz de captar informações e traduzi-las em uma linguagem compreensível (RICARDO *et al.*, 2005). Assim como demonstrado na figura 1, esses dispositivos apresentam como unidades básicas, o receptor ou transdutor, o comunicador e o processador de dados (TREVISAN; POPPI, 2006). Dessa forma, a substância alvo da investigação, também denominada analito, irá interagir com a camada receptora, gerando assim, um sinal químico (ROSINI; ANTONA; POLLEGIONI, 2020). Esse sinal precisa ser traduzido pelo transdutor em um sinal compreensível que pode ser elétrico, óptico ou mecânico.

Nos transdutores eletroquímicos, a interação analito-receptor, pode gerar uma diferença de potencial ou reações de óxido-redução, que serão compreendidas por meio dos sinais eletroquímicos potenciométricos em que a diferença de potencial na interface eletrodo- solução é verificada na ausência de corrente, amperométricos em que a corrente gerada por

processos de oxirredução de espécies eletroativas é verificada através de um potencial fixo, ou condutométricos no qual o transdutor mede a condutividade da solução na presença de corrente elétrica (PORFÍRIO; GIAROLA; PEREIRA, 2016).

Dentre os benefícios destes dispositivos, encontram-se, a alta sensibilidade capaz de gerar análises precisas de compostos em diferentes matrizes; a seletividade que proporciona a distinção entre as diferentes espécies químicas presentes na amostra,

garantindo resultados confiáveis e livres de interferências; a agilidade diagnóstica ao apresentar a capacidade de fornecer resultados em tempo real ou em um curto intervalo de tempo, otimizando o tempo de análise e a tomada de decisões; a facilidade de uso através de operação simples e intuitiva, permitindo que pessoas com diferentes níveis de experiência os utilizem com eficiência; a versatilidade, uma vez que esses dispositivos são adaptáveis a diversos tipos de análises tornando-os ferramentas universais; o baixo custo o que democratiza o acesso à tecnologia e viabilizando seu uso em larga escala; a possibilidade de portabilidade, uma vez que os equipamentos podem ser compactos e leves, facilitando o transporte e a realização de análises em campo; e, a possibilidade de miniaturização que abre caminho para aplicações em dispositivos vestíveis e miniaturizados (CAMPOS *et al.*, 2023).

Os eletrodos convencionais, como platina, ouro e grafite, são os mais tradicionais e amplamente utilizados em eletroquímica (SOUZA, 1997). A platina é conhecida por sua alta atividade catalítica e excelente resistência à corrosão, desse modo, é frequentemente utilizada em eletrodos para reações de oxidação-redução (NASCIMENTO; ANGNES, 1998). O ouro apresenta alta condutividade elétrica, biocompatibilidade e resistência à corrosão (FOGUEL *et al.*, 2009). O carbono é um material de baixo custo com alta condutividade elétrica e boa biocompatibilidade (MONTEIRO; RIBEIRO; FONSECA, 2014).

Os eletrodos *screen-printed* surgem como alternativa aos eletrodos convencionais, e, se destacam pela simplicidade e baixo custo de fabricação (BERGAMINI; ZANONI, 2005). Tintas condutoras à base de carbono, como grafeno e nanotubos de carbono, oferecem alta condutividade elétrica e boa processabilidade para impressão serigráfica (MONTEIRO; RIBEIRO; FONSECA, 2014). Por meio da técnica de impressão serigráfica, é possível produzir eletrodos em massa com geometrias e designs personalizados, facilitando a miniaturização e a integração em diversos dispositivos.

A escolha do tipo de eletrodo eletroquímico ideal depende das necessidades específicas da aplicação. Os eletrodos convencionais oferecem alta performance e reprodutibilidade,

enquanto os eletrodos vestíveis possibilitam o monitoramento contínuo e a integração à pele. Já os eletrodos *screen-printed* se destacam pela simplicidade e baixo custo de fabricação. Portanto, o conhecimento e a análise comparativa detalhada contribuem para a seleção consciente do tipo de eletrodo mais adequado, otimizando o desempenho e a aplicabilidade do sistema final.

Além da escolha do tipo de eletrodo de trabalho, uma etapa crucial de avaliação é a

análise da necessidade da modificação de superfície dos eletrodos eletroquímicos com nanomateriais, em busca de aprimorar suas propriedades e ampliar suas aplicações (ZHU *et al.*, 2015).

Os nanomateriais oferecem características únicas que podem melhorar a sensibilidade, seletividade, atividade catalítica e estabilidade dos eletrodos. Em biossensores eletroquímicos, além das características químicas dos materiais, a biocompatibilidade e bioquímica devem ser avaliadas em busca de um diagnóstico mais eficiente.

A incorporação de nanomateriais amplia a área superficial, uma vez que a elevada área superficial permite maior adsorção de moléculas reagentes na superfície do eletrodo, aumentando a sensibilidade e a corrente de resposta, maior flexibilidade e conformabilidade, biocompatibilidade aprimorada, sensibilidade aprimorada para biomarcadores (CASTRO *et al.*, 2019).

Diversas técnicas de modificação da superfície de eletrodos podem ser utilizadas, uma vez avaliados os benefícios e desafios associados à técnica. Logo, a eletroquímica se transforma com a introdução dos nanomateriais, proporcionando desta forma, o desenvolvimento de eletrodos com propriedades aprimoradas e aplicações inovadoras. As modificações com materiais permitem controlar a estrutura, a composição e a funcionalidade da superfície do eletrodo em escala nanométrica, resultando em eletrodos com alta sensibilidade, seletividade, atividade catalítica e biocompatibilidade.

2.5 BIOSSENSORES ELETROQUÍMICOS

A introdução de novos materiais como, por exemplo, os polímeros condutores e nanomateriais, e, o aperfeiçoamento das técnicas de imobilização biomolecular contribuiu para impulsionar o desempenho e proporcionar de forma mais efetiva a aplicação desses dispositivos nos diversos ramos dos diagnósticos biológicos (AMADOR SALOMÃO, 2018; D'ORAZIO, 2003; NARESH; LEE, 2021).

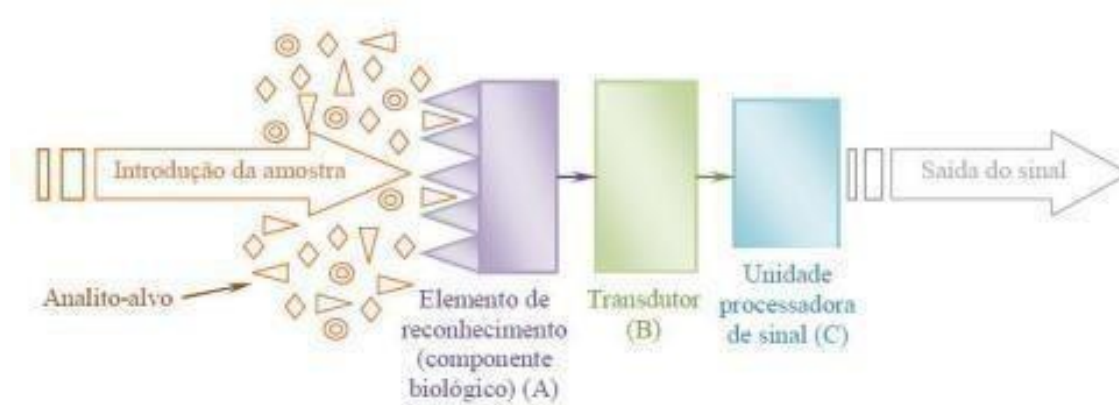
Nos biossensores eletroquímicos, diversos componentes biológicos podem ser integrados a materiais eletroquímicos, a exemplo, enzimas, anticorpos (Ac), antígenos (Ag), materiais genéticos que são biomoléculas que podem ser investigados através destes dispositivos (KAUR; BHOSALE; SHRIVASTAV, 2018).

A imunointeração entre proteínas em solução com suas proteínas complementares, imobilizadas sobre uma superfície, pode ser avaliada por meio de mudanças no índice de

refração, espessura e constante dielétrica da camada de proteínas imobilizadas. Também se podem avaliar essas imunointerações por meio de medidas eletroquímicas e piezoelétricas (KANDIMALLA *et al.*, 2004; HALAMEK *et al.*, 2006).

O funcionamento dos biossensores eletroquímicos como sistemas analíticos de detecção de doenças podem ser explicados por meio da avaliação da interação entre os componentes biológicos finais da avaliação (GRAÇA; FERREIRA, 2015). Assim, essas substâncias biológicas, são ligadas às superfícies transdutoras disponíveis no sistema eletroquímico desenvolvido para esse fim, de modo que, ao serem conectados ao transdutor, os sinais biológicos do biossensor é convertido em sinal elétrico, e é este sinal elétrico que será quantificado e analisado. Essa conversão permite a detecção e análise das amostras biológicas com base nas respostas elétricas geradas pelo dispositivo criado. O esquema representando o funcionamento dos biossensores eletroquímicos pode ser observado na Figura 2, a seguir.

Figura 2: Representação esquemática dos componentes de um biossensor eletroquímico. Mostrando a organização dos seus componentes funcionais. A detecção do analito-alvo é feita por um componente biológico que gera um sinal (A), o qual é convertido (B) e processado(C).



Fonte: Vitoreti, 2014.

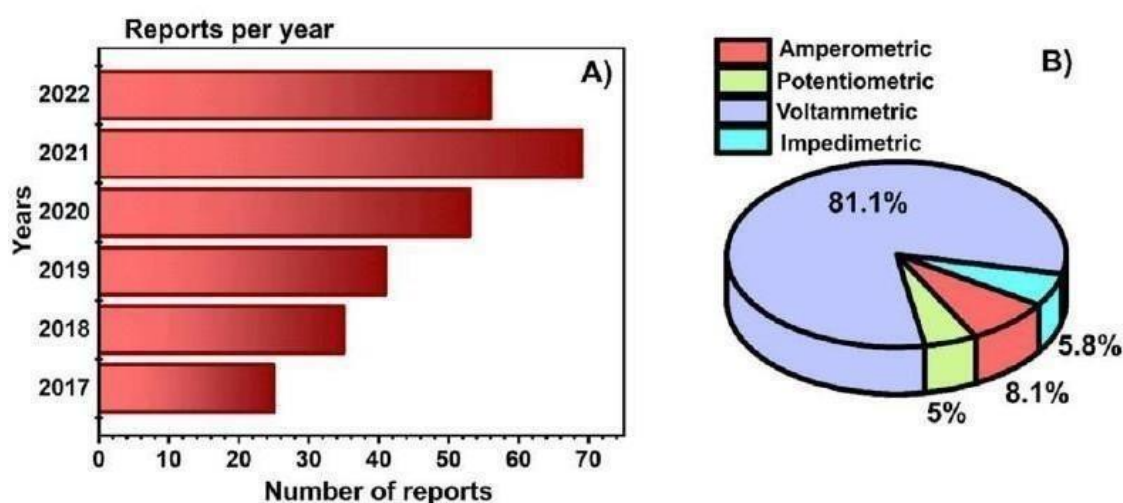
Os biossensores eletroquímicos têm sido amplamente utilizados em aplicações diagnósticas, proporcionando resultados rápidos, sensíveis e precisos (ROCCHITTA *et al.*, 2016; GRIESHABER *et al.*, 2008). Em vista disso, comercialmente podemos observar esses dispositivos aplicados na detecção de biomarcadores de doenças, como glicose para monitoramento de diabetes (CAMPOS *et al.*, 2023; JUSKA; PEMBLE, 2020), monitoramento de troponina para detecção de infarto do miocárdio (FONSECA *et al.*, 2011), marcadores tumorais para o diagnóstico de câncer (BOHUNICKY; MOUSA, 2011).

Biossensores também têm sido aplicados para detecção de patógenos circulantes, como os desenvolvidos para diagnósticos de bactérias (GU *et al.*, 2023; JONES; PADILLA- PARRA, 2016), biossensores para a detecção de vírus (BALVEDI *et al.*, 2014; MIRANDA *et al.*, 2019; SILVA, 2021), protozoários como *Leishmania infantum* (MARTINS *et al.*, 2020), permitindo assim, a rápida identificação de patologias infecciosas.

A interação entre as ciências biológicas, ciências médicas e ciências dos materiais, fornecem um conjunto de conhecimentos essenciais quanto à interação dos componentes biológicos e não biológicos. E representam ferramentas essenciais para a seletividade, reconhecimento do analito de interesse, previsão de aplicação clínica e monitoramento de biocompostos e condições de saúde, desenvolvimento de materiais eletroquímicos avançados, estudo de técnicas de imobilização e interface dos materiais com os componentes biológicos (URBAN, 2018).

A saliva tem se mostrado como uma promissora opção de amostra biológica para o trabalho com biossensores, abaixo a Figura 3 apresenta o número de publicações utilizando a saliva como amostra para detecção eletroquímica e reconhecimento de diferentes analitos/tecnologias de interesse científico.

Figura 3. A) O número de publicações por ano sobre detecção eletroquímica na saliva (2017 a 2022). B) A porcentagem de publicações relacionadas à detecção de saliva usando sensores amperométricos, potenciométricos, voltamétricos e impedimétricos.



Fonte: CARDOSO, *et al.*, 2023.

Tendo em vista, a relevância da eletroquímica, a busca por soluções inovadoras para os desafios da sociedade moderna se torna cada vez mais urgente. Nesse contexto, o

trabalho desenvolvido, aborda os imunossensores eletroquímicos como ferramentas protagonistas para a detecção de HSA. Através de princípios eletroquímicos, o sensor desenvolvido, transforma a presença de um analito em um sinal elétrico mensurável permitindo a quantificação precisa e confiável desta enzima.

3. REFERÊNCIAS BIBLIOGRÁFICAS

- ALVAREZ, S. El bagul dels llibres. 5. Magnetisme: història, mites, literatura i ciència 1. **Revistade la Societat Catalana de Química**, v. 8, p. 48–54, 2007. DOI: 10.2436/20.2003.01.6
- AMADOR SALOMÃO, P. E. Produção e Aplicação de Biossensores: Uma Breve Revisão. **Research, Society and Development**, v. 7, n. 3, p. e1373282, 2018. DOI: 10.17648/rsd-v7i3.282.
- BAI, X. *et al.* 2015. **ACS Appl. Matéria**. Interfaces. 7, 1308–1317. DOI:/10.1021/am507532p.
- BALVEDI, R. P. A. *et al.* Detection of a specific biomarker for epstein-barr virus using a polymer-based genosensor. **International Journal of Molecular Sciences**, v. 15, n. 5, p. 9051–9066, 2014. DOI: 10.3390/ijms15059051.
- BERGAMINI, M. F.; ZANONI, F. C. M. D. O. M. V. B. Análise voltamétrica do corante têxtil do tipo antraquinona empregando eletrodos de carbono impresso . **Ecletica Química**, v. 30, n. 2, p. 53–59, 2005. DOI: 10.1590/S0100-46702005000200007.
- BOHUNICKY, B.; MOUSA, S. A. Biosensors : the new wave in cancer diagnosis. **Nanotechnology, Science and Applications**, p. 1–10, 2011. DOI: 10.2147/NSA.S13465.
- BOULABIAR, A. *et al.* A Historical Analysis of the Daniell Cell and Electrochemistry Teaching in French and Tunisian Textboobresadolks. **Journal of Chemical Education**, v. 81, n. 5, p. 754–757, 2004. DOI: 10.1021/ed081p754.
- BREITKOPF, C.; SWIDER-LYONS, K. Electrochemical Science — Historical Review BT - Springer Handbook of Electrochemical Energy. In: BREITKOPF, C.; SWIDER-LYONS, K. (Eds.). **Springer Handbook of Electrochemical Energy**. Berlin, Heidelberg: Springer Berlin Heidelberg, 2017. p. 1–9. DOI: 10.1007/978-3-662-46657-5_1.
- BRESADOLA, M. Medicine and science in the life of Luigi Galvani (1737 – 1798). **Brain Research Bulletin**, v. 46, n. 5, p. 367–380, 1998. DOI: 10.1016/S0361-9230(98)00023-9.
- BURNS, D. T. *et al.* The State of Chemistry in 1841 London Chemists and Chemistry, Prior to the Formation of the Chemical Society in 1841. **Analytical Proceedings**, v. 30, n. 334, p. 334–337, 1993. DOI: 10.1039/AP9933000334.
- CAJAVILCA, C. *et al.* Luigi Galvani and the foundations of electrophysiology. **Ressucitation**,

v. 80, p. 159–162, 2009. DOI: 10.1016/j.resuscitation.2008.09.020.

CALIL, S. S.; SILVA, P. R. Q. DA Biossensores : estrutura, funcionamento e aplicabilidade. **6ª Mostra de Produção Científica da Pós-Graduação Lato Sensu da PUC Goiás**, p. 1–20, 2011.

CAMPOS, D. A. R. DE *et al.* Biossensores Eletroquímicos Baseados em Peroxidase: Revisão. **Revista Virtual de Química**, p. 1–20, 2023. DOI: 10.21577/1984-6835.20220127.

CARDOSO, A.G. *et al.* Electrochemical sensing of analytes in saliva: Challenges, progress, and perspectives. 2023. **Trends in Analytical Chemistry**. Disponível em: <https://www.sciencedirect.com/science/article/pii/S0165993623000523>. Acesso em: 23 ago 2024.

CASTRO, L. F. DE *et al.* Salivary diagnostics on paper microfluidic devices and their use as wearable sensors for glucose monitoring. **Analytical and Bioanalytical Chemistry**, v. 411, p. 4919–4928, 2019. DOI: 10.1007/s00216-019-01788-0.

CLARK, L. C.; CLARK, E. W. Differential Anodic Enzyme Polarography for the Measurement of Glucose BT - Oxygen Transport to Tissue: Instrumentation, Methods, and Physiology. In: BICHER, H. I.; BRULEY, D. F. (Eds.). **Oxygen Transport to Tissue. Advances in Experimental Medicine and Biology**. Boston, MA: Springer US, 1973. p. 127–133. DOI: 10.1007/978-1-4684-3288-6_18.COTTI.

D’ORAZIO, P. Biosensors in clinical chemistry. **Clinica Chimica Acta**, v. 334, n. 1–2, p. 41–69, 2003. DOI: 10.1016/S0009-8981(03)00241-9.

DE LA ESCOSURA-MUÑIZ, A.; PAROLO, C.; MERKOI, A. Immunosensing using nanoparticles. **Materials Today**, v. 13, n. 7–8, p. 24–34, 1 jul. 2010. DOI: 10.1016/S1369-7021(10)70125-5.

DEUTSCH, O. *et al.* An approach to remove alpha amylase for proteomic analysis of low abundance biomarkers in human saliva. **Electrophoresis**. 2008, 29, 4150–4157.

ELFEKY, S.A, MAHMOUD, S.E, YOUSSEF, A.F, 2017. **J. Adv. Res.** 8, 435–443. DOI: [org/10.1016/j.jare.2017.06.002](https://doi.org/10.1016/j.jare.2017.06.002).

FARA, P. A. Voltametric and the politics of pictures. **Endeavour**, v. 33, n. 4, p. 4–5, 2009. DOI:10.1016/j.endeavour.2009.09.007

FAUSTINO, L. C. *et al.* Miniaturized Electrochemical (Bio) sensing Devices Going Wearable BT - Advances in Bioelectrochemistry Volume 3: Biosensors, Wearable Devices

and Biomedical Applications. In: CRESPILO, F. N. (Ed.). . **Advances in Bioelectrochemistry**

Volume 3. Cham: Springer International Publishing, 2022. p. 51–90. DOI: 10.1007/978-3-03097921-8_3.

FERREIRA, R. No bicentenario de Davy (1778-1829) e de Gay-Lussac (1778-1850).

QuímicaNova, p. 36–38, 1978. Disponível em: http://static.sites.s bq.org.br/quimicanova.s bq.org.br/pdf/Vol1No4_36_v01_n4_%289%29.pdf.

Acesso em: 21 de jul. de 2024.

FOGUEL, M. V. *et al.* Avaliação da limpeza de CDtrodo construídos a partir de CD de ouro gravável/fita adesiva de galvanoplastia. **Eclética Química**, v. 34, n. 2, p. 59–66, 2009. DOI: 0.1590/S0100-46702009000200007.

FONSECA, R. A. S. *et al.* A nanostructured piezoelectric immunosensor for detection of humancardiac troponin T. **Sensors**, v. 11, p. 10785–10797, 2011. DOI: 10.3390/s111110785.

FREIRE, R. S.; PESSOA, C. A.; KUBOTA, L. T. Emprego de monocamadas auto-organizadas no desenvolvimento de sensores eletroquímicos. **Quim. Nova**, v. 26, n. 3, p. 381– 389, 2003. DOI: 10.1590/S0100-40422003000300016.

GRAÇA, J. S.; FERREIRA, M. Encapsulação de Biomoléculas em Lipossomos : Aplicações em Biossensores Enzimáticos e Imunossensores. **Revista Virtual de Química**, v. 7, n. 4, p. 1552– 1564, 2015. DOI: 10.5935/1984-6835.20150084.

GRANGER D.A, *et al.* Salivary alpha-amylase in biobehavibucal research: recent developments and applications. **Ann N Y Acad Sci.** 2007;1098:122–144. DOI: [org/10.1196/annals.1384.008](https://doi.org/10.1196/annals.1384.008)

GRIESHABER, D. *et al.* Electrochemical Biosensors - Sensor Principles and Architectures. **Sensors**, v. 8, n. 3, p. 1400–1458, 2008. DOI: 10.3390/s80314000.

GU, R. *et al.* Fiber-Optic-Based Biosensor as an Innovative Technology for Point-of-Care Testing Detection of Foodborne Pathogenic Bacteria To Defend Food and Agricultural Product Safety. **Journal of Agri. and Food Chemistry**, v. 71, n. 29, p. 10982–10988, 2023. DOI: 10.1021/acs.jafc.3c02067.

GUEDES, E. M. V. Bicentenário da Invenção da Pilha por Alessandro Volta. **Electricidade**,

v. 367, p. 145, 1999. Disponível em: <https://paginas.fe.up.pt/histel/Voltapilha.pdf>. Acesso em: 25 de jul. de 2024.

GUERRA, A. C. S. **Biossensor como proposta alternativa para o ensino de eletroquímica.** [s.l.] Brasil, 2018. Disponível em: <https://repository.ufrpe.br/handle/123456789/873>. Acesso em 25 de jul. de 2024.

HALAMEK, J. *et al.* EQCN based cholinesterase biosensors. **Electrochimica Acta**, v. 51, n. 24, p. 5174, 2006. DOI:org/10.1016/j.electacta.2006.03.047

HEILIGTAG, F.J., Niederberger, M. **Journal. Mat. Tod.** 16, 262-271.2013
Doi: org/10.1016/j.mattod.2013.07.004.

HIRA, A. *et al.* Fabrication of a salivary amylase electrochemical sensor based on surface confined MWCNTs/ β -cyclodextrin/starch architect for dental caries in clinical samples. **Bioelectrochemistry**. 2024. DOI: 10.1016/j.bioelechem.2024.108774.

JONES, D. M.; PADILLA-PARRA, S. The β -Lactamase Assay: Harnessing a FRET. Biosensor Analyze Viral Fusion Mechanisms. **Sensors**, v. 16, n. 7, p. 950, 2016. DOI: 10.3390/s16070950.

JUSKA, V. B.; PEMBLE, M. E. A critical review of electrochemical glucose sensing: Evolution of biosensor platforms based on advanced nanosystems. **Sensors (Switzerland)**, v. 20, n. 21, p. 1–28, 2020. DOI: 10.3390/s20216013.

KANDIMALLA V. B. *et al.* Regeneration of ethyl parathion antibodies for repeated use in immunosensor: a study on dissociation of antigens from antibodies. **Biosensors and Bioelectronics**, v. 20, n. 4, p. 903, 2004. DOI: 10.1016/j.bios.2004.03.027

KHAN, I., SAEED, K., KHAN, I. Árabe. **J. Química.** 2017.On-line, 1-24. <http://dx.doi.org/10.1016/j.arabjc.2017.05.011>. Acesso em: 10 de ago. de 2024.

KAUR, H.; BHOSALE, A.; SHRIVASTAV, S. Biosensors: Classification, Fundamental Characterization and New Trends: A Review. **International Journal of Health Sciences & Research (www.ijhsr.org)**, v. 8, n. 6, p. 315–333, 2018.
Disponível em: https://www.researchgate.net/profile/Kaur-17/publication/339676977_Biosensors_Classification_Fundamental_Characterization_and_New_Trends_A_Review/links/5e5f735fa6fdccbeba1889f1/Biosensors-Classification-Fundamental-Characterization-and-New-Trends-A-Review.pdf. Acesso em: 10 de ago. de 2024.

- KNIGHT, D. M. Humphry Davy: science and social mobility. **Endeavour**, v. 24, n. 4, p. 165–169, 1 dez. 2000. DOI: 10.1016/S0160-9327(00)01326-0.
- KORYTA, J. Theory and applications of ion-selective electrodes. Part 8. **Analytica Chimica Acta**, v. 233, p. 1–30, 1990. DOI: 10.1016/S0003-2670(01)95071-8.
- KREUTER, J., 2006. **Int. J. Phar.** 331, 1-10. DOI: 10.1016/j.ijpharm.2006.10.021.
- LIMA, P. H. C. *et al.* Polímeros condutores com propriedades eletrocrômicas: uma revisão. **Revista Eletrônica de Materiais e Processos**, v. 13, n. 1, p. 1–17, 2018. Disponível em: <http://www2.ufcg.edu.br/revistaremap/index.php/REMAP/article/viewArticle/645>. Acesso em 10 de ago. de 2024.
- LUBERT, K. H.; KALCHER, K. History of Electroanalytical Methods. **Electroanalysis**. v. 22, n. 17–18, p. 1937–1946, 2010. DOI: 10.1002/elan.201000087.
- MARTINS, B. R. *et al.* Development of an electrochemical immunosensor for specific detection of visceral leishmaniasis using gold-modified screen-printed carbon electrodes. **Biosensors**, v. 10, n. 8, p. 1–15, 2020. DOI: 10.3390/bios10080081.
- MIRANDA, P. H. Q. *et al.* Biossensores para diagnóstico de doenças causadas por vírus: uma revisão. **Hegemonia**, v. 27, n. 27, p. 22–22, 1 jan. 2019. DOI: 10.47695/hegemonia.vi27.283.
- MONTEIRO, S. P.; RIBEIRO, L. A. DE R.; FONSECA, W. Determinação de Chumbo em Águas de Abastecimento Utilizando Filmes de Bismuto Crescidos in situ Sobre Eletrodos de Pasta de Carbono. **Orbital - The Electronic Journal of Chemistry**, v. 6, n. 1, p. 29–38, 2014.
- NARESH, V.; LEE, N. A Review on Biosensors and Recent Development of Nanostructured Materials-Enabled Biosensors. **Sensors**, v. 21, n. 4, p. 1109, 5 fev. 2021. DOI: 10.3390/s21041109.
- NASCIMENTO, V. B.; ANGNES, L. Eletrodos fabricados por “silk-screen”. **Química Nova**, v. 21, n. 5, p. 614–629, 1998. DOI: 10.1590/S0100-40421998000500014.
- PHOOHINKONG, W., FOOPHOW, T., PECHARAPA, W., 2017. Adv. **Nat. Ciência: Nanosci. Nanotecnologia** 8, 035003. DOI: 10.1088/2043-6254/aa7223.
- PETROVIC, S. History of Electrochemistry. **Electrochemistry Crash Course for**

- Engineers**, p. 1–2, 2021. Disponível em: < <https://link.springer.com/book/10.1007/978-3-030-61562-8>>. Acesso em: 18 de ago. de 2024.
- PICCOLINO, M. Animal electricity and the birth of electrophysiology: the legacy of Luigi Galvani. **Brain Research Bulletin**, v. 46, n. 5, p. 381–407, 15 jul. 1998. DOI: 10.1016/S0361-9230(98)00026-4
- PICCOLINO, M. Luigi Galvani 's path to animal electricity. **Comptes Rendus Biologies**, v. 329, n. 5–6, p.303–318, 2006. DOI: 10.1016/j.crv.2006.03.002.
- PORFÍRIO, F.; GIAROLA, J.; PEREIRA, A. Biosensor and Beverages - Review. **Revista Virtual de Química**, v. 8, p. 1366–1391, 2016. DOI: 10.21577/1984-6835.20160097.
- REBELO, T. S. C. R. *et al.* A Disposable Saliva Electrochemical MIP-Based Biosensor for Detection of the Stress Biomarker α -Amylase in Point-of-Care Applications. **Electrochem** 2021, 2, 427–438. Disponível em: <https://doi.org/10.3390/electrochem2030028>. Acesso em 22 de ago de 2024.
- REGO-FILHO, F.G. *et al.* IR-to-visible frequency upconversion in Yb³⁺/Tm³⁺ co-doped phosphate glass. 2017. **Op. Materials**. 73, 1-6. DOI: 10.1016/j.optmat.2017.07.037.
- RICARDO, C. *et al.* Polímeros biomiméticos em química analítica. Parte 2: Aplicações de MIP (“Molecularly imprinted polymers”) no desenvolvimento de sensores químicos. **Química Nova**, v. 28, n. 6, p. 1087–1101, 2005. DOI: 10.1590/S0100-40422005000600025.
- ROCCHITTA, G. *et al.* Enzyme Biosensors for Biomedical Applications: Strategies for Safeguarding Analytical Performances in Biological Fluids. **Sensors 2016, Vol. 16, Page 780**, v. 16, n. 6, p. 780, 2016. DOI: 10.3390/s16060780.=.
- ROMEIRO, F.C. *et al.* Rapid synthesis of Co, Ni co-doped ZnO nanoparticles: Optical and electrochemical properties. **Journal of Solid State Chemistry** 230. 2015 DOI: 10.1016/j.jssc.2015.07.026.
- ROSINI, E.; ANTONA, P. D.; POLLEGIONI, L. Biosensors for D-Amino Acids : Detection Methods and Applications. **International Journal of Molecular Sciences**, v. 21, p. 4574, 2020.DOI: 10.3390/ijms21134574.
- ROSS, C. E. How the public successes of a poetic scientist — Humphry Davy (1778 – 1829)— changed English literature. **International Congress Series**, v. 1242, p. 495–501, 2002. DOI: 10.1016/S0531-5131(02)00716-1.

SABIR, S., ARSHAD, M., CHAUDHARI, S.K., Zinc Oxide Nanoparticles for Revolutionizing Agriculture: Synthesis and Applications 2014. **Sci. Wor. J.** 1-8. DOI: 10.1155/2014/925494.

SANTOS, J.L., *et al.* Copy number polymorphism of the salivary amylase gene: implications in human nutrition research. **J Nutrigenet Nutrigenomics.** 2012; 5(3):117-31. DOI: 10.1159/000339951

SEQUEIRA, M. A. S. Estudo da Relação entre a Composição Proteica da Saliva e a Sensibilidade para o Gosto Amargo. 2013. 68f. Dissertação de mestrado – Escola de Ciências e Tecnologia, Universidade de Évora, Janeiro, 2013.

SHUKLA, A. K.; KUMAR, T. P. ECS Classics: Pillars of Modern Electrochemistry. **The Electrochemical Society Interface**, v. 17, n. 3, p. 31–39, 2008. DOI 10.1149/2.F01083IF.

SILVA, S. J. R. DA. **Desenvolvimento e validação de plataformas do tipo “Point-of-Care” para o diagnóstico molecular de arbovírus emergentes.** [s.l: s.n.]. 2021. Disponível em: < <https://www.arca.fiocruz.br/handle/icict/60550>> . Acesso em: 15 de ago. de 2024.

MO, Z. J. *et al.* Observation of giant magnetocaloric effect under low magnetic field in $\text{Eu}_{1-x}\text{Ba}_x\text{TiO}_3$. 2017 **J. Todos Comp.** 708, 619-622. DOI:10.1016/j.jallcom. 2017.03.066.

SOUZA, M. DE F. B. Eletrodos quimicamente modificados aplicados à eletroanálise: uma breve abordagem. **Química Nova**, v. 20, n. 2, p. 191–195, 1997. DOI: 10.1590/S0100-40421997000200011.

SZABADVÁRY, F.; BELCHER, R.; GORDON, L. **History of Analytical Chemistry: International Series of Monographs in Analytical Chemistry.** [s.l.] Elsevier, 2016.

Disponível em:< <https://books.google.com.br/books?hl=pt-BR&lr=&id=icn9BAAQBAJ&oi=fnd&pg=PP1&dq=SZABADV%C3%81RY,+F.%3B+BELCHER,+R.%3B+GORDON,+L.+History+of+Analytical+Chemistry:+International+Series+of+Monographs+in+Analytical+Chemistry%20in%20Analytical%20Chemistry.%20%5Bs.l.%5D%20Elsevier%2C%202016.&f=false>>. Acesso Em: 11 deabr. de 2024.

TREVISAN, M. G.; POPPI, R. J. QUÍMICA ANALÍTICA DE PROCESSOS. **Química Nova**, v. 29, n. 5, p. 1065–1071, 2006. DOI: 10.1590/S0100-40422006000500029.

URBAN, P. L. Prototyping Instruments for Chemical Laboratory Using Inexpensive Electronic Modules. **A Journal of the Gesellschaft Deutscher Chemiker Angewandte**

chemie, p. 1–6, 2018. DOI: 10.1002/anie.201803878.

VANMAEKELBERGH, D., VAN VUGT, LK, ZnO nanowire lasers. 2011. **Nanoescala**. 3, 2783–2800. DOI: 10.1039/C1NR00013F.





VITORETI, A.B.F. “Desenvolvimento de um imunossensor eletroquímico para identificação de toxinas de serpentes”. 2014. 55f. Dissertação de mestrado – Instituto de Química de São Carlos, Universidade de São Paulo, São Carlos, 2014.

ZHU, C. *et al.* Electrochemical Sensors and Biosensors Based on Nanomaterials and Nanostructures. **Analytical Chemistry**, v. 87, n. 1, p. 230–249, 2015. DOI: 10.1021/ac5039863.

4. APÊNDICE A – PUBLICAÇÕES REFERENTES AO TEMA DA TESE



Immunosensor Based on Zinc Oxide Nanocrystals Decorated with Copper for the Electrochemical Detection of Human Salivary Alpha-Amylase

Beatriz Rodrigues Martins ¹, Tainá Marques Sampaio ², Ana Karoline Silva Rocha de Farias ², Rheltheer de Paula Martins ¹ , Renata Roland Teixeira ³, Robson Tadeu Soares Oliveira, Jr. ¹, Carlo Jose Freire Oliveira ¹, Marcos Vinícius da Silva ¹ , Virmondes Rodrigues, Jr. ¹, Noelio Oliveira Dantas ⁴, Foued Salmen Espindola ³, Anielle Christine Almeida Silva ^{4,5}  and Renata Pereira Alves-Balvedi ^{1,2,*} 

- ¹ Physiological Science, Federal University of Triangulo Mineiro, Uberaba, MG 38025-180, Brazil; d201811482@uftm.edu.br (B.R.M.); rheltheer.martins@uftm.edu.br (R.d.P.M.); robson.junior@uftm.edu.br (R.T.S.O.J.); carlo.oliveira@uftm.edu.br (C.J.F.O.); marcos.silva@uftm.edu.br (M.V.d.S.); virmondes.rodrigues@uftm.edu.br (V.R.J.)
- ² Biological Science, Federal University of Triangulo Mineiro, Iturama, MG 38280-180, Brazil; d201511169@uftm.edu.br (T.M.S.); d201710610@uftm.edu.br (A.K.S.R.d.F.)
- ³ Institute of Biotechnology, Federal University of Uberlandia, Uberlandia, MG 38405-319, Brazil; rolandteixeira@ufu.br (R.R.T.); foued@ufu.br (F.S.E.)
- ⁴ Laboratory of New Nanostructured and Functional Materials, Institute of Physics, Federal University of Alagoas, Maceió, AL 57072-900, Brazil; noelio@fis.ufal.br (N.O.D.); acalmeida@fis.ufal.br (A.C.A.S.)
- ⁵ Rede Nordeste de Biotecnologia (RENORBIO), Federal University of Alagoas, Maceió, AL 57072-900, Brazil
- * Correspondence: renata.balvedi@uftm.edu.br; Tel.: +55-34-3415-2500



Citation: Martins, B.R.; Sampaio, T.M.; de Farias, A.K.S.R.; de Paula Martins, R.; Teixeira, R.R.; Oliveira, R.T.S., Jr.; Oliveira, C.J.F.; da Silva, M.V.; Rodrigues, V., Jr.; Dantas, N.O.; et al. Immunosensor Based on Zinc Oxide Nanocrystals Decorated with Copper for the Electrochemical Detection of Human Salivary Alpha-Amylase. *Micromachines* **2021**, *12*, 657. <https://doi.org/10.3390/mi12060657>

Academic Editors: Nam-Trung Nguyen, Katsuo Kurabayashi and Pengyu Chen

Received: 17 April 2021
Accepted: 31 May 2021
Published: 3 June 2021

Publisher's Note: MDPI stays neutral with regard to jurisdictional claims in published maps and institutional affiliations.

Abstract: (1) Background: Nanocrystals (NCs)-based electrochemical sensors have been proposed for biomarkers detection, although immunosensors using ZnO NCs decorated with copper are still scarce. (2) Methods: Electrochemical immunodetection of human salivary alpha-amylase (HSA) used ZnO, CuO, and ZnO:xCu (x = 0.1, 0.4, 1.0, 4.0, and 12.0) NCs. (3) Results: Substitutional incorporation of Cu²⁺ in the crystalline structure of ZnO and formation of nanocomposite were demonstrated by characterization. Graphite electrodes were used and the electrochemical signal increased by 40% when using ZnO:1Cu and 4Cu (0.25 mg·mL⁻¹), in an immunosensor (0.372 mg·mL⁻¹ of anti-alpha- amylase and 1% of casein). Different interactions of HSA with the alpha-amylase antibody were registered when adding the NCs together, either before or after the addition of saliva (4 µL). The immunosensor changed specificity due to the interaction of copper. The ZnO:1Cu and ZnO:4Cu samples showed 50% interference in detection when used before the addition of saliva. The immunosensor showed 100% specificity and a sensitivity of 0.00196 U·mL⁻¹. (4) Conclusions: Results showed that the order of NCs addition in the sensors should be tested and evaluated to avoid misinterpretation in detection and to enable advances in the validation of the immunosensor.

Keywords: zinc oxide nanoparticles; copper; nanocomposite; electrochemical detection; human salivary alpha-amylase; antibody; biomarker



Copyright: © 2021 by the authors. Licensee MDPI, Basel, Switzerland. This article is an open access article distributed under the terms and conditions of the Creative Commons Attribution (CC BY) license (<https://creativecommons.org/licenses/by/4.0/>).

1. Introduction

Nanoparticle research has been underway since the 1960s, with its first biological application in the 1980s [1]. There are odd properties associated with design, and this field presents a new universe with vast possibilities and enormous technological potential, mainly in the development of biosensor speed, low cost, and portability. Both organic (viral or protein) and inorganic (metal) nanoparticles exist in nature. However, they do not present controlled synthesis, which means a sample will not be homogeneous when collected at different sites or conditions [2,3].

Some reviews that have discussed scientific motivation to develop nanoparticles have applied progressively controllable synthesis techniques, used more sensitive characterization tools, and, finally, suggested theoretical models from experimental observations [4–7].

Among all different types of nanoparticles, zinc oxide (ZnO) has drawn more attention due to its remarkable properties and chemical features. Besides being an inexpensive material, it is already on the market as an agent for bioimaging and electrical devices with piezo and pyroelectrical properties [8–10]. Beyond the miniature size and the increase in surface area, bimetallic nanoparticles are better in catalyst form; they have attracted more attention than monometallic nanoparticles [11–13]. ZnO nanoparticles doped with other metals (Cu, Cr, N, Au, Ag, Al, Sn, Ga, Fe, Mn, and Co) become new materials with desired properties that cannot be achieved by monometallic nanoparticles [14–16]. In four decades of research, it has been found that the synthesis of these doped nanoparticles and nanocomposites can be evaluated from the electrochemical point of view, aiming at several technological applications [16–18].

The detection of HSA has been investigated as a stress biomarker in saliva, a fluid that is easy and non-invasive to collect. Studies of these biomarkers for both psychological stress and physical stress have been performed with the measurement of the enzymatic activity of alpha-amylase in the salivary fluid and its immunodetection by Western blot [19–22]. Electrochemical immunosensors, among others, have also been used for this purpose [23–26]. The incorporation of nanomaterials in biosensors aims to optimize detection performance, offering biocompatibility, additional connections, and electrical properties that improve signal strength.

An immunosensor to detect HSA using ZnO nanocrystals (NCs) decorated with Copper (Cu^{2+} ions) may be an attractive option due to the property of copper in interacting with salivary proteins, including HSA [27,28]. HSA is a calcium-binding protein, capable of binding two Ca^{2+} ions. One of the binding sites is exclusive to Ca^{2+} ; in the other enzyme site, the Cu^{2+} ions are bound by electrostatic interaction, like Ca^{2+} [28–30]. The interaction of CuO nanoparticles with the protease–amylase complex also revealed that the oxygen present in the nanoparticle forms hydrogen bonds and binds copper through van der Waals interactions to specific amino acids at the interaction site [31].

However, there are still several challenges for the development of sensors using electrochemical and optical methods with intelligent interfaces to evaluate biomarkers in salivary fluid, including those using antibodies and nanomaterials, such as the one in the present study [26]. Among the challenges are glassy carbon electrodes, as the working electrode constitutes the conventional electrochemical biosensor detection system [32] due to their larger size and the need for a surface treatment-limiting integration miniaturized portable design [33–35]. For the advancement of portable biosensor technologies capable of meeting the appeal of the advantages of using salivary fluid, such as the measurement of biomarkers in situ, some limitations can be overcome, such as using bench equipment and trained personnel for these analyzes [26].

Salivary fluid has been described as a complementary and potential fluid for the diagnosis of diseases and oxidative stress. Many pathologies and physiological changes caused, for example, by physical exercise have alterations in the oxidative stress biomarkers [36,37]. However, there are certain challenges, such as the need for sensitivities and resolution of the biosensors, since many of these biomarkers are in saliva in a much lower concentration than in plasma [38]. In addition, factors inherent to the salivary fluid, such as its secretion rate, pH, viscosity, and the complex environment of the oral cavity, can influence the determination of biomarkers [39–42].

In search of high sensitivity, response time, good performance, easy handling, accurate reporting, portability, low cost, and reliable detection of biomarkers, in this work, we developed an immunosensor based on ZnO NCs decorated with Cu for the electrochemical detection of HSA. Completing the research, we intended to evaluate the best interaction of these ZnO:xCu NCs with the sensor and the HSA available in the electrochemical sensor, confirming the entire process.

2. Materials and Methods

2.1. Reagents and Samples

Ultra-high purity water (deionized water, Milli-Q® IX Water, Merck, Brazil) was used for the preparation of aqueous solutions, and all experiments were conducted at room temperature (25 ± 1 °C).

Reference [27] showed, for the first time, a bioelectrode based on the immobilization of a specific antibody for salivary alpha-amylase (Ab-0.744; $0.372 \text{ mg} \cdot \text{mL}^{-1}$). The blocking of the binding of non-specific biomolecules on the electrode surface was done with casein (1% and 10%), and it was stored at a temperature of 20 °C until use.

Seven types of NCs were used: 6 types of ZnO (pure, and with Cu (0.1, 0.4, 1, 4, 12)) and 1 type of CuO that was synthesized based on previous methodologies [17,18]. Stock solutions were prepared ($0.5 \text{ mg} \cdot \text{mL}^{-1}$). The redox solution was 5 mM $[\text{Fe}(\text{CN})_6]^{3-/4-}$ and 0.1 M KCl (FF/KCl), pH 7.4. All were stored at 4 °C until use.

Saliva samples from healthy human volunteers ($n = 4$, non-smokers) were collected in the morning, without stimulation, centrifuged (1500 rpm, 3 min), and stored at 20 °C until use for detection of human saliva alpha-amylase (HSA-Ag).

The alpha-amylase enzyme (AAE-Browin, Łódź, Polônia) and trypsin DPCC treated, type XI (TXI-Sigma-Aldrich, São Paulo, Brazil), were used for the specificity test and prepared in $0.25 \text{ mg} \cdot \text{mL}^{-1}$.

All samples were analyzed simultaneously in triplicate to assess repeatability and used as proof of concept.

Investigations were carried out following the rules of the Declaration of Helsinki of 1975, revised in 2013. According to point 23 of this declaration, approval from an ethics committee was obtained before undertaking the research. This study was conducted according to the ethical guidelines of the Brazilian Ministry of Health, with protocols and procedures approved by the Research Ethics Committee/UFTM, under protocol number 3.938.388, approved in 2020.

2.2. Apparatus for Characterization and Electrochemical Analysis

X-ray diffractograms (XRDs) were taken with an XRD-6000 (Shimadzu Corp., Tokyo, Japan), using monochromatic Cu-K α 1 ($\lambda = 1.54056 \text{ \AA}$) radiation. The XRDs patterns confirmed ZnO and CuO NCs formation, crystal structure, average size, doping effects, and nanocomposite formation.

Analysis of the surface morphological characterization for a graphite electrode in the absence or presence of NCs was assessed through atomic force microscopy (AFM) Spm9600 (Shimadzu Corp., Tokyo, Japan).

To assess the conductivity of electrodes and for optimization of detection, cyclic voltammetry (CV) was used. The voltammetry measurements were performed using a Potentiostat EmStat1 (PalmSens, The Netherlands) with PSTrace 5.4 software (PalmSens, Houten, The Netherlands).

The measurements for detections were carried out in FF/KCl using a $100.0 \text{ mV} \cdot \text{s}^{-1}$, -0.8 and $+0.8 \text{ V}$, 1scan, one-compartment cell, carbon screen-printed electrode (C110 220, DropSens, Spain). The working (WE) and auxiliary (AE) electrodes were made of carbon, while the reference electrode (RE) was made of silver. All electrochemical assays were conducted in triplicate.

2.3. Electrochemical Selection and Use of the Nanocrystals

Among types of ZnO NCs, we tested different dilutions to select the one with the best electrochemical conductivity onto the electrode. We used $4 \mu\text{L}$ of the NC solution on the surface of the WE for 20 min. Then, the electrode was washed with $100 \mu\text{L}$ of deionized water and dried in a vacuum dryer. Subsequently, $80 \mu\text{L}$ of FF/KCl was used to close the circuit (WE, RE, AE) and evaluate the electrochemical sign, by cyclic voltammetry (CV), for each type of NCs.

After that, we selected the NCs that best responded electrochemically and used them in the molecular recognition between the immobilized Ab and the monitored HSA-like antigen (Ag).

2.4. Immunosensor

The adsorption of anti-alpha-amylase polyclonal (Ab) as a probe was carried out by applying 4 μL on the WE surface. In the next step, the electrode received 4 μL of casein. After that, 4 μL of saliva (target-HSA) was applied to this same electrode with the antibody. The procedure was performed to check the differences with the introduction of 4 μL NCs that best responded electrochemically: before, together, and after the application of human saliva.

After the sensor was set up, we evaluated its electrochemical signal, employing CV in one-compartment electrochemical cells connected to a potentiostat. These signals were measured by using 80 μL FF/KCl as a supporting electrolyte.

All the interactions were carried out at 25 ± 1 °C for 20 min, and at each step, the electrode was washed with deionized water and dried with a vacuum dryer.

3. Results

3.1. Characterization of ZnO:Cu Nanocrystals

Figure 1 illustrates the following: (A) the change of color in powdered samples with doping, according to Cu^{2+} or CuO concentration; (B) the XRD patterns of the ZnO NC samples and of those samples with increasing concentrations of Cu; and (C) the crystal structure of the ZnO and CuO, subsequently exemplifying the doping process and composites in NCs. In Figure 1B, observed in the XRD results of the ZnO sample, narrow peaks confirmed the high crystallinity of the sample, and the Bragg diffraction peaks were characteristic of hexagonal wurtzite ZnO (JCPDS-EF 36-1451). The observed peaks for high concentrations of Cu correspond to single-phase CuO with a monoclinic structure (JCPDS-05-0661). The crystalline planes of ZnO and CuO were added. The zoom of the shaded region illustrates the changes with Cu concentration. For concentrations below ZnO:1Cu, only a major ZnO peak shift could be seen, indicating the substitutional incorporation of Cu^{2+} ions by Zn^{2+} ions into the ZnO crystal structure. Moreover, no additional peaks corresponding to CuO formation were observed, indicating that there was no significant CuO formation to be detected in the diffractograms. The concentrations above 1Cu exhibited the formation of a nanocomposite consisting of Cu-doped ZnO NCs and CuO NCs. The grain size was obtained from the XRD line-broadening measurement, using the Scherrer equation; being 20 nm, it confirmed the formation of NCs.

Figure 1C shows the crystal structure of ZnO and CuO, subsequently exemplifying the doping process and composites. The doping process consisted of the substitution of ions in the crystalline structure of the nanocrystal. The composite is a fascinating due synergism of properties [15]. Based on the XRD results, samples with concentrations of 0.1, 0.4, and 1.0 were Cu-doped ZnO NCs, and the concentrations of 4.0 and 12.0 were composites, i.e., the simultaneous presence of Cu-doped ZnO NCs and CuO NCs. Figure 1D shows the AFM results, whose surface roughness analysis (Rq) was used in the construction of the column chart. After adding different concentrations of NCs onto the electrode surface, the results showed that ZnO:0.4Cu (3th bar) presented 26.21% higher roughness compared with ZnO.

3.2. Electrochemical Analysis of ZnO:Cu Nanocrystals

The NCs' electrochemical reactivity was evaluated with a redox probe FF/KCl through a donation of hydrogen and electrons during the anodic current (oxidation) and return hydrogen and electrons during the cathodic current (reduction).

Different NCs and concentrations (0.5, 0.25, 0.125, and 0.0625 $\text{mg}\cdot\text{mL}^{-1}$) were tested. Both currents may have increased or decreased when NCs were included on the electrode surface. To select the NCs and the optimal concentration, seven types of NC and different dilutions (0.5, 0.25, 0.125, and 0.062 $\text{mg}\cdot\text{mL}^{-1}$) were tested.

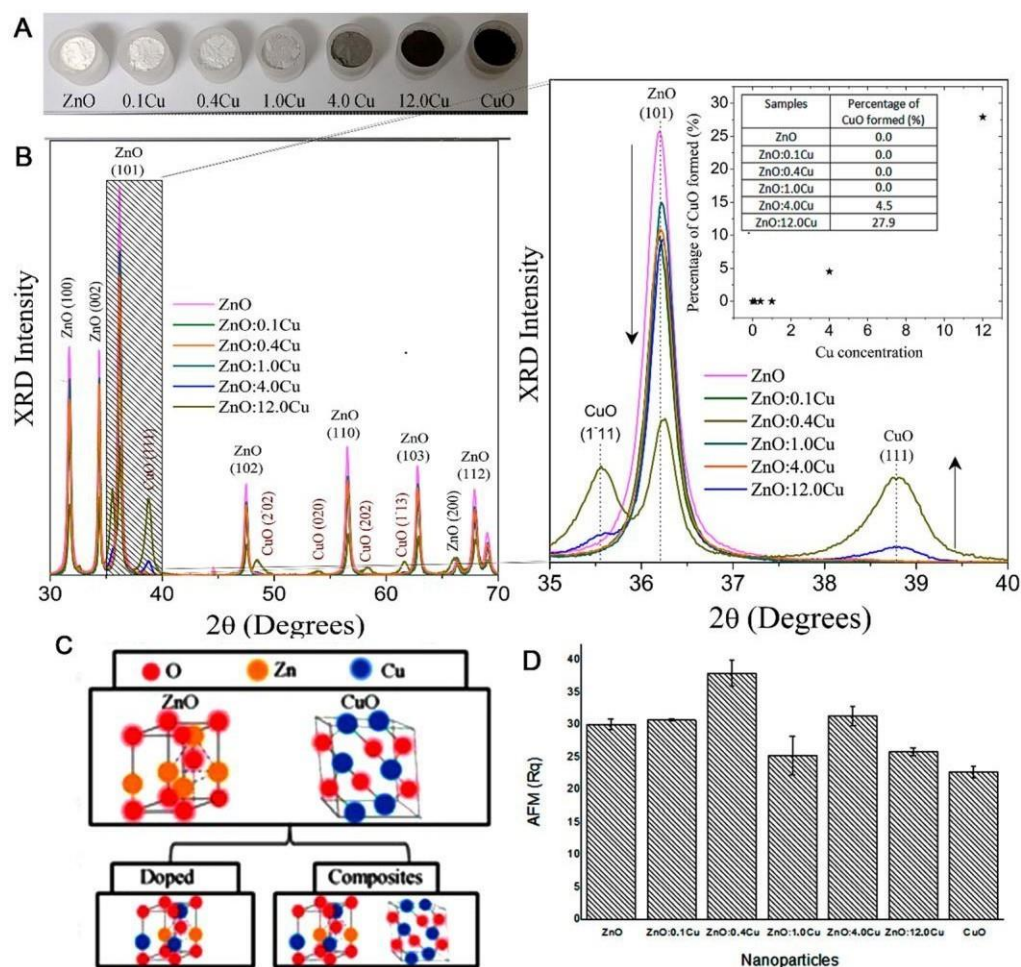


Figure 1. (A) Powdered samples, (B) XRD patterns of the ZnO samples with increasing Cu concentrations, (C) crystal structure of ZnO and CuO, exemplifying the doping process and composites, and (D) surface roughness analysis by AFM of the samples onto electrodes.

Figure 2A,B shows the electrochemical response in the presence of different NCs and concentrations (different dilutions). The oxidation and reduction peaks were used in the construction of the column chart. The electrochemical analysis shows that, in $0.25 \text{ mg}\cdot\text{mL}^{-1}$, there was an increase in the current response of the redox probe (oxidation and reduction) for NC ZnO:1Cu (4th bar) and ZnO:4Cu (5th bar). It may be that these NCs provided an increase in surface area and could potentially improve sensitivity or cause minor capacitive interference in the immunosensor.

3.3. Immunosensor and Electrochemical Analysis

We investigated a modified platform with NCs to evaluate their interactions. In the sensor, we tested two different concentrations of Ab (0.744 ; $0.372 \text{ mg}\cdot\text{mL}^{-1}$), and we tested two different concentrations of casein (1% and 10%). The best results in the electrochemical sensor were found with $0.372 \text{ mg}\cdot\text{mL}^{-1}$ of Ab and 1% of casein. Based on this sensor construction, we made modifications to study the interaction of NCs, as shown in Figure 3. Figure 4 presents the current response for each step of the biosensor construction. (A) and (B) show the oxidative and reductive analysis, in which the bar charts present the current signals. The steps were 1. immobilization of the antibody anti-HSA (Ab) (a); 2. HSA (Ag) recognition with Ab only (Ab-Ag) (b); 3. immobilization of the antibody anti-HSA (Ab) and the addition of ZnO:4Cu (Ab-4Cu) (c); 4. HSA recognition with Ab and ZnO:4Cu (Ab-4Cu-Ag) (d); 5. HSA recognition with Ab, followed by ZnO:4Cu (Ab-Ag-4Cu) (e); 6. water with Ab, followed by ZnO:4Cu (Ab-H₂O-4Cu) (f). (C) shows the CV graphic whose peaks

were used in the construction of the column chart. (D) shows the CV graphic of the sensor with saliva and ZnO:4Cu NCs mixed in one solution.

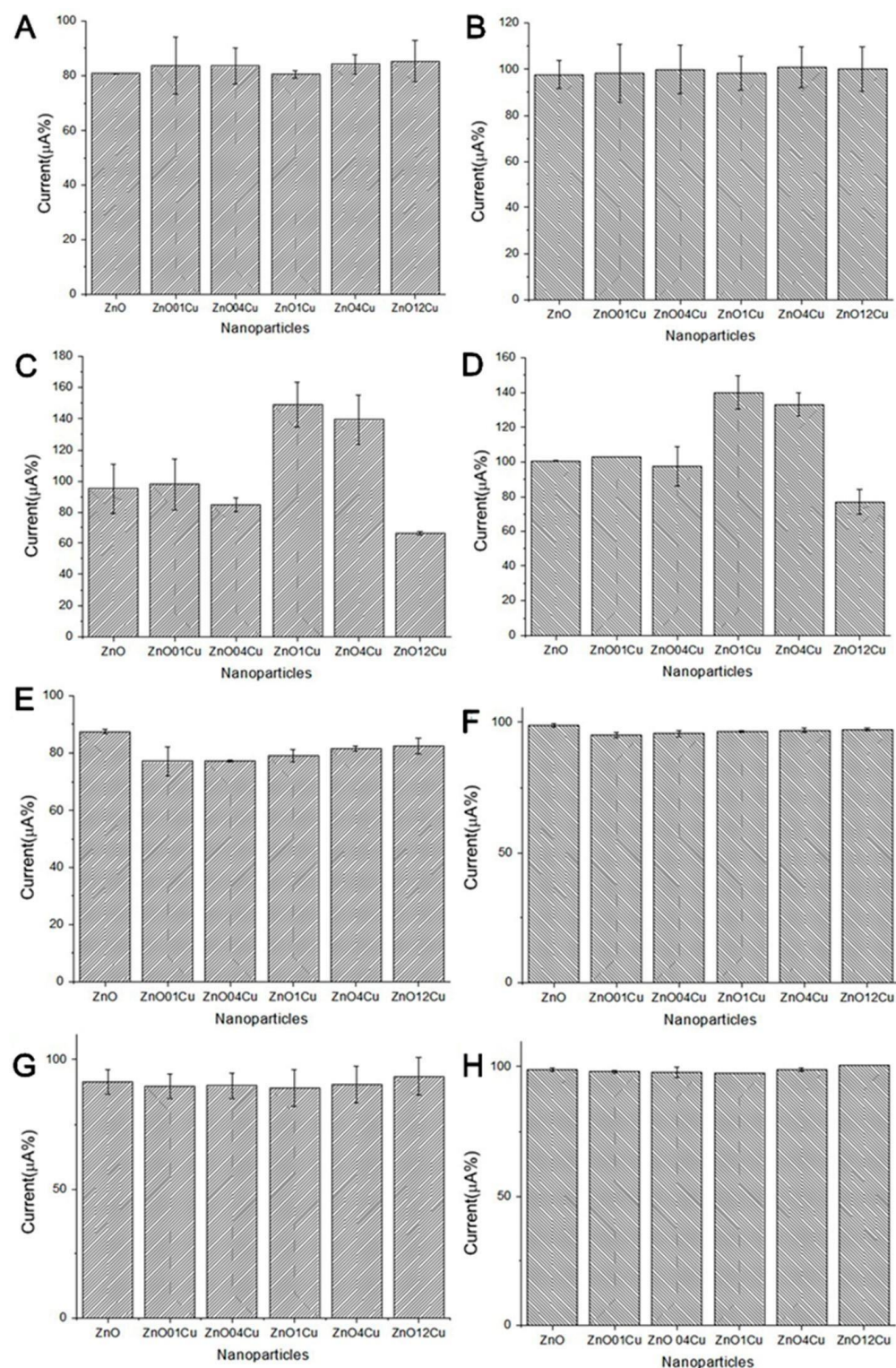


Figure 2. Electrochemical responses of FF/KCl in the presence of different NCs and different concentrations ($\text{mg}\cdot\text{mL}^{-1}$): 0.50 (A,B), 0.25 (C,D), 0.125 (E,F), and 0.625 (G,H). Oxidation peaks (first column) and reduction peaks (second column) in the cyclic voltammogram (CV) used in the construction of the column chart. Indicator electrolyte solution $[\text{Fe}(\text{CN})_6]^{-3/-4}$ and KCl, electrode C110, scan rate = $100.0 \text{ mV}\cdot\text{s}^{-1}$.

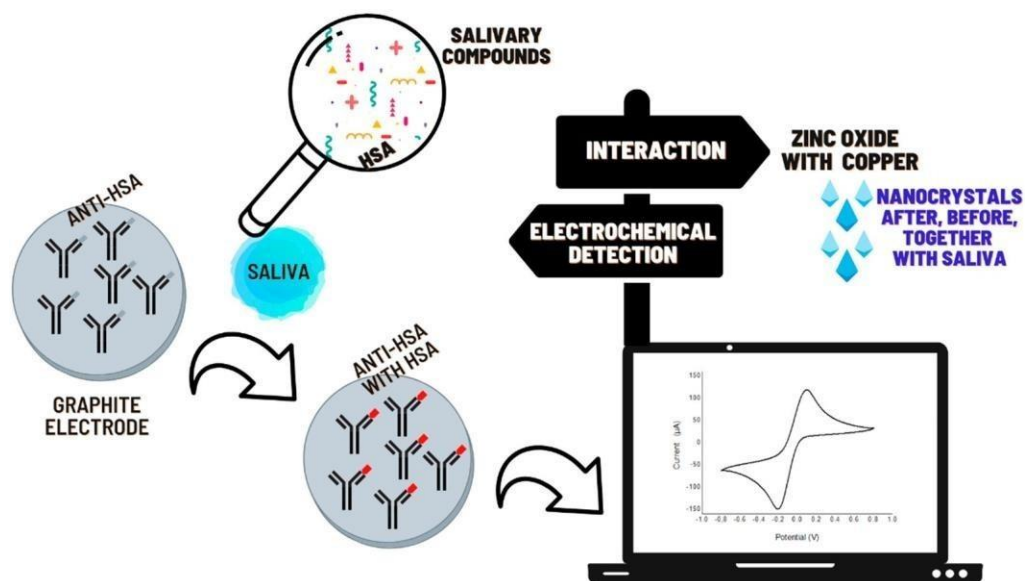


Figure 3. Schematic representation of the immunosensor development detection of HSA with ZnO:Cu NCs.

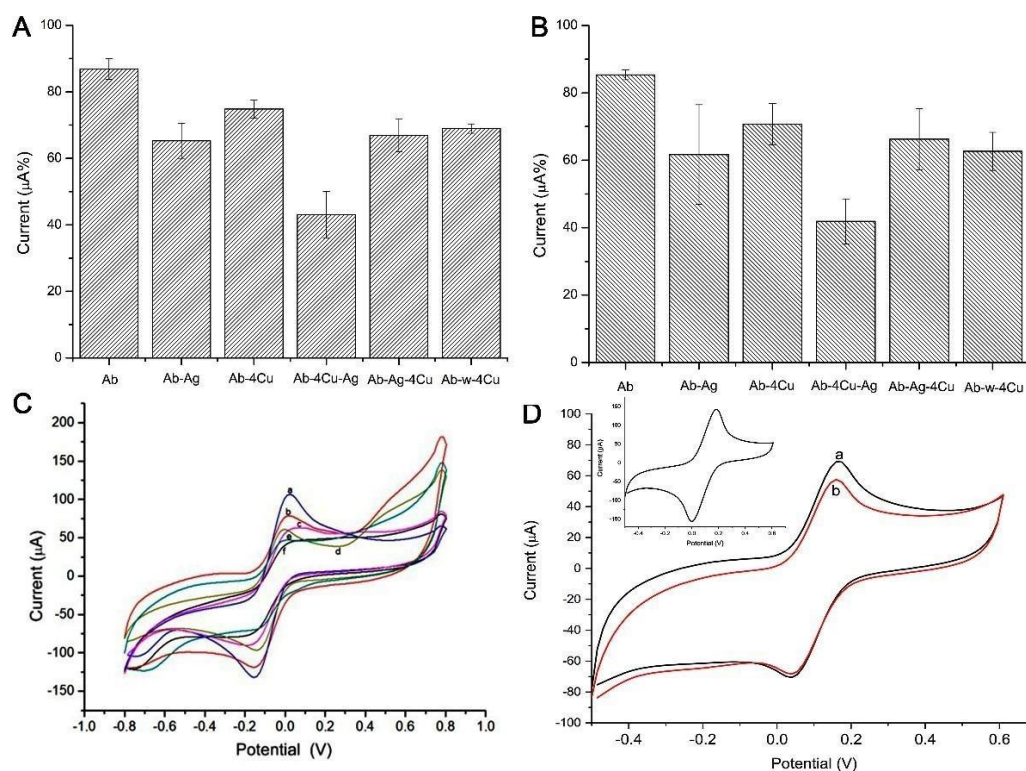


Figure 4. Sensor 01 and 02 presented column chart (A) oxidation peaks and (B) reduction peaks, sensor 01 (bars 1, 2, and 5) and sensor 02 (bars 3, 4, and 6), with ZnO:4Cu. Graphic (C) cyclic voltammetry (CV) (CV a, e, and d) and Sensor 02 (CV b, f, and c), whose peaks were used in the construction of the column chart. (D) CV of the sensor with saliva and ZnO:4Cu NCs mixed in one solution. The insert shows the cyclic voltammogram used to assess the electrodes' conductivity. Indicator electrolyte solution $[Fe(CN)_6]^{-3/-4}$ and KCl, electrode C 110, scan rate = $100.0\text{ mV}\cdot\text{s}^{-1}$. Note: all construction steps of this biosensor were shown.

To facilitate understanding, we could consider that we had two sensors at this stage: “Sensor 01”, evaluated on bars 1, 2, and 5, and “Sensor 02”, evaluated on bars 3, 4, and 6, shown in Figure 4. Note that bars 4 and 5 present the current signals for a changing order, i.e., ZnO:4Cu addition before and after the HSA (Ag).

The most significant electrochemical current drop happened with step 4 (Ab-4Cu-Ag), compared with step 5 (Ab-Ag-4Cu), with 53.3% values, emphasizing that, here, the greater resistivity process occurred. Sensor 01 in step 2 (Ab-Ag) presented a current decrease of 77.6%. An additional test (Ab-Ag mixed with 4Cu) presented a current decrease of 78.2%, emphasizing that the specific recognition process did not occur the same way when NCs were pipetted in different orders.

The results presented in Figure 5A,B show the oxidative and reductive analysis made with the ZnO:1Cu, in which bar charts present the current signals. In this case, “Sensor 3”, the steps were 1. immobilization of the antibody anti-HSA (Ab) and the addition of ZnO:1Cu (Ab-1Cu) (a); 2. HSA recognition with Ab with ZnO:1Cu (Ab-1Cu-Ag) (b); 3. HSA recognition with Ab, followed by ZnO:1Cu (Ab-Ag-1Cu) (c). (C) shows the CV whose peaks were used in the construction of the column chart. (D) shows the CV of the sensor with saliva and NCs ZnO:1Cu mixed in one solution. Note that bars 2 and 3 present the current signals for a changing order, i.e., the addition of ZnO:1Cu before and after the HSA (Ag).

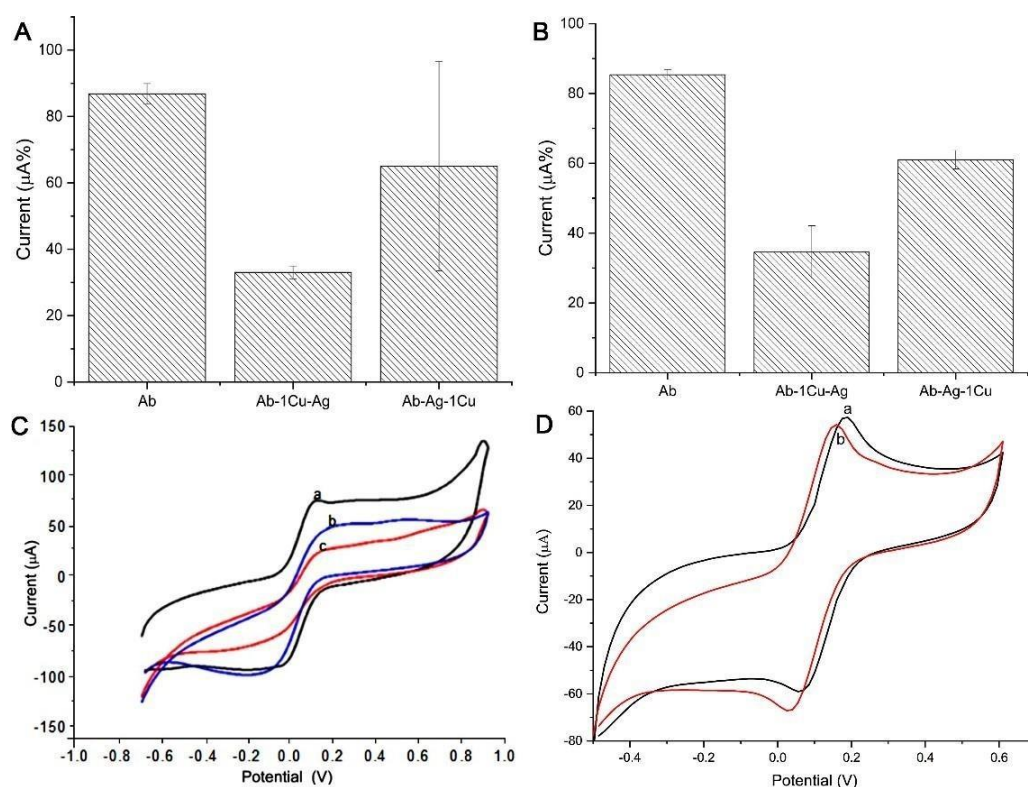


Figure 5. Sensor 03 presented column chart (A) oxidation peaks and (B) reduction peaks (bar 1, 2, and 3), with ZnO:1Cu. Graphic (C) CV (a, b, and c) whose peaks were used in the construction of the column chart. (D) CV of the sensor with saliva and ZnO:1Cu NCs mixed in one solution. Indicator electrolyte solution $[\text{Fe}(\text{CN})_6]^{-3/-4}$ and KCl, electrode C110, scan rate = $100.0 \text{ mV}\cdot\text{s}^{-1}$. Note: all construction steps of this biosensor were shown.

With Sensor 03, the most significant electrochemical current drop happened at step 2 (Ab-1Cu-Ag) compared to step 3 (Ab-Ag-1Cu), with 58.7% values, emphasizing that here the greater resistivity process occurred. An additional test (Ab-Ag mixed with 1Cu) presented a current decrease of 94.8%, emphasizing that the specific recognition process did not occur the same way when NCs were pipetted in different orders, as also noted in Figure 4.

Figure 6 shows the calibration curve in indirect detection evaluating the peak oxidation of FF/KCl at different saliva dilutions (pure (1 = $7.3887 \text{ U}\cdot\text{mL}^{-1}$, 1:10; 1:100; 1:1000;

1:10,000)). The graph shows a linear range of current peak vs. dilution. The logarithmic function (log) was used in the dilution values to achieve linearity in the graph.

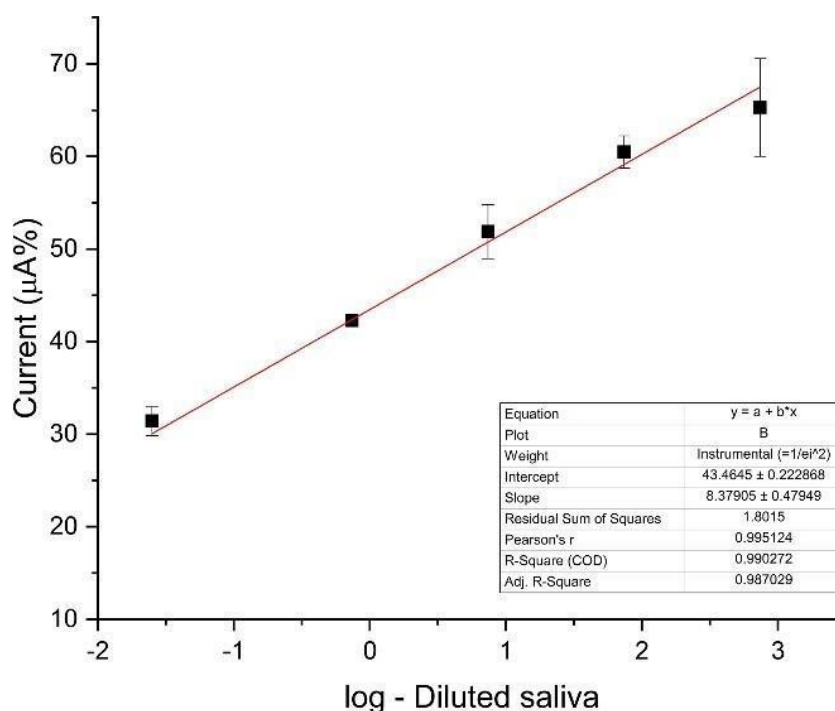


Figure 6. Electrochemical response for the oxidation of FF/KCl obtained after the recognition of the electrode containing the probe anti-HSA with different concentrations of HSA (log-diluted saliva). The inset shows R square, slope, and intercept values. Indicator electrolyte solution $[\text{Fe}(\text{CN})_6]^{-3/-4}$ and KCl, electrode C110, scan rate = $100.0 \text{ mV} \cdot \text{s}^{-1}$.

Evaluating the R square, slope, and intercept, we note that the oxidation graph had better results. This plot presents the correlation coefficient of 0.990272 (for the equation: $i(\mu\text{A}\%) = 8.37905 \times [\text{saliva dilution ratio}] + 43.4645$), an estimated limit of detection of $0.00196 \text{ U} \cdot \text{mL}^{-1}$, and limit of quantification of $0.00594 \text{ U} \cdot \text{mL}^{-1}$. The lowest dilution values (1:30,000; 1:50,000; 1:100,000) did not show significant differences in detection (results not shown).

Figure 7 shows the current response for the specificity test with alpha-amylase enzyme (AAE) and trypsin DPCC treated, type XI (TXI); both were prepared in $0.25 \text{ mg} \cdot \text{m}^{-1} \cdot \text{L}^{-1}$. (A) The steps were 1. immobilization of the antibody anti-HSA (Ab) (a); 2. HSA pure (Ag) recognition with Ab (Ab-Ag) (b); 3. AAE recognition with Ab (Ab-Ag) (c); 4. HSA (1:10.000) (Ag) recognition with Ab (d). (B) The steps were 1. electrode without any biomolecules (a); 2. immobilization of the antibody anti-HSA (Ab) (b); 3. TXI without recognition with Ab (c).

3.4. Sensor and Electrochemical Analysis

To study the interaction of NCs and saliva, a sensor without anti-HSA (Ab) was designed. Figure 8 shows the current response for each step of the other construction. (A) and (B) show the CV analysis of ZnO:4Cu and ZnO:1Cu, respectively, without steps 1 (immobilization of the antibody anti-HSA (Ab)). Step 1: adsorption of HSA (Ag) and ZnO:4Cu (Ag-4Cu) (a); step 2: adsorption of HSA (Ag) with ZnO:4Cu (Ag mixed with 4Cu) (b); step 3: adsorption of ZnO:4Cu and HSA(Ag) (4Cu-Ag) (c), and the same process was performed using ZNO:1Cu.

This analysis evaluated different responses of saliva and NCs when compared with sensors 01, 02, and 03.

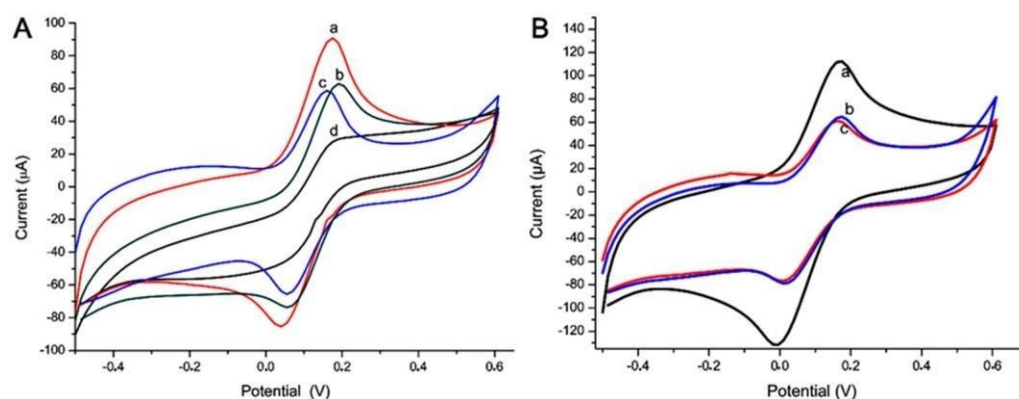


Figure 7. Electrochemical response of the biosensor with HSA, alpha-amylase enzyme, and trypsin for the specificity test. In this case, only saliva and AAE were detected (A), and (B) shows that TXI was not detectable. Indicator electrolyte solution $[\text{Fe}(\text{CN})_6]^{-3/-4}$ and KCl, electrode C110, scan rate = $100.0 \text{ mV}\cdot\text{s}^{-1}$.

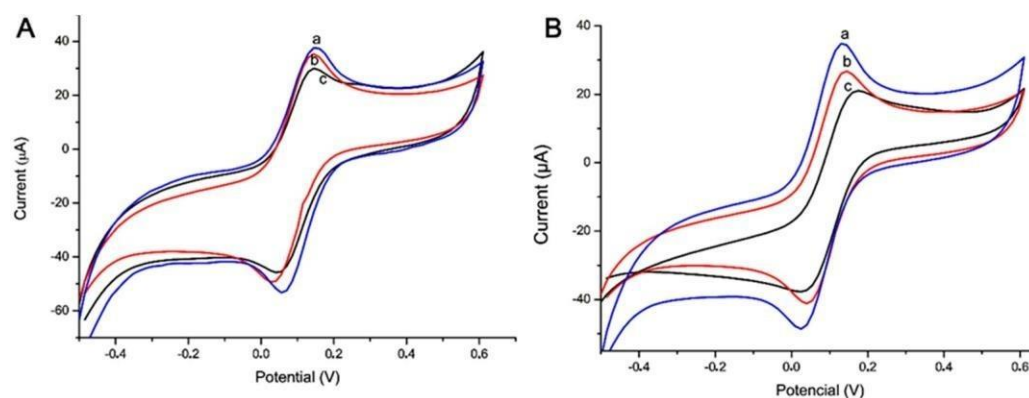


Figure 8. Electrochemical response of the electrode without antibody anti-HSA (Ab). In this case, it only had saliva and two types NCs in different orders. (A) ZnO:4Cu and (B) ZnO:1Cu. Indicator electrolyte solution $[\text{Fe}(\text{CN})_6]^{-3/-4}$ and KCl, electrode C110, scan rate = $100.0 \text{ mV}\cdot\text{s}^{-1}$.

4. Discussion

The study of the physical properties of nanomaterials is essential for the development of new technologies [43]. ZnO has a wide bandgap, chemical stability, and large exciton binding energy that outshines other oxide semiconductors for applications in diverse fields of electronics and piezoelectric outcomes [44,45]. Thus, in this work, we confirmed the formation of pure and Cu-doped ZnO nanocrystals, as well as the formation of nanocomposites (Cu-doped ZnO + CuO Ncs), and investigated the electrical responses in electrochemical sensors.

The surface roughness analysis (AFM) of the ZnO:0.4Cu NCs (Cu-doped ZnO NCs) system appeared to be much more intense when compared with ZnO NCs. Increasing the Cu^{2+} concentration to 4% (ZnO:4Cu-nanocomposite), the formation of the nanocomposite, and the synergism between the nanocrystals of Cu-doped ZnO and CuO NCs intensified the results, as shown in similar research [46,47].

We call attention to two groups of the NCs: doped (Cu-doped ZnO) and nanocomposite (Cu-doped ZnO + CuO NCs). In Cu-doped ZnO nanocrystals, copper ions were located both on the surface and inside the nanocrystal. Cu ions located on the nanocrystalline surface allowed interaction with specific biomolecules, facilitating interaction, as well as promoting mass transfer, promoting electron transfer, and avoiding photo-corrosion of nanocomposites, which enhanced its efficiency [48–50].

In the current study, an attempt was made to develop an immunosensor. Starting from the principle that the choice of NCs must occur from its interaction with all the molecules of a sensor, we started the electrochemical evaluations. These indicated the

NCs with better electrochemical conductivities. The current responses of the two NCs, ZnO:1Cu (Cu-doped ZnO) and ZnO:4Cu (Cu-doped CuO-ZnO + CuO NCs), occurred because the first one presented maximum doping, and the second was the composite with the lowest concentration. This high conductivity occurred due to copper segregation in the NC contours, causing a drop in resistance, indicating that the Cu^{2+} ions inserted in the Zn network played the role of an acceptor-type impurity [51].

In the development of a biosensor, we used the same specific polyclonal antibodies, purified by immunoaffinity, as described in others' works [24,52]. This sensor was improved using anti-HSA diluted 100 times in dw. Our results showed better electrochemical salivary enzyme detection in this concentration, and even specificity and selectivity tests were evaluated in the recognition Ab-Ag process, shown above.

The redox pair, potassium ferrocyanide/potassium ferricyanide, acted efficiently as an indicator on the electrode surface, resulting in an efficient change of the peak current in the presence of specific NCs and biomolecules. The electrochemical analysis, the values oxidation, and reduction could be used for diagnosis analysis in cyclic voltammetry (first cycle) [53,54].

In this work, tests revealed that saliva presented a more efficient diagnosis behavior in oxidation without NCs. The presence of ZnO:4Cu or ZnO:1Cu, shown in Figures 3 and 4, produced a greater drop in current when NCs were placed on the sensor before saliva.

These NCs, pipetted after Ab but before the saliva sample, altered the specificity. This result occurred because the sensor had free copper ions connectable to HSA. When the NCs were added after the saliva, we observed a current drop during the Ab-Ag recognition. We also observed that the presence of NCs did not significantly increase the current, showing that the specific coupling was partially interfered with, owing to the interaction of Cu^{2+} ions.

The third example was of that when the NCs were added together in the saliva. We did not observe a current drop during the recognition. The Cu^{2+} ion bound to HSA at the same site as the Ab binding, blocking the Ab-Ag interaction.

The electrochemical analysis presented more selectivity in the presence of NC ZnO with Cu after the saliva. The NCs collaborated to evaluate how the interference of other NCs present in saliva occurred, using small amplitude voltage.

This result could be explained because salivary proteins, including amylase, have metal-binding capacities like Cu^{2+} and Zn^{2+} [27,55,56].

The Cu^{2+} present in the surface of ZnO NCs or CuO NCs can bind with this protein through electrostatic interaction following a mechanism similar to Ca^{2+} . Studies have shown that alpha-amylase has two metal-binding sites, one exclusively for Ca^{2+} and the other for Cu^{2+} and Fe^{3+} [28,56]. These reports corroborated our findings and indicated the intense interaction of Cu^{2+} with human salivary alpha-amylase.

The calibration curve had better result in the oxidation test. In this case, the redox probe could produce the tests when this reagent lost electrons during the electrochemical reaction.

The specificity of this immunosensor was validated with the enzyme TXI. Commercial alpha-amylase had the same capacity to recognize a real sample, confirming molecular recognition using an electrochemical technique [57].

To assess this interaction of alpha-amylase with Cu^{2+} ions, we developed a sensor without Ab. Thus, we were able to evaluate that the NCs, when placed before the saliva, really generated an interaction with the HSA (biggest drop in the current). However, in the absence of Ab, where the NCs were placed after the saliva, we observed an absence of interaction due to allosteric impedance of the Cu^{2+} binding sites with HSA that was directly adsorbed on the electrode. Differently, it occurred when the NC was mixed with saliva, and it freely bound to HSA. We observed an intermediary current flow, proving the interaction between them. Therefore, based on the results achieved, we can say that we have an electrostatic interaction model between HSA and Cu^{2+} that can be evaluated in this immunosensor.

5. Conclusions

We presented a new differential analysis of nanoparticles for better recognition of biological elements, which imparted different currents and potentials in electrochemical detection, implying better diagnostic accuracy.

Challenged by the countless works in electrochemistry using nanocrystals, we evaluated the results obtained in this work and provided opportunities for reflection based on experimental evidence.

We must evaluate the ZnO:Cu NCs, the effect of Cu concentration on physical and chemical properties, and the different ways to put them on the sensors to avoid erroneous interpretations of the results.

The results showed that the produced immunosensor showed exciting properties, such as good selectivity and sensibility. Thus, it is a promising technique of molecular analysis, and further studies of this advanced technology will extend the system to the determination of other biomolecules in saliva samples.

Author Contributions: Conceptualization, R.P.A.-B., A.C.A.S., and F.S.E.; methodology, R.P.A.-B., A.C.A.S., R.T.S.O.J., B.R.M., T.M.S., A.K.S.R.d.F., R.d.P.M., and R.R.T.; characterization and synthesis of the nanocrystal, N.O.D. and A.C.A.S.; validation, B.R.M., R.d.P.M., T.M.S., A.K.S.R.d.F., and R.R.T.; formal analysis, B.R.M., R.d.P.M., R.P.A.-B., N.O.D., A.C.A.S., and F.S.E.; investigation, R.P.A.-B., A.C.A.S., and F.S.E. resources, M.V.d.S., C.J.F.O., V.R.J., A.C.A.S., and F.S.E.; writing—original draft preparation, R.P.A.-B.; writing—review and editing, all authors; supervision, R.P.A.-B., A.C.A.S., and F.S.E.; project administration, R.P.A.-B., A.C.A.S., and F.S.E.; funding acquisition, N.O.D. and F.S.E. We declare that B.R.M. and T.M.S. were co-first authors. All authors have read and agreed to the published version of the manuscript.

Funding: This research was funded by Fundação de Amparo à Pesquisa do Estado de Minas Gerais (FAPEMIG), grant number NS: ES08310 Project APQ-01083-16; Conselho Nacional de Desenvolvimento Científico e Tecnológico (CNPq) grants of Productivity 1D under the Nr. 311568/2017-3 (N.O.D) and Productivity 2 under the 311730/2020-5 (A.C.A.S); Coordenação de Aperfeiçoamento de Pessoal de Nível Superior (CAPES).

Acknowledgments: UFTM, UFAL, UFU, CAPES, FAPEMIG, and CNPq for the support. The authors would like to take this opportunity to thank all reviewers for their valuable comments for improvement of the article.

Conflicts of Interest: The authors declare no conflict of interest.

References

- Kreuter, J. Nanoparticles—a historical perspective. *Int. J. Pharm.* **2006**, *331*, 1–10. [[CrossRef](#)]
- Colomban, P.; Gouadec, G. The ideal ceramic-fibre/oxide-matrix composite: How to reconcile antagonist physical and chemical requirements? *Ann. Chim. Sci. Mater.* **2005**, *30*, 673–688. [[CrossRef](#)]
- Hough, R.M.; Noble, R.R.P.; Reich, M. Natural gold nanoparticles. *Ore. Geol. Rev.* **2011**, *42*, 55–61. [[CrossRef](#)]
- Heiligt, F.J.; Niederberger, M. The fascinating world of nanoparticle research. *J. Mater. Today* **2013**, *16*, 262–271. [[CrossRef](#)]
- Sabir, S.; Arshad, M.; Chaudhari, S.K. Zinc Oxide Nanoparticles for Revolutionizing Agriculture: Synthesis and Applications. *Sci. World J.* **2014**, *2014*, 1–8. [[CrossRef](#)]
- Elfeky, S.A.; Mahmoud, S.E.; Youssef, A.F. Applications of CTAB modified magnetic nanoparticles for removal of chromium (VI) from contaminated water. *J. Adv. Res.* **2017**, *8*, 435–443. [[CrossRef](#)] [[PubMed](#)]
- Khan, I.; Saeed, K.; Khan, I. Nanoparticles: Properties, applications and toxicities. *Arab. J. Chem.* **2017**, *1*, 1–24. [[CrossRef](#)]
- Vanmaekelbergh, D.; Van Vugt, L.K. ZnO nanowire lasers. *Nanoscale* **2011**, *3*, 2783–2800. [[CrossRef](#)] [[PubMed](#)]
- Bai, X.; Li, L.; Liu, H.; Tan, L.; Liu, T.; Meng, X. Solvothermal Synthesis of ZnO Nanoparticles and Anti-Infection Application in Vivo. *ACS Appl. Mater. Interfaces* **2015**, *7*, 1308–1317. [[CrossRef](#)]
- Haq, A.N.U.; Nadhman, A.; Ullah, I.; Mustafa, G.; Yasin, M.; Khan, I. Synthesis Approaches of Zinc Oxide Nanoparticles: The Dilemma of Ecotoxicity. *J. Nanomater.* **2017**, *2017*, 8510342. [[CrossRef](#)]
- Sharma, G.; Kumar, A.; Sharma, S.; Naushad, M.; Dwivedi, R.P.; AlOthman, Z.A.; Mola, G.T. Novel development of nanoparticles to bimetallic nanoparticles and their composites: A review. *J. King Saud. Univ.* **2017**, *31*, 257–269. [[CrossRef](#)]
- Silva, R.S.; Gualdi, A.J.; Zabotto, F.L.; Cano, N.F.; Silva, A.C.A.; Dantas, N.O. Weak ferromagnetism in Mn²⁺ doped Bi₂Te₃ nanocrystals grown in glass matrix. *J. Alloys Compd.* **2017**, *708*, 619–622. [[CrossRef](#)]
- Rego-Filho, F.G.; Dantas, N.O.; Silva, A.C.A.; Vermelho, M.V.D.; Jacinto, C.; Gouveira-Neto, A.S. IR-to-visible frequency upconversion in Yb³⁺/Tm³⁺ co-doped phosphate glass. *Opt. Mater.* **2017**, *73*, 1–6. [[CrossRef](#)]

14. Salem, W.; Leitner, D.R.; Zingl, F.G.; Schratte, G.; Prassl, R.; Goessler, W.; Reidl, J.; Schilda, S. Antibacterial activity of silver and zinc nanoparticles against *Vibrio cholerae* and enterotoxigenic *Escherichia coli*. *Int. J. Med. Microb.* **2015**, *305*, 85–95. [[CrossRef](#)] [[PubMed](#)]
15. Chu, H.; Liu, X.; Liu, J.; Li, J.; Wu, T.; Li, H.; Lei, W.; Xu, Y.; Pan, L. Synergetic effect of Ag₂O as co-catalyst for enhanced photocatalytic degradation of phenol on N-TiO. *Sci. Eng. B Solid State Mater. Adv. Technol.* **2016**, *2211*, 128–134. [[CrossRef](#)]
16. Phoothong, W.; Foophow, T.; Pecharapa, W. Synthesis and characterization of copper zinc oxide nanoparticles obtained via metathesis process. *Adv. Nat. Sci. Nanosci. Nanotechnol.* **2017**, *8*, 035003. [[CrossRef](#)]
17. Morais, P.V.; Gomes-Junior, V.F.; Silva, A.C.A.; Dantas, N.O.; Schoning, M.J.; Siqueira-Junior, J.R. Nanofilm of ZnO nanocrystals/carbon nanotubes as biocompatible layer for enzymatic biosensors in capacitive field-effect devices. *J. Mater. Sci.* **2017**, *52*, 12314–12325. [[CrossRef](#)]
18. Reis, É.M.; Rezende, A.A.A.; Oliveira, P.F.; Nicolella, H.D.; Tavares, D.C.; Silva, A.C.A.; Dantas, N.O.; Spanó, M.A. Evaluation of titanium dioxide nanocrystal-induced genotoxicity by the cytokinesis-block micronucleus assay and the *Drosophila* wing spot test. *Food Chem. Toxicol.* **2016**, *84*, 55–63. [[CrossRef](#)]
19. Nater, U.M.; Rohleder, N. Salivary alpha-amylase as a non-invasive biomarker for the sympathetic nervous system: Current state of research. *Psychoneuroendocrinology* **2009**, *34*, 486–496. [[CrossRef](#)] [[PubMed](#)]
20. Diaz, M.M.; Bocanegra, O.L.; Teixeira, R.R.; Soares, S.S.; Espindola, F.S. Response of salivary markers of autonomic activity to elite competition. *Int. J. Sports Med.* **2012**, *33*, 763–768. [[CrossRef](#)] [[PubMed](#)]
21. Teixeira, R.R.; Díaz, M.M.; Santos, T.V.; Bernardes, J.T.; Peixoto, L.G.; Bocanegra, O.L.; Neto, M.B.; Espindola, F.S. Chronic stress induces a hyporeactivity of the autonomic nervous system in response to acute mental stressor and impairs cognitive performance in business executives. *PLoS ONE* **2015**, *10*, e0119025. [[CrossRef](#)] [[PubMed](#)]
22. Giacomello, G.; Scholten, A.; Parr, M.K. Current methods for stress marker detection in saliva. *J. Pharm. Biomed. Anal.* **2020**, *191*, 113604. [[CrossRef](#)]
23. Yamaguchi, M.; Deguchi, M.; Wakasugi, J.; Ono, S.; Takai, N.; Higashi, T.; Mizuno, Y. Hand-held monitor of sympathetic nervous system using salivary amylase activity and its validation by driver fatigue assessment. *Biosens. Bioelectron.* **2006**, *21*, 1007–1014. [[CrossRef](#)]
24. Santos, T.V.S.; Teixeira, R.R.; Franco, D.L.; Madurro, J.M.; Brito-Madurro, A.G.; Espindola, F.S. Bioelectrode for detection of human salivary amylase. *Mater. Sci. Eng. C* **2012**, *32*, 530–535. [[CrossRef](#)]
25. Malon, R.S.P.; Sadir, S.; Balakrishnan, M.; Corcoles, E.P. Saliva-based biosensors: Noninvasive monitoring tool for clinical diagnostics. *BioMed Res. Int.* **2014**, *2014*, 962903. [[CrossRef](#)]
26. Zheng, X.; Zhang, F.; Wang, K.; Zhang, W.; Li, Y.; Sun, Y.; Sun, X.; Li, C.; Dong, B.; Wang, L.; et al. Smart biosensors and intelligent devices for salivary biomarker detection. *TrAC Trends Anal. Chem.* **2021**, *140*, 116281. [[CrossRef](#)]
27. Agarwal, R.P.; Henkin, R.I. Metal binding characteristics of human salivary and porcine pancreatic amylase. *J. Biol. Chem.* **1987**, *262*, 2568–2575. [[CrossRef](#)] [[PubMed](#)]
28. Hong, J.H.; Duncan, S.E.; Dietrich, A.M.; O’Keefe, S.F.; Eigel, W.N.; Mallikarjunan, K. Interaction of copper and human salivary proteins. *J. Agric. Food Chem.* **2009**, *57*, 15–6967. [[CrossRef](#)] [[PubMed](#)]
29. Linden, A.; Mayans, O.; Meyer-Klaucke, W.; Antranikian, G.; Wilmanns, M. Differential regulation of a hyperthermophilic α -amylase with a novel (Ca, Zn) two-metal center by zinc. *J. Biol. Chem.* **2003**, *278*, 9875–9884. [[CrossRef](#)] [[PubMed](#)]
30. Zhang, C.; Liu, J.; Yu, W.; Sun, D.; Sun, X. Susceptibility to corrosion of laser welding composite arch wire in artificial saliva of salivary amylase and pancreatic amylase. *Mater. Sci. Eng. C Mater. Biol. Appl.* **2015**, *55*, 267–271. [[CrossRef](#)]
31. Murugappan, G.; Sreeram, K.J. Nano-biocatalyst: Bi-functionalization of protease and amylase on copper oxide nanoparticles. *Colloids Surf. B Biointerfaces* **2021**, *197*, 111386. [[CrossRef](#)]
32. Ngamchuea, K.; Chaisiwamongkol, K.; Batchelor-McAuley, C.; Compton, R.G. Chemical analysis in saliva and the search for salivary biomarkers—A tutorial review. *Analyst* **2018**, *143*, 81–99. [[CrossRef](#)]
33. Yao, Y.; Li, H.; Wang, D.; Liu, C.; Zhang, C. An electrochemiluminescence cloth-based biosensor with smartphone-based imaging for detection of lactate in saliva. *Analyst* **2017**, *142*, 3715–3724. [[CrossRef](#)]
34. Khanna, P.; Walt, D.R. Salivary diagnostics using a portable point-of-service platform: A review. *Clin. Therapeut.* **2015**, *37*, 498–504. [[CrossRef](#)]
35. Vinitha, T.U.; Ghosh, S.; Milleman, A.; Nguyen, T.; Ahn, C.H. A new polymer lab-on-a-chip (LOC) based on a microfluidic capillary flow assay (MCFA) for detecting unbound cortisol in saliva. *Lab Chip* **2020**, *20*, 1961–1974. [[CrossRef](#)]
36. Arunkumar, S.; Arunkumar, J.S.; Krishna, N.B.; Shakuntala, G.K. Developments in Diagnostic Applications of Saliva in Oral and Systemic Diseases—A Comprehensive Review. *J. Sci. Innov. Res.* **2014**, *3*, 372–387. Available online: http://www.jsirjournal.com/Vol3_Issue3_16.pdf (accessed on 5 January 2021).
37. Souza, A.V.; Giolo, J.S.; Teixeira, R.R.; Vilela, D.D.; Peixoto, L.G.; Justino, A.B.; Caixeta, D.C.; Puga, G.M.; Espindola, F.S. Salivary and Plasmatic Antioxidant Profile following Continuous, Resistance, and High-Intensity Interval Exercise: Preliminary Study. *Oxid. Med. Cell Longev.* **2019**, 5425021. [[CrossRef](#)]
38. Jayathilaka, W.A.D.M.; Qi, K.; Qin, Y.; Chinnappan, A.; Serrano-García, W.; Baskar, C.; Wang, H.; He, J.; Cui, S.; Thomas, S.W. Significance of nanomaterials in wearables: A review on wearable actuators and sensors. *Adv. Mater.* **2019**, *31*, 1805921. [[CrossRef](#)]
39. Mishra, S.; Saadat, D.; Lee, O.Y.; Choi, W.S.; Kim, J.H.; Yeo, W.H. Recent advances in salivary cancer diagnostics enabled by biosensors and bioelectronics. *Biosens. Bioelectron.* **2016**, *81*, 181–197. [[CrossRef](#)]

40. Ilea, A.; Andrei, V.; Feurdean, C.N.; Băbțan, A.-M.; Petrescu, N.B.; Câmpian, R.S.; Bosca, A.B.; Ciui, B.; Tertis, M.; Săndulescu, R. Saliva, a magic biofluid available for multilevel assessment and a mirror of general health—A systematic review. *Biosensors* **2019**, *9*, 27. [[CrossRef](#)]
41. Ehtesabi, H. Carbon nanomaterials for salivary-based biosensors: A review. *Mater. Today Chem.* **2020**, *17*, 100342. [[CrossRef](#)]
42. Mani, V.; Beduk, T.; Khushaim, W.; Ceylan, A.E.; Timur, S.; Wolfbeis, O.S.; Salama, K.N. Electrochemical sensors targeting salivary biomarkers: A comprehensive review. *TrAC. Trends Anal. Chem.* **2020**, 116164. [[CrossRef](#)]
43. Rao, C.N.R.; Biswas, K. Characterization of Nanomaterials by Physical Methods. *Annu. Rev. Anal. Chem.* **2009**, *2*, 435–462. [[CrossRef](#)] [[PubMed](#)]
44. Quintana, A.; Gómez, A.; Baró, M.D.; Surinach, S.; Pellicer, E.; Sort, J. Self-templating faceted and spongy single-crystal ZnO nanorods: Resistive switching and enhanced piezoresponse. *Mater. Des.* **2017**, *133*, 54–61. [[CrossRef](#)]
45. Li, F.; Gou, Q.; Xing, J.; Tan, Z.; Jiang, L.; Xie, L.; Wu, J.; Zhang, W.; Xiao, D.; Wu, J. The piezoelectric and dielectric properties of sodium–potassium niobate ceramics with new multiphase boundary. *J. Mater. Sci. Mater. Electron.* **2017**, *28*, 18090–18098. [[CrossRef](#)]
46. Bhardwaj, R.; Bharti, A.; Singh, J.P.; Chae, K.H.; Goyal, N. Influence of Cu doping on the local electronic and magnetic properties of ZnO nanostructures. *Nanoscale Adv.* **2020**, *2*, 4450–4463. [[CrossRef](#)]
47. Dolatabadi, J.E.N.; de la Guardia, M. Nanomaterial-based electrochemical immunosensors as advanced diagnostic tools. *Anal. Methods* **2014**, *6*, 3891–3900. [[CrossRef](#)]
48. Charde, S.J.; Sonawane, S.S.; Rathod, A.P.; Sonawane, S.H.; Shimpi, N.G.; Parate, V.R. Copper-Doped Zinc Oxide Nanoparticles: Influence on Thermal, Thermo Mechanical, and Tribological Properties of Polycarbonate. *Polym. Compos.* **2017**, *39*, E1398–E1406. [[CrossRef](#)]
49. Thiawong, T.; Onlaor, K.; Chaithanatkun, N.; Tunhoo, T. Preparation of Copper Doped Zinc Oxide Nanoparticles by Precipitation Process for Humidity Sensing Device. *AIP Conf. Proc.* **2018**, *2010*, 020022. [[CrossRef](#)]
50. Das, S.; Srivastava, V.C. An overview of the synthesis of CuO-ZnO nanocomposite for environmental and other applications. *Nanotechnol. Rev.* **2018**, *7*, 267–282. [[CrossRef](#)]
51. Egelhaaf, H.J.; Oelkrug, D. Luminescence and nonradiative deactivation of excited states involving oxygen defect centers in polycrystalline ZnO. *J. Cryst. Growth* **1996**, *161*, 190–194. [[CrossRef](#)]
52. Cho, I.H.; Kim, D.H.; Park, S. Electrochemical biosensors: Perspective on functional nanomaterials for on-site analysis. *Biomater. Res.* **2020**, *24*, 6. [[CrossRef](#)] [[PubMed](#)]
53. Zhou, N.; Chen, H.; Li, J.; Chen, L. Highly sensitive and selective voltammetric detection of mercury (II) using an ITO electrode modified with 5-methyl-2-thiouracil, graphene oxide and gold nanoparticles. *Microchim. Acta* **2013**, *180*, 493–499. [[CrossRef](#)]
54. Martins, B.R.; Barbosa, Y.O.; Andrade, C.M.R.; Pereira, L.Q.; Simão, G.F.; de Oliveira, C.J.; Correia, D.; Oliveira, R.T.S., Jr.; da Silva, M.V.; Silva, A.C.A.; et al. Development of an Electrochemical Immunosensor for Specific Detection of Visceral Leishmaniasis Using Gold-Modified Screen-Printed Carbon Electrodes. *Biosensors* **2020**, *10*, 81. [[CrossRef](#)] [[PubMed](#)]
55. Shatzman, A.R.; Henkin, R.I. Metal-binding characteristics of the parotid salivary protein gustin. *Biochim. Biophys. Acta.* **1980**, *623*, 107–108. [[CrossRef](#)]
56. Baker, E.N.; Anderson, B.F.; Baker, H.M.; Haridas, M.; Norris, G.E.; Rumball, S.V.; Smith, C.A. Metal and anion binding sites in lactoferrin and related proteins. *Pure Appl. Chem.* **1990**, *62*, 1067–1070. [[CrossRef](#)]
57. Sadik, O.A.; Aluoch, A.O.; Zhou, A. Status of biomolecular recognition using electrochemical techniques. *Biosens. Bioelectron.* **2009**, *24*, 2749–2765. [[CrossRef](#)]

APÊNDICE B - SÍNTESE E CARACTERIZAÇÃO DE ESTRUTURA METAL-ORGÂNICA (MOF) E PROVA DE CONCEITO NO DESENVOLVIMENTO DE BIOCENSORES PARA DETECÇÃO DE ALFA-AMILASE SALIVAR HUMANA

Síntese e caracterização de estrutura metal-orgânica (MOF) e prova de conceito no desenvolvimento de biossensor para detecção de alfa-amilase salivar humana

Rhéltheer de P. Martins^a, Beatriz R. Martins^a, Amanda B. Nascimento^b,
Rodrigo A.A. Muñoz^b, Robson T. S de Oliveira^a Renata P. Alves^a.

^aUniversidade Federal do Triângulo Mineiro – UFTM, Uberaba, Brasil;

^bUniversidade Federal de Uberlândia – UFU, Uberlândia, Brasil.

Resumo

Este trabalho segue uma rota de síntese de uma estrutura metal-orgânica de nióbio. Foram necessárias adequações na rota de síntese e no tratamento final das amostras sintetizadas. A Nb-MOF foi sintetizada e caracterizada pelas metodologias de difração de raios X (DRX), microscopia eletrônica de varredura (MEV), espectroscopia de raio-X por energia dispersiva (EDS), espectroscopia de absorção na região do infravermelho por transformada de Fourier (FTIR) e espectroscopia Raman. Após o bom resultado obtido nas caracterizações, a Nb-MOFH foi testada como prova de conceito em um imunossensor eletroquímico para a detecção da Alfa-amilase salivar humana (HSA). As propriedades eletroquímicas foram avaliadas por voltametria cíclica (VC) (0,1 V.s⁻¹). O par redox Ferri/Ferrocianeto de Potássio, possibilitaram a análise dos picos de corrente anódicas e catódicas. Os resultados foram obtidos pelo potenciostato EmStat1/software PsTrace8. A Nb-MOFH apresentou ganho de corrente depois da adsorção no eletrodo comercial de grafite. O imunossensor decorado com Nb-MOFH apresentou especificidade e seletividade. Portanto, com os resultados observados neste trabalho este imunossensor tem potencial promissor como um dispositivo para detecção de HSA, presentes na saliva.

Palavras-chave: Estrutura metal-orgânica (MOF); Biossensor; Nb-MOF; Alfa-amilase salivar humana.

Introdução

Os avanços das metodologias de síntese e das técnicas de caracterizações, o desenvolvimento e a aplicação de materiais porosos tem sido muito estudado e desperta grande interesse científico (Hussain *et al.* 2024).

Os polímeros de coordenação foram descritos em 1954, podendo ser definidos como uma extensa rede de íons ou agrupamentos metálicos coordenados às moléculas orgânicas, com poros de tamanhos controláveis e formas geométricas definidas. As redes metalorgânicas são uma nova classe de polímeros de coordenação cristalinos, tendo os centros metálicos, constituídos por íons metálicos ou por aglomerados de metais, que estão ligados por moléculas orgânicas, oportunizando a formação de compostos poliméricos altamente organizados (Almeida *et al.* 2012).

O termo redes metalorgânicas ou do inglês “metal-organic framework” (MOF) surgiu na literatura em 1995. A União Internacional de Química Pura e Aplicada (IUPAC) define MOF como sendo um polímero de coordenação com uma rede aberta contendo vazios potenciais. Mesmo tendo uma ampla definição é enfatizado que os poros precisam estar disponíveis e desobstruídos de moléculas como as de solvente (Batten, *et al.* 2012).

As formas geométricas das redes metalorgânicas, irão depender das características dos metais e dos ligantes que formará estas redes. Os ligantes funcionam como pilares dos poros da estrutura. Os ligantes utilizados na síntese das MOFs são compostos orgânicos com anéis aromáticos e com átomos doadores de elétrons. Estes ligantes devem apresentar pelo menos duas ramificações funcionalizadas, disponíveis para se ligarem em dois ou mais sítios metálicos na estrutura da MOF, como mostra a Figura 1 (Jiang e Xu 2011) (Oliveira, 2019).

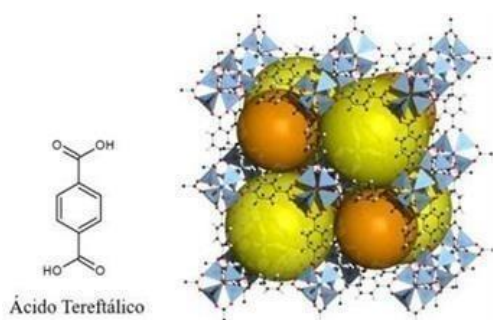


Figura 1 – Estrutura química do ácido tereftálico e esquematização da MOF.

O Politereftalato de Etileno (PET) é um polímero termoplástico da família dos poliésteres que tem como características básicas a leveza, a resistência e a transparência. Ele chegou ao Brasil em 1988, sendo utilizado primeiramente na indústria têxtil. A partir de 1993 passou a ter forte expressão no mercado de embalagens, sendo largamente utilizado em todo o mundo para a fabricação de embalagens (Deleu *et al.* 2016).

O PET é produzido industrialmente através da esterificação direta do ácido tereftálico purificado com o monoetileno glicol, o PET pós-consumo pode ser utilizado para a obtenção do ácido tereftálico. Percebendo que mais de 85% do peso do PET pós-consumo consiste em ácido tereftálico, ele se torna um resíduo de grande interesse como reagente para o desenvolvimento de pesquisas que envolvem a síntese de novos materiais (Krisbiantoro *et al.* 2024)

A reciclagem terciária também conhecida como a decomposição química do PET se baseia na reversibilidade da sua polimerização, na qual pode ser realizada através das reações de hidrólise, glicólise, metanólise e aminólise podendo ser catalisada por ácidos, bases, ou catalisadores neutros. Uma grande vantagem da utilização da hidrólise, ou seja, sua despolimerização é a produção de ácido tereftálico, que após purificação pode ser repolimerizado. Este fato, sozinho, possibilita a economia de 130 milhões de dólares por ano em importações de fontes p-ftálicas (ácido tereftálico e tereftalato de dimetila), além da redução no uso de derivados do petróleo (Di Souza, 2008).

Historicamente, as substâncias metálicas têm desempenhado um grande papel na indústria mineral brasileira. As de novas descobertas de depósitos naturais de metais no território brasileiro ocasionou relevante impacto na economia nacional, impulsionando o processo de industrialização brasileira.

Segundo o United States Geological Survey – USGS, o Brasil possui 98,43%, quase a totalidade das reservas globais lavráveis de nióbio, seguido pelo Canadá com 1,11% e a Austrália com 0,46%. Com isso, a USGS afirma que os recursos mundiais de nióbio conhecidos são suficientes para atender as necessidades mundiais do metal por mais de duzentos anos (Gusmão, K. B., Pergher, S. B. C., Santos dos, E. N, 2017).

Nas últimas décadas, uma variedade de materiais contendo nióbio ganharam destaque devido a suas aplicações nas indústrias tecnológicas. Na década de 90, esses materiais

ganharam espaço nas pesquisas, após a publicação de trabalhos que demonstraram um aumento considerável da atividade catalítica, seletividade e estabilidade química de catalisadores tradicionais quando adicionados pequenas quantidades de nióbio a eles (Lopes *et al.* 2015).

Frente a esta pesquisa bibliográfica, propomos sintetizar e caracterizar uma Nb-MOF fazendo alguns ajustes em uma rota de síntese já relatada na literatura. E posteriormente utilizar esta Nb-MOF como prova de conceito no desenvolvimento de biossensor para detecção de alfa-amilase salivar humana.

Experimental

Todos os reagentes eram de grau analítico (Merck), e todas as soluções foram preparadas usando água ultrapura obtida de um sistema (Synergy Milli-Q). O ácido tereftálico foi obtido a partir do PET e depois juntamente com os outros reagentes, utilizado para a síntese da MOF de nióbio (Nb-MOF). A síntese dos materiais foi realizada de acordo com Oliveira (2019), sendo realizadas algumas adequações.

Para a obtenção do ácido tereftálico (AT) a partir do PET preparamos 25mL de uma solução de hidróxido de sódio com concentração de $5,0\text{mol L}^{-1}$, na qual foi acrescentado 5,5g de PET previamente triturado e peneirado. A suspensão formada foi aquecida a 100°C sob agitação magnética por 5 h em refluxo.

Após a reação, foram adicionados 250mL de água destilada para a completa dissolução do precipitado formado. Em seguida, a solução formada foi acidificada com ácido sulfúrico PA até alcançar pH próximo a zero, o pH foi medido com o auxílio de um pHmetro (Marca: HANNA Modelo: HI 9321). Após acidificação, a mistura formada foi centrifugada a 5000rpm por 5 minutos para a retirada do líquido sobrenadante. Posteriormente, o sólido branco foi levado à estufa por 24 h a 75°C para secagem, logo após, o mesmo foi submetido à maceração e armazenagem.

A partir da obtenção do AT foi sintetizado a Nb-MOF. Em um béquer (A) foi adicionado 2g do oxalato amoniacal de nióbio ($\text{NH}_4\text{NbO}(\text{C}_2\text{O}_4)_2 \cdot \text{H}_2\text{O}$), na qual foi levado ao ultrassom até completa dissolução. Adicionou-se 0,8g de permanganato de potássio (KMnO_4). Foi adicionado ácido sulfúrico PA até pH próximo a 1. A adição de permanganato de potássio tem como objetivo a oxidação do oxalato a fim de deixar os sítios de nióbio disponíveis para a complexação com o AT.

Em outro béquer (B), foi adicionado 1,2g de AT obtido do PET e 0,6g de hidróxido de sódio em água destilada. A mistura foi levada ao ultrassom até completa dissolução. A solução contida no béquer A e foi submetida a aquecimento. Após ebulição da solução no balão de fundo redondo, a solução contida no béquer B foi gotejada sobre a solução A.

Em seguida, ao empregar a proporção molar de 1:1, o balão contendo as duas soluções (A e B) foram submetidas a aquecimento e refluxo por 24 h. Após o decorrer deste tempo, o material sintetizado foi lavado, centrifugado a 5000 rpm por 5 minutos e seco a 100°C por 7 dias em estufa. Logo após a secagem, o Nb-MOF sintetizado foi macerado e armazenado até a sua utilização.

Após a síntese da Nb-MOF os poros podem estar obstruídos, impedindo assim que as MOFs utilizem a área superficial total que possuem. Para o tratamento dos poros, adicionou-se em um béquer 20mL de metanol e 300mg da MOF. Após a sedimentação do material, retirou-se o metanol e adicionou-se 20mL de diclorometano. Este procedimento foi repetido por 3 vezes em cada solvente com intervalos de 24hrs. Logo após secagem obteve-se a Nb-MOF tratada.

A fim de avaliarmos o efeito deste tratamento da Nb-MOF, foi separada para as análises posteriores uma porção do material sintetizado sem fazermos a tratamento da mesma. Sendo assim, teremos nas análises duas amostras, a saber: Nb-MOF (sem tratamento) e a Nb-MOFH (com tratamento).

Os reagentes precursores e as Nb-MOF e Nb-MOFH foram caracterizadas pelas técnicas: difração de raios X (DRX), microscopia eletrônica de varredura (MEV), espectroscopia de raios-X por energia dispersiva (EDS), espectroscopia de absorção na região do infravermelho por transformada de Fourier (FTIR) e espectroscopia Raman.

As medidas de DRX foram realizadas em um difratômetro Shimadzu (modelo XRD6000) utilizando radiação de $\text{CuK}\alpha$, $\lambda = 1,5418\text{\AA}$ com voltagem de 40kV e corrente de 30mA. As amostras foram analisadas em uma velocidade de passo de $0,5^\circ \text{min}^{-1}$ e em um intervalo de 10° a 70° .

As morfologias foram analisadas em microscópio Tescan (modelo VEJA 3 LMU) operado em 10kV. Junto com o MEV utilizou-se o detector de microanálises por espectroscopia por energia dispersiva (EDS) Oxford (modelo INSCA X-ACT) para verificar os elementos químicos nas amostras.

As medidas de espectroscopia de absorção na região do infravermelho por transformada de Fourier foram realizadas em um espectrômetro PerkinElmer (modelo Spectrum Two), no modo de reflectância total atenuada (ATR) com detector de CsI. Foram realizadas 16 varreduras para cada espectro na região de 500 a 4000 cm^{-1} .

As medidas por espectroscopia Raman foram realizadas em um espectrômetro Horiba (modelo LabRAM HR Evolution), utilizando o software HORIBA Scientific's LabSpec – (LABSpec 6 Spectroscopy Suite), com detector OSD Sincerity. As medidas foram realizadas utilizando o laser de 532 nm, com potência de 50mW.

Para a análise do uso da Nb-MOF e Nb-MOFH como prova de conceito para detecção da alfa-amilase salivar humana em biossensor eletroquímico foram utilizadas as seguintes soluções: solução de ferri/ferrocianeto de potássio ($[\text{Fe}(\text{CN})_6]^{3-}/[\text{Fe}(\text{CN})_6]^{4-} \cdot 3\text{H}_2\text{O}$) 5mol/L, contendo 0,1 mol/L⁻¹ KCl, pH 7,4; como sonda foi usado solução de anti-alfa amilase (anti-HSA) 0.372mg/mL⁻¹; como solução de bloqueio foi a caseína1% e as soluções de saliva e das MOFs tiveram suas concentrações adequadas às plataformas e equipamentos eletroquímicos. A enzima alfa-amilase (AAE-Browin, Łódz, Polônia) e a tripsina DPCC tratada, tipo XI (TXI-Sigma-Aldrich, São Paulo, Brasil), foram utilizadas para o teste de especificidade, sendo preparadas na concentração de 0,250mg/mL⁻¹.

Para a plataforma eletroquímica foram utilizados eletrodos screen-printed (grafite (DPR-110) da DropSens, Asturias, Espanha), (WE), (AE) de Platina e (RE) Ag/AgCl . Todos os experimentos foram realizados na temperatura ambiente (25 ± 2 °C). As análises eletroquímicas foram realizadas pelo equipamento EmStat1 (PalmSens BV, The Netherlands) com *software* PStace 5.4 (PalmSens,Houten, Holanda). A Voltametria Cíclica (CV) foi utilizada para avaliar a condutividade dos eletrodos e a otimização da detecção.

Utilizamos 4 μL da solução da MOF na superfície do WE deixando o tempo necessário para secagem. Em seguida, 80 μL de FF / KCl foram usados para fechar o circuito (WE, RE, AE) e avaliar o sinal eletroquímico. A imobilização do anticorpo 4 μL sob a superfície do WE foi por adsorção do anticorpo policlonal anti-alfa amilase, após a secagem o eletrodo foi lavado com 80 μL de água ultrapura. Em seguida depois de secar foi aplicado 4 μL de caseína, após a secagem e lavagem foi aplicado no WE 4 μL de saliva diluída (HSA-alvo). Depois destas montagens avaliarmos o sinal eletroquímico, empregando 80 μL de FF / KCl

usados para fechar o circuito (WE, RE, AE) e avaliar o sinal eletroquímico.

A análise estatística foi realizada com o *software* OriginPro versão 8.0. Todas as amostras foram analisadas em triplicata para avaliar a repetibilidade e usado como prova de conceito. Em suma, todos os resultados foram considerados significativos a um nível de significância de $P < 0,05$.

Resultado e discussão

As amostras de Nb-MOF foram caracterizadas por DRX a fim de averiguar a formação da fase cristalina e a cristalinidade do material de acordo com o diferente tratamento de cada amostra. Sabe-se que a variação de temperatura e tempo de síntese afetam a cristalinidade dos materiais, tornando o material mais cristalino conforme variação destes parâmetros.

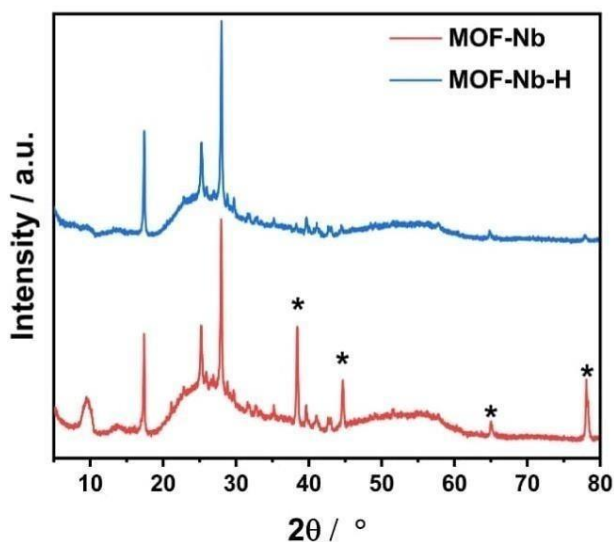


Figura 2 – Difratogramas para amostras de Nb-MOF e Nb-MOFH em diferentes condições de tratamento: Nb-MOF(em vermelho); Nb-MOFH (em azul).

A partir da Figura 2 é possível observar a presença de picos de difração em destaque são caracterizados pelo alumínio, estes picos são provenientes do porta amostra utilizado para análise. As propriedades dos MOFs vêm por conta da alta cristalinidade. O DRX é utilizado para ver essa cristalinidade. Um material com alta cristalinidade apresenta os picos

no DRX bem definidos e finos. As amostras apresentaram perfis semelhantes no DRX, sugerindo que o tratamento das MOFs não culminou em amostras distintas. Os picos observados em $2\theta = 18,2^\circ$, $26,1^\circ$ e $28,4^\circ$ indicam que a estrutura Nb-MOF foi construída com sucesso (Nizamidin *et al.* 2022).

Realizou-se a caracterização das amostras de Nb-MOF por espectroscopia de absorção no infravermelho por transformada de Fourier (FTIR) com o intuito de verificar bandas características, assim como verificar a presença de impurezas no material. A Figura 3 apresenta os espectros FTIR obtidos para as amostras.

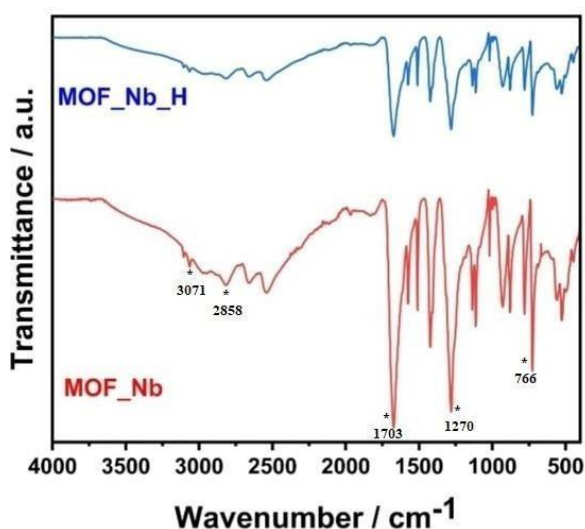


Figura 3 – Espectros de FTIR para as amostras de Nb-MOF e Nb-MOFH em diferentes condições de tratamento: Nb-MOF(em vermelho); Nb-MOFH (em azul).

A partir da Figura 3 é possível observar que os espectros de FTIR para as amostras de Nb-MOF e Nb-MOFH apresentam bandas que se repetem para os materiais sintetizados nas condições trabalhadas.

As bandas características da região de alta frequência $3071\text{--}2858\text{cm}^{-1}$ (vibração de N–H), 1703cm^{-1} (vibração de C=O), 1579cm^{-1} (vibração do esqueleto do anel de benzeno), 1345cm^{-1} (O–C–O), 1270cm^{-1} , (vibração de C–N) e $924\text{--}519\text{cm}^{-1}$ (C–H) representa a construção bem sucedida da estrutura Nb-MOF. (Qi, Z. M., Honma, I., Zhou, H, 2006) (Zang *et al.* 2021) (Choi *et al.* 2021) (Nizamidin *et al.* 2022).

Também foram analisados os reagentes químicos precursores utilizados do processo de síntese das Nb-MOFs, os espectros de FTIR destes precursores e as Nb-MOFs estão

apresentados na Figura 4.

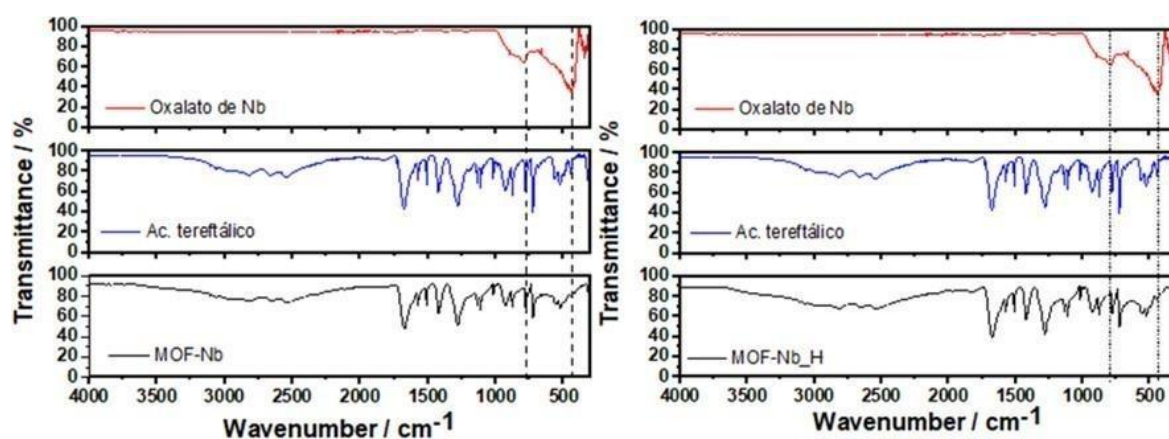


Figura 4: Espectros de FTIR para as amostras de Nb-MOF e Nb-MOFH com os reagentes químicos utilizados na rota de síntese das MOFs.

As bandas presentes da região de menor frequência $500-750\text{cm}^{-1}$ apresentaram modificações e deslocamento, quando comparadas com os reagentes precursores da síntese, nos dando indícios do sucesso na formação da Nb-MOF.

A fim de averiguar a morfologia das Nb-MOF sintetizadas, as amostras foram caracterizadas por microscopia eletrônica de varredura. A Figura 5 apresenta as imagens obtidas por MEV para as amostras.

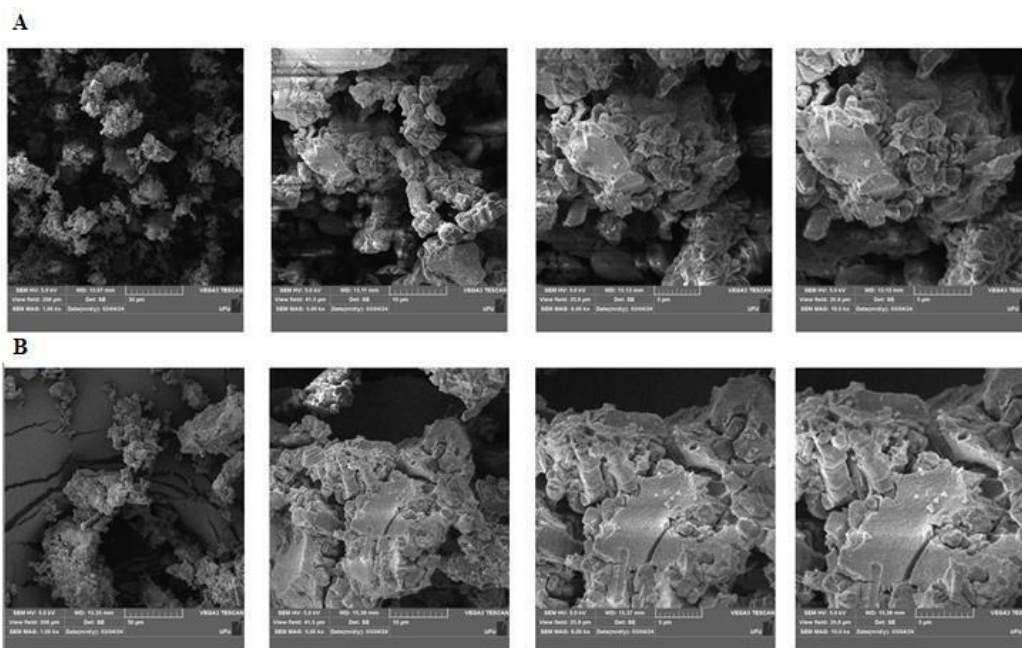


Figura 5 – Imagens de MEV das amostras: (A) Nb-MOF e (B) Nb-MOFH.

A partir da MEV pode-se verificar que as alterações do tratamento de ativação não influenciaram na morfologia das amostras de Nb-MOF e Nb-MOFH, pois, nas duas amostras o material apresenta o formato de blocos com as faces definidas e com a presença de poros.

Além da caracterização por MEV, também foi feita a análise utilizando espectroscopia por energia dispersiva (EDS). O espectro de EDS e o mapa elemental para cada amostra encontram-se nas Figuras 6 e 7.

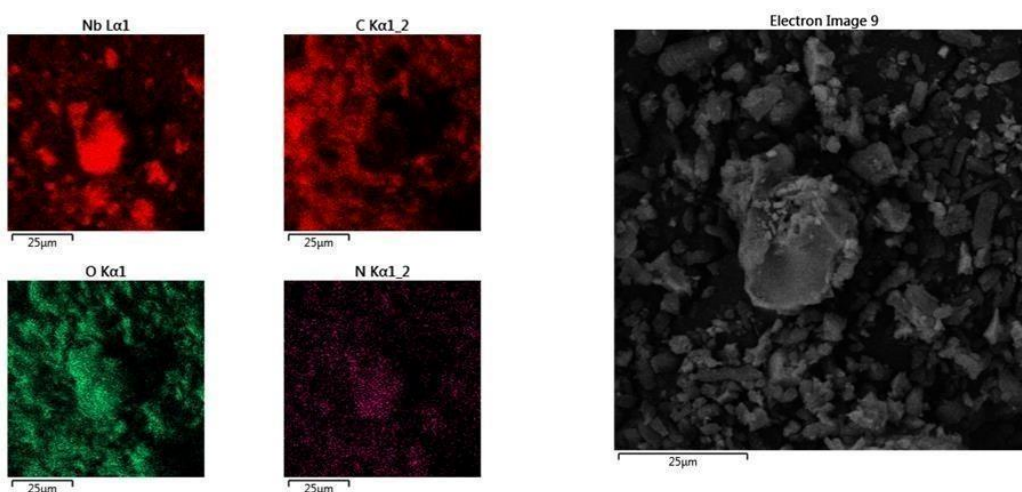


Figura 6 – Mapa elemental para átomos de nióbio (Nb), oxigênio (O), nitrogênio (N) e carbono (C); para amostra de Nb-MOF.

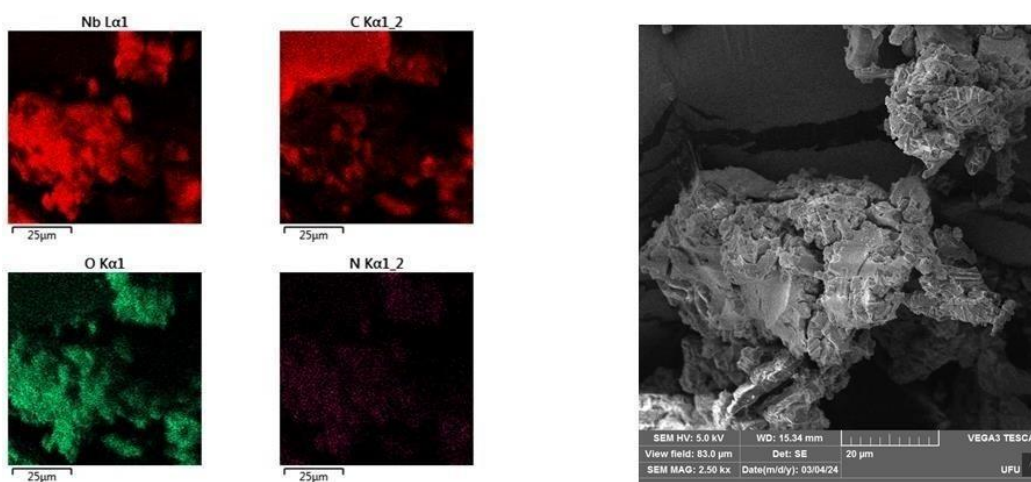


Figura 7 – Mapa elemental para átomos de nióbio (Nb), oxigênio (O), nitrogênio (N) e carbono (C); para amostra de Nb-MOFH.

A partir das Figuras 6 e 7 é possível observar a presença de nióbio, oxigênio, nitrogênio e carbono em todas as amostras sintetizadas. A presença destes quatro elementos já era esperada uma vez que são os constituintes das Nb-MOFs.

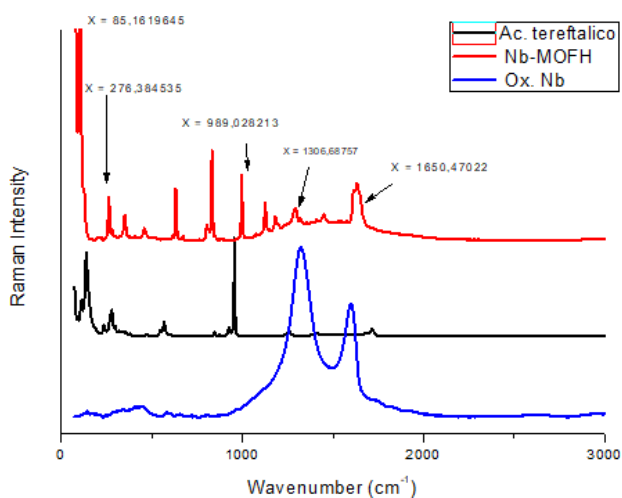


Figura 8: Espectros Raman para ácido tereftálico (em preto), Nb-MOFH (em vermelho) e oxalato de nióbio (em azul).

Analisando as bandas presentes nos espectros Raman da Figura 08 observa-se as bandas características para oxalato de nióbio, ácido tereftálico e da Nb-MOFH. Analisando as bandas características do Nb-MOFH separadamente, observa-se que para a Nb-MOFH existem bandas características em 85, 276, 989, 1306 e 1650 cm^{-1} . A banda em 85 cm^{-1} , indica uma vibração de baixa frequência, que está associada, geralmente, as vibrações de rede ou modos de movimento coletivo em materiais sólidos. Em materiais contendo metais como nióbio, uma banda nessa faixa (abaixo de 100 cm^{-1}) pode indicar vibrações de ligação metal-metal ou interações de redes coordenadas.

Por sua vez, a banda em 276 cm^{-1} que corresponde as vibrações de estiramento ou flexão envolvendo ligações entre átomos de metal e oxigênio, vibrações de flexão Nb-O-Nb ou estiramento Nb-O. Dependendo da geometria de coordenação, essa banda pode estar associada a vibrações de ligação Nb-O ou Nb-ligante. A banda em 989 cm^{-1} ou nesta região (980-1000 cm^{-1}) é observada devido às vibrações de estiramento entre Nb=O (ligação dupla) e também pode estar relacionado a estiramentos Nb-O-Nb, dependendo da estrutura cristalina e do ambiente local do metal. As bandas 1306 e 1650 cm^{-1} , são características de oxalato de nióbio e o aparecimento destas bandas em uma estrutura coordenada dependerão dos ligantes do nióbio.

Como prova de conceito utilizamos as Nb-MOFs para funcionalizar o biossensor de HSA.

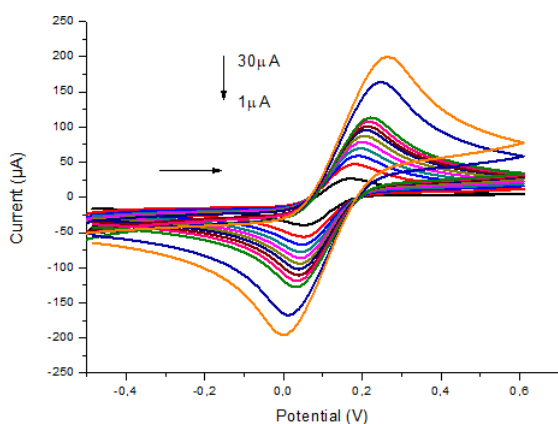


Figura 9: Voltamogramas cíclicos representando a varredura com diferentes variações de corrente.

Avaliamos a diferença de condutividade antes e após a adsorção das Nb-MOF e Nb-MOFH. A figura 10 mostra o gráfico de colunas utilizado para avaliar a condutividade dos eletrodos. Solução eletrolítica indicadora $[\text{Fe}(\text{CN})_6]^{-3/-4}$ e KCl, eletrodo C 110, taxa de varredura = $100,0 \text{ mV} \cdot \text{s}^{-1}$.

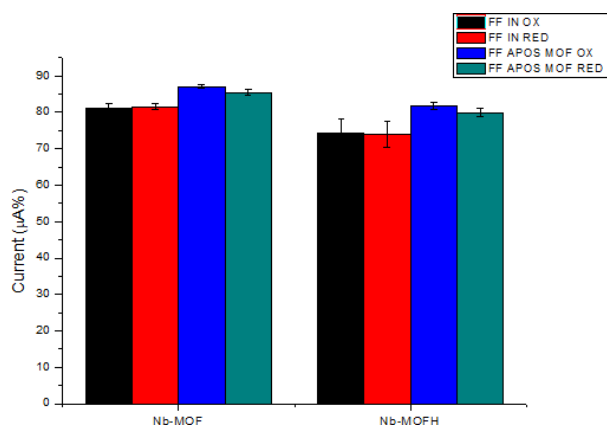


Figura 10: Comparação da diferença de condutividade do eletrodo de grafite antes e após a adsorção das amostras Nb-MOF e Nb-MOFH. As barras de erro representam à média e o desvio padrão (DP) de medições triplicadas para cada condição experimental.

Há maior diferença de condutividade mostrada nos picos de oxidação e redução nos eletrodos com adsorção da Nb-MOFH, reafirmando a necessidade de realizar-se o tratamento após a síntese da MOF. Acredita-se que este tratamento possibilite a

desobstrução dos poros da amostra sintetizada.

Posteriormente, avaliamos a necessidade de se fazer um tratamento na superfície do eletrodo de grafite a fim de melhorar a adsorção das Nb-MOFs no WE. Este tratamento foi realizado com a solução eletrolítica de KCl 0.1M, onde foram realizados 1 ciclo 0,0 e 1,0V (ativação), posteriormente 10 ciclos entre 0.015 e 1.5V (redução) e logo em seguida outro ciclo de ativação nas mesmas condições mencionadas.

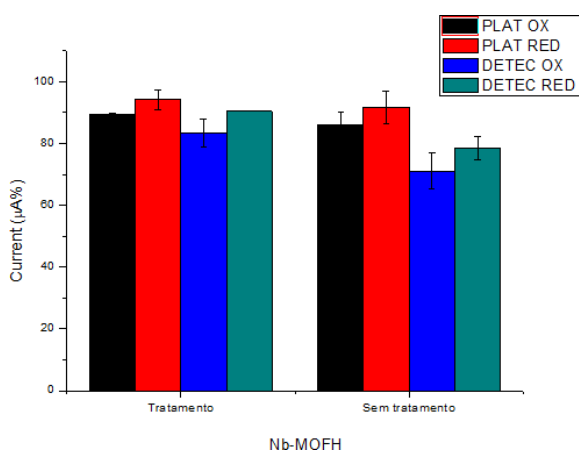


Figura 11: Comparação dos picos de oxidação e redução da Nb-MOFH, no eletrodo de grafite com e sem o tratamento da superfície do eletrodo. As barras de erro representam à média e o desvio padrão (DP) de medições triplicadas para cada condição experimental.

Observa-se maior diferença de condutividade nos picos de oxidação e redução nos eletrodos sem o tratamento da superfície com adsorção da Nb-MOFH.

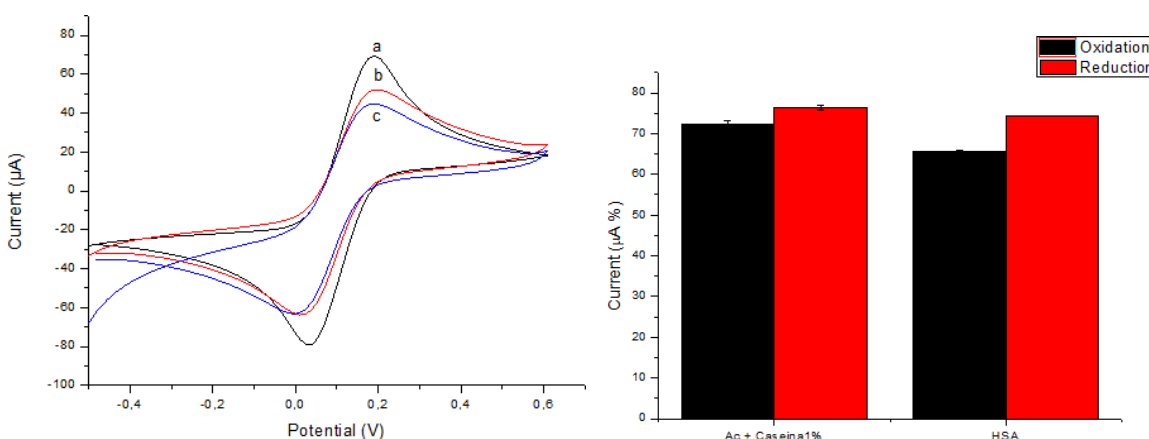


Figura 12: Voltamogramas cíclicos para a sonda redox e gráficos de barras representando dados referentes à detecção de HSA em saliva diluída 1-50.000 em uma plataforma de grafite comercial com adsorção de Nb-MOFH. Ressaltamos que em "a"

representamos o voltamograma após a adsorção o Nb-MOFH em "b" representamos a plataforma eletroquímica consistindo de uma superfície modificada com biomoléculas, como anti-HSA e caseína 1%, neste caso a caseína atua como uma camada de bloqueio, enquanto o anticorpo serve como um sítio de reconhecimento para o analito. Em "c" representamos o analito, neste caso, a HSA, que se liga ao anticorpo na superfície da plataforma eletroquímica, desencadeando uma resposta eletroquímica mensurável, esta resposta é usada para detectar e quantificar a presença da HSA na amostra testada. As barras de erro representam à média e o desvio padrão (DP) de medições triplicadas para cada condição experimental.

O teste de especificidade com a enzima comercial alfa-amilase (AAE) e tratado com tripsina DPCC, tipo XI (TXI), são apresentados na figura 13 ambos foram preparados em $0,25 \text{ mg/mL}^{-1}$. (A) Gráfico de barras representando os cálculos percentuais dos dispositivos desenvolvidos para TXI e AAE. (B) As etapas foram 1. adsorção do Nb-MOFH na superfície do WE, (a); 2. imobilização do anticorpo anti-HSA (1:200) (Ab) (b); 3. reconhecimento de AAE com Ab (Ab-Ag) (c). (C) As etapas foram 1. adsorção do Nb-MOFH na superfície do WE, (a); 2. imobilização do anticorpo anti-HSA (1:200) (Ab) (b); 3. sem reconhecimento da TXI com Ab (Ab-Ag) (c).

Gráfico de barras picos de oxidação e redução, mostrando a resposta eletroquímica do biossensor funcionalizado com Nb-MOFH/ anti-HSA, enzima AAE e TRX para o teste de Solução eletrolítica indicadora $[\text{Fe}(\text{CN})_6]^{-3/4}$ e KCl, eletrodo C110, taxa de varredura = $100,0 \text{ mV} \cdot \text{s}^{-1}$.

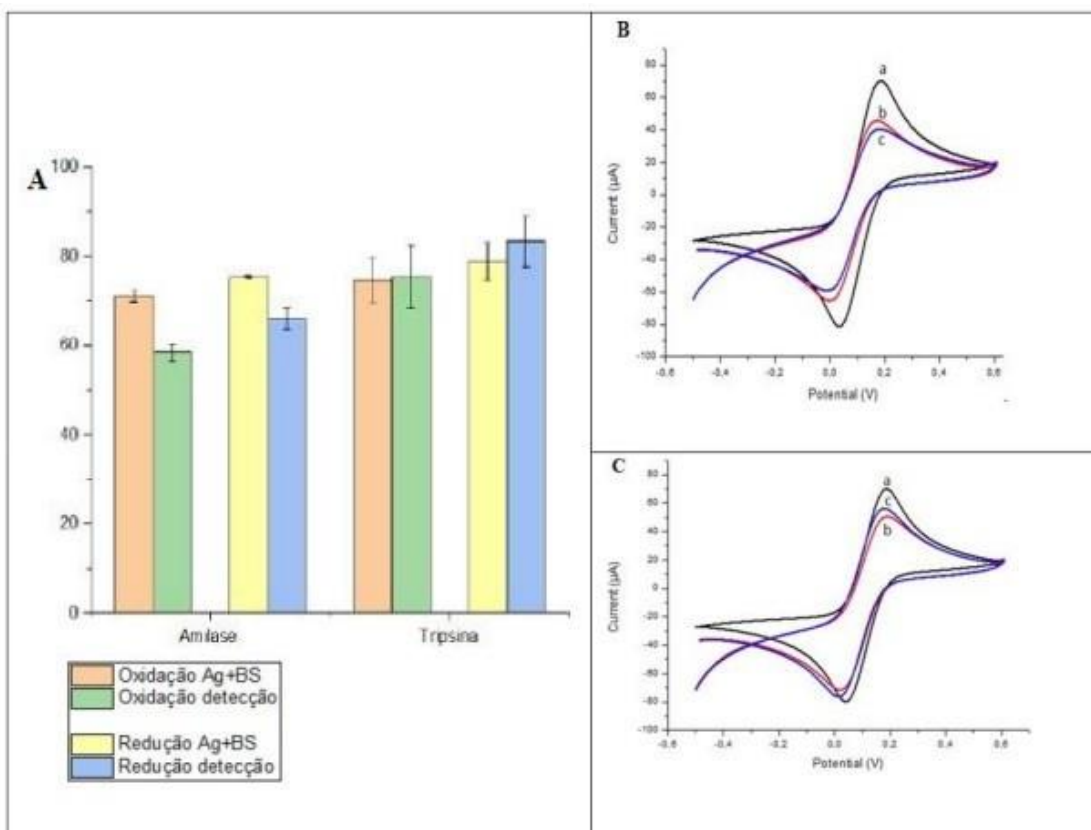


Figura 13: Gráficos de barras e voltamogramas cíclicos para a sonda redox representando dados referentes a especificidade do sensor com Nb-MOFH na detecção da amilase comercial (AAE) e o não reconhecendo da tripsina (TXI).

O par redox, ferrocianeto de potássio/ferricianeto de potássio, atuou eficientemente como indicador na superfície do eletrodo, resultando em uma mudança eficiente da corrente de pico na presença da Nb-MOFH e biomoléculas específicas.

A análise eletroquímica apresentou maior seletividade na presença de Nb-MOFH. Este resultado pode ser explicado porque as proteínas salivares, incluindo a amilase, possuem capacidades de ligação com metais como: Cu^{2+} e Zn^{2+} (Baker *et al.* 2009). Estudos demonstraram que a alfa-amilase possui dois sítios de ligação ao metal, um exclusivamente para Ca^{2+} e outro para Cu^{2+} e Fe^{3+} (Hong *et al.* 2009).

comercial teve a mesma capacidade de reconhecer uma amostra real, confirmando o reconhecimento molecular utilizando uma técnica eletroquímica.

Conclusões

O estudo das propriedades físicas dos nanomateriais é essencial para o desenvolvimento de novas tecnologias. Neste trabalho, confirmamos a formação da Nb-MOF. Partindo do princípio de que a escolha do nanomaterial deve ocorrer a partir da sua interação com todas as moléculas de um sensor, iniciamos as avaliações eletroquímicas que indicaram que a Nb-MOFH apresenta melhores respostas no biossensor eletroquímico.

Nossos resultados mostraram melhora na detecção eletroquímica da HSA em eletrodos funcionalizados com Nb-MOFH, e ainda testes de especificidade e seletividade foram avaliados no reconhecimento Nb-MOFH-Ab-Ag.

Desafiados pelos inúmeros trabalhos em eletroquímica utilizando nanomateriais, avaliamos os resultados obtidos neste trabalho e proporcionaram oportunidades de reflexão com base em evidência.

Os resultados mostraram que o imunossensor produzido apresentou propriedades excitantes, como boa seletividade e sensibilidade. Assim, é uma técnica promissora de detecção molecular da HSA, e estudos posteriores mais avançados desta tecnologia serão necessários para melhores esclarecimentos e elucidações. A fim de uma posterior utilização para determinação de outras biomoléculas.

Referências Bibliográficas

- Almeida, P. F. A., Klinowski, J., Vilela, S. M. F., Tomé, J. P.C., Cavaleiro, J. A. S., Rocha, J. **2012**. Ligand Design for Functional Metal-Organic Frameworks. *Chemical Society Reviews*. 41, 1088-1110. doi: [10.1039/C1CS15055C](https://doi.org/10.1039/C1CS15055C).
- Baker, E. N., Anderson, B. F., Baker, H. M., Haridas, M., Norris, G. E., Rumball, S. V., Smith, C. A. **2009**. Metal and anion binding sites in lactoferrin and related proteins. *Pure Appl. Chem*. V.62, p.1067–1070. doi: [10.1351/pac199062061067](https://doi.org/10.1351/pac199062061067).
- Batten, S. R., Champness, N. R., Chen, X., Martinez, J. G., Kitagawa, S., Öhrström, L., O’Keeffe, M., Suh, M.P., Reedijk, J. **2012**. Coordination Polymers, Metal Organic Frameworks and the Need for Terminology Guidelines; *CrystEngComm*,14: 3001-3004. doi: [10.1039/C2CE06488J](https://doi.org/10.1039/C2CE06488J).
- Choi, J., Yoo, K. S., Kim, D., Kim, J., Othman, M. R. **2021**. Microporous Mo-UiO-66 Metal–Organic Framework Nanoparticles as Gas Adsorbents. *ACS Applied Nano Materials*. 4, 5, 4895–4901. doi: [10.1021/acsanm.1c00444](https://doi.org/10.1021/acsanm.1c00444).

- Deleu, W.P.R., Stassen, I., Jonckheere, D., Amellot, R. Vos, D.E. 2016. Waste PET (Bottles) as a Resource or Substrate for MOF Synthesis. *J. Mater. Chem. A*. v.4, 9519-9525. doi:[10.1039/C6TA02381A](https://doi.org/10.1039/C6TA02381A).
- Di Souza, L., Adhemar, R.F., Torres, M.C.M. 2008. Despolimerização Do Poli (Tereftalato de Etileno) - PET: Efeitos de Tensoativos e Excesso de Solução Alcalina. *Polímeros: Ciência e Tecnologia*, v. 18, n4, p.334-341. doi:[10.1590/S0104-14282008000400013](https://doi.org/10.1590/S0104-14282008000400013)
- Gusmão, K. B., Pergher, S. B. C., Santos dos, E. N. 2017. Um panorama da Catálise no Brasil nos últimos 40 anos. *Química Nova*, v. 40, n. 6, p. 650-655. doi:[10.21577/0100-4042.20170083](https://doi.org/10.21577/0100-4042.20170083).
- Hong, J.H., Duncan, S. E., Dietrich, A. M., O'Keefe, S. F., Eigel, W. N., Mallikarjunan, k. 2009. Interaction of copper and human salivary proteins. *J. Agric. Food Chem* 57:6967-6975. doi:[10.1021/jf804047h](https://doi.org/10.1021/jf804047h).
- Hussain, E., Shahadat, M., Ahtesham, A., Mohamad, N., Ibrahim, M. 2024. Synthesis, characterization, and applications of ambi-functional PANI/GO/MOF-Fe₃O₄ magnetic nanocomposite for removing industrial dye and emerging contaminant. *Separation and Purification Technology* 351: 128052. doi:[10.1016/j.seppur.128052](https://doi.org/10.1016/j.seppur.128052).
- Jiang, H. L., Xu, Q. 2011. Porous Metal-Organic Frameworks as Platforms for Functional Applications. *Chem. Commun.* 47: 3351-3370. doi:[10.1039/C0CC05419D](https://doi.org/10.1039/C0CC05419D).
- Krisbiantoro, P. A., Kuo, T.J., Chang, Y.C., Liao, W., Sun, J. P., Yang, C.Y., Kamiya, Y., Shieh, F. S., Chen, C. C., Wu, K.W. 2024. PET-derived bis(2-hydroxyethyl) terephthalate as a new linker source for solvent-free and hydrothermal synthesis of BDC-based MOFs. *Materials Today Nano*.v. 25: 1-12. doi:[10.1016/j.mtnano.2024.10045](https://doi.org/10.1016/j.mtnano.2024.10045).
- Lopes, O. F., De Mendonça, V.R., Silva, F.B.F., Ribeiro, C. 2015. Óxidos de nióbio: uma visão sobre a síntese do Nb₂O₅ e sua aplicação em fotocatalise heterogênea. *Química Nova*. N.0,1-12. doi:[10.5935/0100-4042.20140280](https://doi.org/10.5935/0100-4042.20140280).
- Nizamidin, P., Yang, Q., Guo, C., Wufuer, A., Yimit, A. Muhammad, T. 2022. Fabrication and Surface Modification of Niobium Metal–Organic Framework Membrane and its Gas Sensing Application. *Advanced Materials Interfaces*. v.9. 1-11. doi:[10.1002/admi.202200742](https://doi.org/10.1002/admi.202200742)
- Oliveira, N.R. 2019. Síntese e caracterização de MOFs à base de ácido tereftálico obtido através do pet e sua utilização na remoção de contaminantes do petróleo. *Dissertação de*

mestrado (Mestrado em Química) - Centro Federal de Educação Tecnológica de Minas Gerais, Belo Horizonte, p. 122.

Qi, Z. M., Honma, I., Zhou, H. 2006. Chemical gas sensor application of open-pore mesoporous thin films based on integrated optical polarimetric interferometry. *Analytical Chemistry*, 78(4), 1034-1041. doi:[10.1021/ac051380f](https://doi.org/10.1021/ac051380f).

Zhang, Y., Lv, S., Jiang, L., Liu, F., Wang, J., Yang, Z., Wang, B., You, R., Wang, C., Yan, X., Sun, P., Gao, Y., Liang, X., Lu, G. 2021. Room-Temperature Mixed-Potential Type ppb-Level NO Sensors Based on K₂Fe₄O₇ Electrolyte and Ni/Fe-MOF Sensing Electrodes. *ACS Sensors*. 6. 12. 4435–4442. doi: [10.1021/acssensors.1c01838](https://doi.org/10.1021/acssensors.1c01838).

ANEXO A – Demais trabalhos publicados durante o doutorado

We are IntechOpen,
the world's leading publisher of
Open Access books
Built by scientists, for scientists

5,900

Open access books available

145,000

International authors and editors

180M

Downloads

154

Countries delivered to

Our authors are among the

TOP 1%

most cited scientists

12.2%

Contributors from top 500 universities

Selection of our books indexed in the Book Citation Index
in Web of Science™ Core Collection (BKCI)

Interested in publishing with us?
Contact book.department@intechopen.com

Numbers displayed above are based on latest data collected.
For more information visit www.intechopen.com



Sensor Surface Design with NanoMaterials: A New Platform in the Diagnosis of COVID-19

Eliete A. Alvin, Anna V.B. e Borges, Rhéltheer de P. Martins, Marcela R. Lemes, Rafaela M. Barbosa, Carlo J.F. de Oliveira, Diógenes Meneses, Bruno G. Lucca, Noelio O. Dantas, Virmondes R. Junior, Renata P.A. Balvedi, Fabiane C. de Abreu, Marcos V. da Silva and Anielle C.A. Silva

Abstract

Mass testing for COVID-19 is essential to defining patient management strategies, choosing the best clinical management, and dimensioning strategies for controlling viral dissemination and immunization strategies. Thus, it is of utmost importance to search for devices that allow a quick and reliable diagnosis of low cost that can be transposed from the bench to the bedside, such as biosensors. These devices can help choose the correct clinical management to minimize factors that lead to infected patients developing more severe diseases. The use of nanomaterials to modify biosensors' surfaces to increase these devices' sensitivity and their biofunctionality enables high-quality nanotechnological platforms. In addition to the diagnostic benefits, nanotechnological platforms that facilitate the monitoring of anti-SARS-CoV-2 antibodies may be the key to determining loss of protective immune response after an episode of COVID-19, which leads to a possible chance of reinfection, as well as how they can be used to assess and monitor the success of immunization strategies, which are beginning to be administered on a large scale and that the extent and duration of their protection will need to be determined.

Therefore, in this chapter, we will cover nanomaterials' use and their functionalities in the surface design of sensors, thus generating nanotechnological platforms in the various facets of the diagnosis of COVID-19.

Keywords: COVID-19, SARS-CoV-2, nanotechnological platforms, nanomaterials, biosensors, diagnosis, sensor surface design

1. Introduction

SARS-CoV-2 is a virus in the coronavirus family, discovered in December 2019 in Wuhan, China, and the cause of COVID-19 [1]. Coronaviruses (CoV) are RNA viruses and can cause anything from the common cold to more serious diseases with neurological, gastrointestinal, and pulmonary involvement [2]. They are zoonotic viruses;

Biotechnology to Combat COVID-

that is, they can be transmitted between animals and people due to their ability to

recombine their viral proteins between coronaviruses of different hosts [3].

COVID-19 was defined as Pandemic on March 11, 2020 (1), and by February 1, 2021, there are already 103,221,369 individuals infected worldwide, and the number of global deaths already exceeds 2,232,563 [4]. Before SARS-CoV-2, two other CoVs causing a pandemic disease were identified: the first was SARS-CoV in 2002, originating in Foshan (China), which caused Severe Acute Respiratory Syndrome (SARS); the second was MERS-CoV, which originated in the Arabian Peninsula in 2012, causing the Middle East Respiratory Syndrome (MERS) [5].

A significant bottleneck in COVID-19 is mass diagnosis. The real-time reverse-transcription polymerase chain reaction (RT-PCR) is the “gold standard” method for demonstrating the presence of SARS-CoV-2. This diagnosis is reliable; however, most countries have suffered from a lack of supplies and equipment and its high cost. IgM and IgG antibodies can be detected in the serum of patients with COVID-19, where their monitoring can indicate recent or late infection and the duration of the post-infection protective immune response.

The development of easy-to-use alternative platforms is encouraged with specific attention paid to sensitivity and simplicity to specifically detect targets at a very low concentration, in about minutes, enabling portable on-site screening upon further optimizations of the detection limit. However, the accuracy of these techniques depends on several factors; variations in these factors might significantly lower the sensitivity of detection.

Nanomaterials can be applied in several types of sensors due to their physical and chemical properties, making them possible to detect by colorimetric, fluorescence, magnetism, surface plasmon resonance, and electrochemical [6–10]. In electrochemical sensing, the conductive nanomaterials are interesting for application due to their well-known ability to improve the catalytic activity, the electron transfer speed, and the conductivity of the sensors. Furthermore, the superficial area and amplify the analytical signal can be increased by deposition of nanomaterials over electronic surfaces, enhancing the sensitivity regarding target analytes' detection. Therefore, the group has been working with several nanomaterials to develop sensors.

Therefore, in this book chapter, we describe case reports and proof-of-concept for a simple, label-free electrochemical sensor for the fast and direct detection of SARS-CoV-2 through the detection of the specific probe. Early and widespread testing has proven to reduce mortality rates and improve contact tracing. However, the value of testing is directly linked to the availability and accuracy of diagnostic tests as concerns grow. Additionally, we have demonstrated in this work the possibility of a biorecognition element between the target concentration and the viral load exploring different electrode materials and redox markers allows for improved sensor properties with higher effectiveness than the commercially available assay or traditional diagnostic methods.

2. Diagnosis of COVID-19: the old and the gold

Coronaviruses infect human cells mainly by binding proteins from viral spikes (spike proteins) to molecules of the angiotensin-converting enzyme 2 (ACE2), [11] widely expressed in human organs and tissues, such as nasal, bronchial epithelial cells, and pneumocytes. After entering the cell, viral replication occurs and the host cell's subsequent death, whether epithelial, endothelial, or immune cells [12].

Due to the increase in viral replication, the epithelial-endothelial barrier's integrity is compromised, accentuating the inflammatory response, causing edema

Sensor Surface Design with NanoMaterials: A New Platform in the Diagnosis of COVID-19
DOI: <http://dx.doi.org/10.5772/intechopen.97056>

and inflammatory infiltrates. Furthermore, it compromises coagulation pathways, increasing fibrin degradation products and alterations in leukocytes

and red blood cells. Together with the inflammatory infiltrate, the resulting edema contributes to the ground-glass opacities seen in imaging studies and too low oxygenation [13].

Symptoms and clinical evolution depend on the triad: virus strain, host immunity, and pre-existing conditions, known as comorbidities, such as hypertension, obesity, diabetes, cardiovascular disease, chronic lung disease, chronic kidney disease, and malignancies [14]. Symptoms range from the most common in flu-like conditions, such as fever, cough, and shortness of breath, nausea, diarrhea, loss of smell and taste, and more severe symptoms such as pneumonia leukopenia, kidney failure, myocarditis, meningitis, and thromboembolic events [15].

The immune response against COVID-19 has been extensively investigated and is directly related to clinical evolution. The presence of lymphopenia and increased production of chemokines and proinflammatory cytokines have been demonstrated in patients with COVID-19, especially in the most severe cases, which can worsen tissue damage [16]. Serum levels of chemokines (IL-8) and proinflammatory cytokines (TNF- α , IL-1, IL-6, IFN- γ , IP-10, and MCP-1) are found in greater quantities in patients with COVID-19 severe when compared with individuals with mild disease. This fact indicates that the cytokine storm is associated with the severity of the disease and adverse outcomes, suggesting a possible role of hyperinflammatory responses in the pathogenesis of COVID-19 [16, 17].

Studies on the humoral immune response demonstrate that antibodies, such as IgA, IgM, and IgG against SARS-CoV-2, appear on the first day after the onset of symptoms [18, 19]. IgM levels appear on days 0 to 7, increasing on days 8 to 14 and reaching a plateau, while IgA levels increased from days 0 to 14, whereas IgG levels were detected on days 0 to 7, increased on days 8 to 14, continued to increase until the 15th to the 21st and reached a plateau on the 21st [18]. This kinetics of antibody levels indicates a rapid and almost simultaneous response of these three isotypes during the first weeks of infection by SARS-CoV-2, IgA and IgG remain with higher titers for a longer time when compared to IgM [20, 21].

The amount of antibodies in samples from patients with COVID-19 is dependent on the number of viral RNA present: the lower the viral load, the lower the level of antibodies present, and the severity of clinical evolution [19–21]. Initial data indicate a lower concentration of anti-SARS-CoV-2 antibodies in asymptomatic patients, but more quickly, while in mild symptomatic ones, there is a slower but more continuous production. Serious patients have high levels of antibodies, mainly IgA and IgG. However, there are still gaps about whether specific humoral and cellular immune memory persist and for how long [20]. Despite these limitations in understanding the long-term humoral immune response, the determination of IgA, IgM, and IgG antibodies are widely used in laboratory tests for the detection of COVID-19. Early diagnosis also allows the infected patient to have faster access to medical care and increases their chances of a better prognosis. It will enable the initiation of treatment when the viral load is in low concentrations.

Antibody determination is also important to monitor patients who have been vaccinated since immunization stimulates the immune system's production without having to be infected [22]. Results about vaccines against COVID-19 showed that vaccinated patients increased the production of specific antibodies and their affinity to levels similar to those observed in patients who recovered from COVID-19 [23–25]. Data show that a standardized quantification/determination of antibody levels may be sufficient to monitor vaccinated patients and estimate the quality and duration of this protection [24].

To date, quantitative real-time reverse-transcription polymerase chain reaction (RT-PCR), qRT-qPCR assay is the gold standard for the early detection of virus

Figure 1.

Major steps of qRT-PCR as a diagnostic tool at COVID-19 (1) A patient suspected of COVID-19 undergoes collection of cells infected with SARS-CoV-2 through a nasopharyngeal swab. (2–3) Viral RNA is extracted and purified. The enzyme reverse transcriptase converts RNA into cDNA.

(major steps presented in **Figure 1**), but the CRISPR–Cas12-based lateral flow, Immunochromatographic, ELISA, loop-mediated isothermal amplification (LAMP) and other techniques has been developed and applied to screening or to confirm positive COVID-19 patients allowing prompt clinical and quarantine decisions this infection (**Table 1**).

To minimize the cost and logistical problems of sample collection and diagnostics, rapid diagnostic systems based on classical methodological approaches, such as immunochromatography, were quickly implemented in the detection of SARS-CoV-2 antigens or antibodies produced against it. However, the accuracy of these techniques depends on several factors. The bioavailability of the researched molecule, as viral genetic material, viral antigens, and various subclasses of antibodies, the stability of these biomolecules to the procedures of sample collection and transport to the diagnostic platforms, the possibility of storage for later evaluation are significant bottlenecks that have impaired mass testing, especially in developing countries and variations in these factors might significantly lower the sensitivity of detection. The degree of reliability is uncertain in many of them, and implementing a faster and accurate diagnosis system is essential to monitor the disease and define policies to control viral spread.

Biosensors are one of the most popular types of point-of-care devices in various diagnostics areas, which offer several advantages such as the low cost, the capability of miniaturization, and high sensitivity and selectivity. The transposition of the molecular and immunological diagnosis to miniaturization platforms like point-of-care systems implies a drastic reduction in the amount of sample needed, increases specificity, reliable measurements in real-time, and portability. The development of easy-to-use alternative platforms is encouraged with specific attention paid to sensitivity and simplicity to detect targets at a very low concentration in about minutes, enabling portable on-site screening upon further optimizing the detection limit.

Detection	Sensitivity	Specificity	LOD of	Biom.	Biom.	Methodology	Detection	Nanomaterials	Database	References
RT-dPCR	90	100	2 copies/ reaction μL	Primers	Viral RNA	Real - time Transcripta to Reverse Digital PCR	—	—	P/S/WS	[30]
RT-LAMP	90–100	Low	100 copies/ μL	Primers	Viral RNA	Isothermal amplification of the Transcript reversed	30–40	—	P/S/WS	[29, 31, 32]
CRISPR-cas12	95–100	100	10–100 copies/ μL	gRNA	Viral RNA	gRNA binds to the target segment making precise cutting	45–75	—	P/S/WS	[33]
RT-RPA	98	100	7.659 copies/ μL	Primers	Viral RNA	Real-time Transcript to Reverse Recombinase Polymerase Amplification	< 20	—	P/S	[34]
ELISA	86–100 *	89–100	—	Anti-antibody IgM	IgM	Indirect	60–300	—	P/S/WS	[31]
ELISA	86–100 *	89–100	—	Anti-antibody IgG	IgG	Indirect	60–300	—	P/S	[35]
ELISA	*	100	—	Antibody	Ag	Sandwich	60–300	—	P/S/WS	[31]
Lateral flow immunoassay	60–80	85–100	—	Ag	IgM	Immunoassay/Quick Test	2–20	—	P/S/WS	[31]

Detection type	Sensitivity %	Specificity %	LOD	Biom. of the probe	Biom. target	Methodology	Detection time (m)	Nanomaterials	Database	References
Lateral flow immunoassay	60–80	85–100	—	Ag	IgG	Immunoassay/Quick Test	2–20	—	P/S/WS	[31]
Lateral flow immunoassay	91.2 Swab 60.1 Sample solution	100	—	Antibody	Ag	Immunoassay/Quick Test	15–30	—	P/S/WS	[31, 36]
Chimioluminescence	82–97	75–87	—	Ag	IgM	Immunoassay/ Chemiluminescence	30–60	Magnetic microsphere	P/S/WS	[37, 38]
Chimioluminescence	82–97	75–87	—	Ag	IgG	Immunoassay/ Chemiluminescence	30–60	Magnetic microspheres	P/S/WS	[38, 39]

LOD: limit of detection, RPA: Recombinase Polymerase Amplification, Database: Pubmed (P), Scopus (S), and Web of Science (WS).

*Variable sensitivity according to kit and sample collection day.

Table 1.

Comparison of methodologies applied to the diagnosis of (SARS)-CoV-2.

An overview of some methodologies applied to the diagnosis of (SARS)-CoV-2 is presented in **Table 1**. The ELISA-based test was used to validate the antibody-antigen interaction, or RT-PCR was used to validate the primer, particularly the complexity of the assays during inventory shortages, while cyclic voltammetry, electrochemical impedance spectroscopy, differential pulse voltammetry was used to characterize the electrode functionalization.

Multi sensors, lateral flow tests, mobile biosensors, and wearable biosensors are critical parts for precision medicine in COVID-19. Russell, S.M. et al., defined these biosensors' ideal characteristics using some prototypes from recent literature as examples [40]. Multi sensors, lateral flow tests, mobile biosensors, and wearable biosensors are crucial parts for precision medicine in COVID-19. We propose the ideal characteristics of these biosensors using some prototypes from recent literature as examples. Multi sensors, lateral flow tests, mobile biosensors, and wearable biosensors are crucial parts for precision medicine in COVID-19.

In his work, Fukumoto, T. et al. 2020 has developed a fast, easy to use, and inexpensive diagnostic method that is needed to help control the current outbreak of the new coronavirus based on microfluidic microdevices. A new detection kit - the 2019 Novel Coronavirus Detection Kit (nCoV-DK) - cuts detection time in half, eliminating RNA extraction and purification steps. The nCoV-DK test effectively detects SARS-CoV-2 in all types of samples, including saliva, while reducing the time required for detection and risk of human error [41].

Laghrib, F. et al., showed the leading current trends and strategies in diagnosing n-SARS-CoV-2 based on emerging and traditional assessment technologies for continuous innovation. Addressing recent biosensors trends to build a fast, reliable, more sensitive, accessible, friendly system with easily adaptable n-SARS-CoV-2 detection and monitoring technology [42]. Overall, we address and identify evidence from research that supports biosensors' use based on the premise that screening people for n-SARS-CoV-2 is the best way to stem its spread. The detection and notification of infectious pathogens in a fast, sensitive, and specific way is essential for managing the patient and surveillance of outbreaks. With their ability to diagnose in real-time with the high specificity of a low concentration sample, biosensors are much more reliable than the rapid test for coronavirus detection.

The use of nano biosensors has been considered the most promising approach for detecting new n-SARSCoV-2 coronavirus disease. Meanwhile, the current work has also tried to improve biosensors' detection sensitivity, simplicity, and performance.

Hui, X. et al. 2020, showed in his work, G quadruplex-based Biosensor: A potential tool for SARS-CoV-2 detection to discover additional advantageous attributes of G-quadruplex as potential to be used in new biosensors, such as ligand binding enhanced and unique folding properties [43]. The newly developed G-quadruplex biosensors include electrochemical and optical biosensors that have shown better performance with potential applications with a wide detection range and a broad spectrum of pathogens SARS-CoV-2, the causative agent of COVID-19 disease.

G-quadruplex is a non-canonical nucleic acid structure formed by the folding of guanine-rich DNA or RNA.

3. Platform with nanomaterials in the diagnosis of COVID-19: a brave new world

Biosensors are analytical devices that incorporate a biological recognition element capable of detecting the presence, activity, or concentration of the sample under analysis connected to a transducer. This biological element can be a

Sensor Surface Design with NanoMaterials: A New Platform in the Diagnosis of COVID-19

micro-organism, an antibody, oligonucleotides, lectins, biomolecule enzymes that can interact with the target substrate. About the transducer, it can be an electrode, fiberoptic, or oscillating quartz [42, 44]. Thus, biosensors are one of the most popular types of point-of-care devices in various areas of diagnostics, which offer several advantages such as low cost, the capability of miniaturization, and high sensitivity and selectivity.

Immunosensors are analytical devices of the biosensor class, which detect and transmit information regarding biochemical changes involving integrating a biological element with an electronic interface [45, 46]. This integration can convert a biological signal into an electrical response that is proportional to the concentration of the analyte. Thus, these biosensors can recognize a specific antibody or antigen by forming an antigen–antibody immunocomplex. The recognition event is detected and converted, through a transducer, to a measurable signal (such as electrical current, for example). The primary transducers used in immunosensors are electrochemical, optical, and piezoelectric. Therefore, the incorporation of specific nanomaterial can be intensified by improving the biosensor's sensitivity and versatility.

Genosensors can also be used, a specific type of biosensor based on nucleic acid chemistry phenomena, such as the hybridization process [47]. Nucleic acids have been widely used in the development of biosensors for drug detection, identification of pathogenic microorganisms and other biological substances, and the diagnosis of diseases. The sensory technique through hybridization involves the

immobilization of an oligonucleotide probe on the surface of a transducer and subsequent sensor exposure to a sample containing the complementary sequence (target oligonucleotide) with consequent hybridization.

Complementary DNA (cDNA) is a DNA synthesized from a messenger RNA molecule in a reaction catalyzed by the enzyme reverse transcriptase. Thus, the incorporation of nanomaterials on the biosensor's surface ensures the enhancement of the electrochemical response.

Our group has been demonstrating through publications and patents expertise in the development of nanomaterials with specific properties, such as increased sensitivity of some devices, biocompatibility, and low genotoxicity, essential properties in developing nanotechnological platforms [48–53]. Toxicity is an important parameter in nanomaterials, but depending on synthesis methodologies it is possible to decrease toxicity. For example, Silva et al. demonstrated some toxicities of nanomaterials, some influenced by the crystalline phase, composition or type of material [54–61]. In relation to quantum dots, synthesis methodologies were developed, making it possible to increase cellular viability and specificity aiming at several applicability as biological probes [52, 53, 62–68].

The development of artificial intelligence software enables more accurate detection and quantification and low-cost analytical platforms [69, 70]. These nanotechnological platform [71] s can be used in large-scale production, with low cost and low consumption of samples and reagents [6, 72].

High-quality, low-cost nanotechnological platforms based on the detection of anti-SARS-CoV-2 antibodies may be the key to defining groups already exposed to the disease, even if asymptomatic, that have a potentially protective immune response, a crucial factor for delimitation priority immunization groups. Besides, we can determine the loss of protective immune response after an episode of

COVID-19, which leads to a possible chance of reinfection. Some advantages are the amount of sample of interest, in the order of μL , simultaneous analysis of several analytes in the same device and miniaturization, being portable, light, and easy to use the equipment. Also, nanotechnological platforms can be used to assess and monitor the success of immunization strategies, which should soon begin to be administered on a large scale, and the extent and duration of their protection will

DOI: <http://dx.doi.org/10.5772/intechopen.97056>

Several diagnostic methods have been reported, aiming at biomedical applications, especially in the diagnosis of covid-19, to detect the coronavirus in clinical, research, and public health laboratories. Based on biosensors for SARS-CoV-2, diagnostic methods presented have analytical performance and response times ranging from a few minutes to several hours, which make them promise for practical use in health care points, showing as a strong ally for control of endemics and pandemics.

An overview of current efforts to improve point-of-care diagnostic systems based on biosensors using different nanomaterials at COVID-19 is presented in **Table 2**.

Currently, diverse electrochemical biosensors have been lately developed for the detection of the SARS-CoV-2 using modified electrodes with metallic nanoparticle or nano-islands or nanostars, carbon nanofiber (CNF), using inorganic quantum dots, zinc oxide nanowires (ZnO NWs) or nanorods, bimetallic nanoparticles, Graphene Oxide (GO) nanosheet and other modifications show in **Table 2**. These nanomaterials showed excellent applications in biosensors because of their ease of functionalization, large surface area, stability, on the stable immobilization of probe molecules, the blocking reagent to minimize nonspecific binding, high electronic conductivity (accelerate the electron transfer), high carrier/charge mobility, and strong adsorption capability that increase the sensitivity of electrochemical platform due to their excellent unmatched properties followed by enhancement in the electrochemical response toward the selective detection of SARS-CoV-2.

Vadlamani, B S. et al., the synthesis of a TiO₂ functionalized with cobalt but susceptible electrochemical sensor based on nanotubes (Co-TNTs) for rapid detection of SARS-CoV-2 using peak detection (binding domain receptor (RBD)) present on the virus surface [83]. A simple, low-cost, one-step electrochemical anodization route was used to synthesize TNTs, followed by an incipient wetting method for cobalt functionalization of the TNT platform, which was connected to a potentiostat for data collection. This sensor specifically detected the S-RBD protein from SARS-CoV-2, even at very low concentrations (range 14 to 1400 nM (nanomolar)). Besides, our sensor showed a linear response in the detection of viral protein in the concentration range. Thus, our Co-TNT sensor is highly effective in detecting the SARS-CoV-2 S-RBD protein in approximately 30s.

Cuy and Zhou, 2019, showed in their review work that timely detection and diagnosis are urgently needed to guide epidemiological measures, infection control, antiviral treatment, and vaccine research [86]. In this review, biomarkers/indicators for diagnosis of coronavirus 2019 disease or detection of severe acute respiratory syndrome coronavirus 2 in the environment are summarized and discussed. However, antibody detection methods can be combined with real-time quantitative polymerase reverse transcriptase chain reaction to improve diagnostic sensitivity and specificity and boost vaccine research significantly. The deep throat saliva and induced sputum are desired for the RT-qPCR test or other early detection technologies. The ultra-sensitive and specific laboratory diagnostic method and portable devices are essential to control the rapidly evolving COVID-19 pandemic associated with SARS-CoV-2. Currently, computed tomography, RT-qPCR, and LFICS based on the colloid Au NPs (colloidal gold method) have been developed.

Based on the table results, we can verify that the biosensors that showed the best sensitivities are using carbon-based materials due to their conductive properties, metallic oxides (ZnO and TiO₂) with supercapacitor properties, and nanocomposites (containing the capacitive and metallic systems).

In nanomaterials, the effects of size, morphology, and chemical structures have a strong influence on the optical, electrical, and magnetic properties. Thus, the tuning of these parameters allows maintaining the same material and intensifying the biosensors' responses. Another critical parameter is the

Detection type	Sensitivity %	Specificity %	LOD	RSD %	Biom. of probe	Biom. target	Methodology	Detection time (m)	Nanomaterials	Database	References
Electrochemical biosensor	—	—	—	—	cRNA	Viral RNA	Genosensors	—	—	P/S	[73]
Electrochemical biosensor	—	—	1 fg/mL	—	Antibodies with 1-pyrenobutyric acid N-hydroxysuccinimide	Ag. Protein S	Field effect transistor FET	< 4	Grafeno leaves	P/S/WS	[74]
Electrochemical biosensor	—	—	—	—	Ag. Protein S	Antibody	Impedance Spectroscopy	—	Polyethylene terephthalate	P/S/WS	[75]
Electrochemical biosensor	Lowest PCR	—	20 ng/mL	—	Antibody Anti- Protein S	Ag. Protein S	Impedance Spectroscopy/ Cyclic voltammetry/ Square wave voltammetry	45	Graphene layer/1-Pyrene butyric acid N-hydroxysuccinimide ester linker (PBASE)	P/S/WS	[76]
Electrochemical biosensor	100	90	1 ng/mL	4.2 for IgG and 3.3 for IgM	Ag. Protein S	IgM/IgG Antibodies	Paper platform	30	—	P/S	[77]
Ultra- sensitive	High	High	3 aM	—	cDNA	Viral RNA	Differential pulse	181	Modified SPCE	P/S/WS	[78]

Detection type	Sensitivity %	Specificity %	LOD	RSD %	Biom. of probe	Biom. target	Methodology	Detection time (m)	Nanomaterials	Database	References
Electrochemical biosensor	High	High	6.5 pfu/mL	—	Antibody Anti-Protein S and N	Ag. Protein S and N in saliva	Immunosensor/ Differential pulse voltammetry	30	Magnetic nanoparticle/Black carbon	P/S/WS	[80]

nanomaterials, several biosensors using more than one type of nanomaterials to further improve sensitivity. Thus, unfortunately, this systematic study of the literature in biosensors does not exist, being difficult to compare the sensitivity properties using different materials and nanocomposites.

4. Conclusion

Therefore, this chapter showed use of systems in diagnosis COVID-19 and how the nanomaterials may enable an improvement in sensitivity when being incorporated in the surface design of sensors, thus generating nanotechnological platforms. The functional improvement of biosensors using nanomaterials has undoubted benefits, both from the point of view of biological samples, ease of technical execution, better distribution and application logistics and better cost-benefit, being able to direct a whole new generation of rapid diagnoses easily transposable to combat other human diseases. These nanotechnological platforms could be the revolution for the mass diagnosis of COVID-19, without implying an increase in investments since it is a low-cost diagnostic proposal. In this way, they can be immediately translated into clinical practice and used in all parts of the health chain used to combat COVID-19, given its simplicity of use, biosafety, and low cost. The use of nanotechnology to modify diagnostic platforms has a special impact as they generate patents, strengthen technology, and arouse worldwide interest for their technological robustness, which may impact the attraction of resources to countries through the export of these or other forms of sharing that be advantageous.

Acknowledgements

This work was supported by grants of CNPq, CAPES, FAPEAL, and FAPEMIG.

Conflict of interest

The authors declare no conflict of interest.

IntechOpen

Author details

Eliete A. Alvin^{1,2,3}, Anna V.B. e Borges⁴, Rhéltheer de P. Martins⁵,
Marcela R. Lemes⁴, Rafaela M. Barbosa⁴, Carlo J.F. de Oliveira⁴, Diógenes Meneses³,
Bruno G. Lucca⁶, Noelio O. Dantas¹, Virmondes R. Junior⁴, Renata P.A. Balvedi⁵,
Fabiane C. de Abreu³, Marcos V. da Silva⁴ and Anielle C.A. Silva^{1,2*}

1 Laboratory of New Nanostructured and Functional Materials, Physics Institute, Federal University of Alagoas, Maceió, AL, Brazil

2 Programa de Pós-Graduação da Rede Nordeste de Biotecnologia (RENORBIO), Federal University of Alagoas, Maceió, AL, Brazil

3 LEMAN, Institute of Chemistry and Biotechnology, Federal University of Alagoas, Maceió, AL, Brazil

4 Department of Microbiology, Immunology and Parasitology, Institute of Biological and Natural Sciences, Federal University of Triângulo Mineiro, Uberaba, MG, Brazil

5 Federal University of Triângulo Mineiro, Iturama, MG, Brazil

6 Institute of Chemistry, Federal University of Mato Grosso do Sul, Campo Grande, MS, Brazil

*Address all correspondence to: acalmeida@fis.ufal.br

© 2021 The Author(s). Licensee IntechOpen. This chapter is distributed under the terms of the Creative Commons Attribution License (<http://creativecommons.org/licenses/by/3.0>), which permits unrestricted use, distribution, and reproduction in any medium, provided the original work is properly cited.

‘Biotechnology to Combat COVID-19’ is a collaborative project with Biotechnology Kiosk

References

- [1] Organization, W.H. Novel Coronavirus (2019-nCoV) Situation Report – 1 2020.
- [2] Benvenuto, D.; Giovanetti, M.; Ciccozzi, A.; Spoto, S.; Angeletti, S.; Ciccozzi, M. The 2019-new coronavirus epidemic: Evidence for virus evolution. *J. Med. Virol.* **2020**, *92*, 455-459, doi:10.1002/jmv.25688.
- [3] Ji, W.; Wang, W.; Zhao, X.; Zai, J.; Li, X. Cross-species transmission of the newly identified coronavirus 2019-nCoV. *J. Med. Virol.* **2020**, *92*, 433-440, doi:10.1002/jmv.25682.
- [4] Hopkings, J. COVID-19 dashboard by the Center for Systems Science and Engineering (CSSE) at Johns Hopkins University (JHU) 2020.
- [5] Cui, J.; Li, F.; Shi, Z.L. Origin and evolution of pathogenic coronaviruses. *Nat. Rev. Microbiol.* 2019, *17*, 181-192.
- [6] de França, C.C.L.; Meneses, D.; Silva, A.C.A.; Dantas, N.O.; de Abreu, F.C.; Petroni, J.M.; Lucca, B.G. Development of novel paper-based electrochemical device modified with CdSe/CdS magic-sized quantum dots and application for the sensing of dopamine. *Electrochim. Acta* **2021**, *367*, doi:10.1016/j.electacta.2020.137486.
- [7] da Silva, M.P.G.; Candido, A.C.L.; de Araújo-Júnior, J.X.; Silva, A.C.A.; Dantas, N.O.; de Aquino, T.M.; de Abreu, F.C. Evaluation of the interaction of a guanilylhydrazone derivative with cobalt ferrite nanoparticles and PAMAM electrochemical and UV/visible spectroscopic techniques. *J. Solid State Electrochem.* **2020**, *25*, 743-752, doi:10.1007/s10008-020-04848-z.
- [8] de Lima França, C.C.; da Silva Terto, E.G.; Dias-Vermelho, M. V.; Silva, A.C.A.; Dantas, N.O.; de Abreu, F.C. The electrochemical behavior of core-shell CdSe/CdS magic-sized quantum dots linked to cyclodextrin for studies of the encapsulation of bioactive compounds. *J. Solid State Electrochem.* **2016**, *20*, 2533-2540, doi:10.1007/s10008-016-3221-8.
- [9] Martins, B.R.; Barbosa, Y.O.; Andrade, C.M.R.; Pereira, L.Q.; Simão, G.F.; de Oliveira, C.J.; Correia, D.; Oliveira, R.T.S.; da Silva, M. V.; Silva, A.C.A.; et al. Development of an Electrochemical Immunosensor for Specific Detection of Visceral Leishmaniasis Using Gold-Modified Screen-Printed Carbon Electrodes. *Biosensors* **2020**, *10*, 81, doi:10.3390/bios10080081.
- [10] Petroni, J.M.; Lucca, B.G.; da Silva Júnior, L.C.; Barbosa Alves, D.C.; Souza Ferreira, V. Paper-based Electrochemical Devices Coupled to External Graphene-Cu Nanoparticles Modified Solid Electrode through Meniscus Configuration and their Use in Biological Analysis. *Electroanalysis* **2017**, *29*, 2628-2637, doi:10.1002/elan.201700398.
- [11] Hoffmann, M.; Kleine-Weber, H.; Schroeder, S.; Krüger, N.; Herrler, T.; Erichsen, S.; Schiergens, T.S.; Herrler, G.; Wu, N.H.; Nitsche, A.; et al. SARS-CoV-2 Cell Entry Depends on ACE2 and TMPRSS2 and Is Blocked by a Clinically Proven Protease Inhibitor. *Cell* **2020**, *181*, 271-280.e8, doi:10.1016/j.cell.2020.02.052.
- [12] Sungnak, W.; Huang, N.; Bécavin, C.; Berg, M.; Queen, R.; Litvinukova, M.; Talavera-López, C.; Maatz, H.; Reichart, D.; Sampaziotis, F.; et al. SARS-CoV-2 entry factors are highly expressed in nasal epithelial cells together with innate immune genes. *Nat. Med.* **2020**, *26*, 681-687, doi:10.1038/s41591-020-0868-6.

- [13] Xu, Z.; Shi, L.; Wang, Y.; Zhang, J.; Huang, L.; Zhang, C.; Liu, S.; Zhao, P.; Liu, H.; Zhu, L.; et al. Pathological findings of COVID-19 associated with acute respiratory distress syndrome. *Lancet Respir. Med.* **2020**, *8*, 420-422, doi:10.1016/S2213-2600(20)30076-X.
- [14] Yang, J.; Zheng, Y.; Gou, X.; Pu, K.; Chen, Z.; Guo, Q.; Ji, R.; Wang, H.; Wang, Y.; Zhou, Y. Prevalence of comorbidities and its effects in coronavirus disease 2019 patients: A systematic review and meta-analysis. *Int. J. Infect. Dis.* **2020**, *94*, 91-95, doi:10.1016/j.ijid.2020.03.017.
- [15] Esakandari, H.; Nabi-Afjadi, M.; Fakkari-Afjadi, J.; Farahmandian, N.; Miresmaeili, S.M.; Bahreini, E. A comprehensive review of COVID-19 characteristics. *Biol. Proced. Online* **2020**, *22*, 19.
- [16] Qin, C.; Zhou, L.; Hu, Z.; Zhang, S.; Yang, S.; Tao, Y.; Xie, C.; Ma, K.; Shang, K.; Wang, W.; et al. Dysregulation of immune response in patients with coronavirus 2019 (COVID-19) in Wuhan, China. *Clin. Infect. Dis.* **2020**, *71*, 762-768, doi:10.1093/cid/ciaa248.
- [17] Huang, C.; Wang, Y.; Li, X.; Ren, L.; Zhao, J.; Hu, Y.; Zhang, L.; Fan, G.; Xu, J.; Gu, X.; et al. Clinical features of patients infected with 2019 novel coronavirus in Wuhan, China. *Lancet* **2020**, *395*, 497-506, doi:10.1016/S0140-6736(20)30183-5.
- [18] Guo, L.; Ren, L.; Yang, S.; Xiao, M.; Chang, D.; Yang, F.; Dela Cruz, C.S.; Wang, Y.; Wu, C.; Xiao, Y.; et al. Profiling early humoral response to diagnose novel coronavirus disease (COVID-19). *Clin. Infect. Dis.* **2020**, *71*, 778-785, doi:10.1093/cid/ciaa310.
- [19] Wang, Y.; Zhang, L.; Sang, L.; Ye, F.; Ruan, S.; Zhong, B.; Song, T.; Alshukairi, A.N.; Chen, R.; Zhang, Z.; et al. Kinetics of viral load and antibody response in relation to COVID-19 severity. *J. Clin. Invest.* **2020**, *130*, 5235-5244, doi:10.1172/JCI138759.
- [20] Carsetti, R.; Zaffina, S.; Mortari, E.P.; Terreri, S.; Corrente, F.; Capponi, C.; Palomba, P.; Mirabella, M.; Cascioli, S.; Palange, P.; et al. Different Innate and Adaptive Immune Responses to SARS-CoV-2 Infection of Asymptomatic, Mild, and Severe Cases. *Front. Immunol.* **2020**, *11*, 3365, doi:10.3389/fimmu.2020.610300.
- [21] Figueiredo-Campos, P.; Blankenhaus, B.; Mota, C.; Gomes, A.; Serrano, M.; Ariotti, S.; Costa, C.; Nunes-Cabaço, H.; Mendes, A.M.; Gaspar, P.; et al. Seroprevalence of anti-SARS-CoV-2 antibodies in COVID-19 patients and healthy volunteers up to 6 months post disease onset. *Eur. J. Immunol.* **2020**, *50*, 2025-2040, doi:10.1002/eji.202048970.
- [22] CDC Vaccines: The Basics 2012.
- [23] Anderson, E.J.; Roupheal, N.G.; Widge, A.T.; Jackson, L.A.; Roberts, P.C.; Makhene, M.; Chappell, J.D.; Denison, M.R.; Stevens, L.J.; Pruijssers, A.J.; et al. Safety and Immunogenicity of SARS-CoV-2 mRNA-1273 Vaccine in Older Adults. *N. Engl. J. Med.* **2020**, *383*, 2427-2438, doi:10.1056/NEJMoa2028436.
- [24] Folegatti, P.M.; Ewer, K.J.; Aley, P.K.; Angus, B.; Becker, S.; Belij-Rammerstorfer, S.; Bellamy, D.; Bibi, S.; Bittaye, M.; Clutterbuck, E.A.; et al. Safety and immunogenicity of the ChAdOx1 nCoV-19 vaccine against SARS-CoV-2: a preliminary report of a phase 1/2, single-blind, randomised controlled trial. *Lancet* **2020**, *396*, 467-478, doi:10.1016/S0140-6736(20)31604-4.
- [25] Xia, S.; Zhang, Y.; Wang, Y.; Wang, H.; Yang, Y.; Gao, G.F.; Tan, W.; Wu, G.; Xu, M.; Lou, Z.; et al. Safety and immunogenicity of an inactivated SARS-CoV-2 vaccine, BBIBP-CorV:

a randomised, double-blind, placebo-controlled, phase 1/2 trial. *Lancet Infect. Dis.* **2021**, *21*, 39-51, doi:10.1016/S1473-3099(20)30831-8.

[26] Wong, H.Y.F.; Lam, H.Y.S.; Fong, A.H.T.; Leung, S.T.; Chin, T.W.Y.; Lo, C.S.Y.; Lui, M.M.S.; Lee, J.C.Y.; Chiu, K.W.H.; Chung, T.W.H.; et al. Frequency and Distribution of Chest Radiographic Findings in Patients Positive for COVID-19. *Radiology* **2020**, *296*, E72–E78, doi:10.1148/radiol.2020201160.

[27] Udugama, B.; Kadhiresan, P.; Kozlowski, H.N.; Malekjahani, A.; Osborne, M.; Li, V.Y.C.; Chen, H.; Mubareka, S.; Gubbay, J.B.; Chan, W.C.W. Diagnosing COVID-19: The Disease and Tools for Detection. *ACS Nano* **2020**, *14*, 3822-3835, doi:10.1021/acsnano.0c02624.

[28] Leblanc, J.J.; Gubbay, J.B.; Li, Y.; Needle, R.; Arneson, S.R.; Marcino, D.; Charest, H.; Desnoyers, G.; Dust, K.; Fattouh, R.; et al. Since January 2020 Elsevier has created a COVID-19 resource centre with free information in English and Mandarin on the novel coronavirus COVID-19. The COVID-19 resource centre is hosted on Elsevier Connect, the company's public news and information. **2020**.

[29] Corman, V.M.; Landt, O.; Kaiser, M.; Molenkamp, R.; Meijer, A.; Chu, D.K.; Bleicker, T.; Brünink, S.; Schneider, J.; Luisa Schmidt, M.; et al. Detection of 2019-nCoV by RT-PCR. *Euro Surveill* **2020**, *25*, 1-8.

[30] Lv, Y.; Wu, R.; Feng, K.; Li, J.; Mao, Q.; Yuan, H.; Shen, H.; Chai, X.; Li, L.S. Highly sensitive and accurate detection of C-reactive protein by CdSe/ZnS quantum dot-based fluorescence-linked immunosorbent assay. *J. Nanobiotechnology* **2017**, *15*, 35, doi:10.1186/s12951-017-0267-4.

[31] Rai, P.; Kumar, B.K.; Deekshit, V.K.; Karunasagar, I.;

Karunasagar, I. Detection technologies and recent developments in the diagnosis of COVID-19 infection. *Appl. Microbiol. Biotechnol.* **2021**, *105*, 441-455, doi:10.1007/s00253-020-11061-5.

[32] Zhang, Y.; Odiwuor, N.; Xiong, J.; Sun, L.; Nyaruaba, R.O.; Wei, H.; Tanner, N.A. Rapid molecular detection of SARS-CoV-2 (COVID-19) virus RNA using colorimetric LAMP. *medRxiv* **2020**, *2*, doi:10.1101/2020.02.26.20028373.

[33] Broughton, J.P.; Deng, X.; Yu, G.; Fasching, C.L.; Servellita, V.; Singh, J.; Miao, X.; Streithorst, J.A.; Granados, A.; Sotomayor-Gonzalez, A.; et al. CRISPR–Cas12-based detection of SARS-CoV-2. *Nat. Biotechnol.* **2020**, *38*, 870-874, doi:10.1038/s41587-020-0513-4.

[34] Lau, Y.L.; Ismail, I. binti; Mustapa, N.I. binti; Lai, M.Y.; Soh, T.S.T.; Hassan, A.H.; Peariasamy, K.M.; Lee, Y.L.; Kahar, M.K.B.A.; Chong, J.; et al. Development of a reverse transcription recombinase polymerase amplification assay for rapid and direct visual detection of Severe Acute Respiratory Syndrome Coronavirus 2 (SARS-CoV-2). *PLoS One* **2021**, *16*, 2-9, doi:10.1371/journal.pone.0245164.

[35] Lassaunière, R.; Frische, A.; Harboe, Z.B.; Nielsen, A.C.Y.; Fomsgaard, A.; Kroghfelt, K.A.; Jørgensen, C.S. Evaluation of nine commercial SARS- CoV-2 immunoassays. *medRxiv* **2020**, 1-15, doi:10.1101/2020.04.09.20056325.

[36] Mertens, P.; De Vos, N.; Martiny, D.; Jassoy, C.; Mirazimi, A.; Cuypers, L.; Van den Wijngaert, S.; Monteil, V.; Melin,

P.; Stoffels, K.; et al. Development and Potential Usefulness of the COVID-19 Ag Respi-Strip Diagnostic Assay in a Pandemic Context. *Front. Med.* **2020**, *7*, doi:10.3389/fmed.2020.00225.

Open

Open

- [37] Cai, X.F.; Chen, J.; Hu, J. li; Long, Q. X.; Deng, H.J.; Liu, P.; Fan, K.; Liao, P.; Liu, B.Z.; Wu, G.C.; et al. A peptide-based magnetic chemiluminescence enzyme immunoassay for serological diagnosis of coronavirus disease 2019. *J. Infect. Dis.* **2020**, *222*, 189-195, doi:10.1093/infdis/jiaa243.
- [38] Giri, B.; Pandey, S.; Shrestha, R.; Pokharel, K.; Ligler, F.S.; Neupane, B.B. Review of analytical performance of COVID-19 detection methods. *Anal. Bioanal. Chem.* **2021**, *413*, 35-48, doi:10.1007/s00216-020-02889-x.
- [39] Infantino, M.; Grossi, V.; Lari, B.; Bambi, R.; Perri, A.; Manneschi, M.; Terenzi, G.; Liotti, I.; Ciotta, G.; Taddei, C.; et al. Diagnostic accuracy of an automated chemiluminescent immunoassay for anti-SARS-CoV-2 IgM and IgG antibodies: an Italian experience. *J. Med. Virol.* **2020**, *92*, 1671-1675, doi:10.1002/jmv.25932.
- [40] Russell, S.M.; Alba-Patiño, A.; Barón, E.; Borges, M.; Gonzalez-Freire, M.; De La Rica, R. Biosensors for Managing the COVID-19 Cytokine Storm: Challenges Ahead. *ACS Sensors* **2020**, *5*, 1506-1513, doi:10.1021/acssensors.0c00979.
- [41] Fukumoto, T.; Iwasaki, S.; Fujisawa, S.; Hayasaka, K.; Sato, K.; Oguri, S.; Taki, K.; Nakakubo, S.; Kamada, K.; Yamashita, Y.; et al. Efficacy of a novel SARS-CoV-2 detection kit without RNA extraction and purification. *Int. J. Infect. Dis.* **2020**, *98*, 16-17, doi:10.1016/j.ijid.2020.06.074.
- [42] Laghrib, F.; Saqrane, S.; El Bouabi, Y.; Farahi, A.; Bakasse, M.; Lahrach, S.; El Mhammedi, M.A. Current progress on COVID-19 related to biosensing technologies: New opportunity for detection and monitoring of viruses. *Microchem. J.* **2021**, *160*, 105606.
- [43] Xi, H.; Juhas, M.; Zhang, Y. G-quadruplex based biosensor: A potential tool for SARS-CoV-2 detection. *Biosens. Bioelectron.* **2020**, *167*, 112494, doi:10.1016/j.bios.2020.112494.
- [44] Turner, A.P.F. Biosensors: Fundamentals and applications - Historic book now open access. *Biosens. Bioelectron.* **2015**, *65*, A1.
- [45] Ermolaeva, T.; Farafonova, O.; Karaseva, N. Possibilities and Prospects of Immunosensors for a Highly Sensitive Pesticide Detection in Vegetables and Fruits: a Review. *Food Anal. Methods* **2019**, *12*, 2785-2801.
- [46] Ramírez, N.B.; Salgado, A.M.; Valdman, B. The evolution and developments of immunosensors for health and environmental monitoring: Problems and perspectives. *Brazilian J. Chem. Eng.* **2009**, *26*, 227-249, doi:10.1590/s0104-66322009000200001.
- [47] Goumi, Y. El Electrochemical Genosensors: Definition and Fields of Application. *Int. J. Biosens. Bioelectron.* **2017**, *3*, doi:10.15406/ijbsbe.2017.03.00080.
- [48] Silva, A.C.A.; Silva, M.J.B.; Da Luz, F.A.C.; Silva, D.P.; De Deus, S.L.V.; Dantas, N.O. Controlling the cytotoxicity of CdSe magic-sized quantum dots as a function of surface defect density. *Nano Lett.* **2014**, *14*, 5452-5457, doi:10.1021/nl5028028.
- [49] Silva, A.C.A.; Da Silva, S.W.; Morais, P.C.; Dantas, N.O. Shell thickness modulation in ultrasmall CdSe/Cd_xSe 1-x/CdS core/shell quantum dots via 1-thioglycerol. *ACS Nano* **2014**, *8*, 1913-1922, doi:10.1021/nn406478f.
- [50] Morais, P. V.; Gomes, V.F.; Silva, A.C.A.; Dantas, N.O.; Schöning, M.J.; Siqueira, J.R. Nanofilm of ZnO nanocrystals/carbon nanotubes as biocompatible layer for enzymatic

biosensors in capacitive field-effect devices. *J. Mater. Sci.* **2017**, *52*, 12314-12325, doi:10.1007/s10853-017-1369-y.

[51] Almeida Silva, A.C.; Gratens, X.; Chitta, V.A.; Franco, S.D.; Souza Da Silva, R.; Condeles, J.F.; Dantas, N.O. Effects of ultrasonic agitation on the structural and magnetic properties of CoFe₂O₄ nanocrystals. *Eur. J. Inorg. Chem.* **2014**, doi:10.1002/ejic.201402563.

[52] Silva, A.C.A.; Freschi, A.P.P.; Rodrigues, C.M.; Matias, B.F.; Maia, L.P.; Goulart, L.R.; Dantas, N.O. Biological analysis and imaging applications of CdSe/CdS_xSe_{1-x}/CdS core-shell magic-sized quantum dot. *Nanomedicine Nanotechnology, Biol. Med.* **2016**, *12*, 1421-1430, doi:10.1016/j.nano.2016.01.001.

[53] Silva, A.C.A.; Azevedo, F.V.P.V.; Zóia, M.A.P.; Rodrigues, J.P.; Dantas, N.O.; Melo, V.R.Á.; Goulart, L.R. Magic Sized Quantum Dots as a Theranostic Tool for Breast Cancer. In *Recent Studies & Advances in Breast Cancer*; Open Access eBooks: Wilmington, 2017; pp. 1-10 ISBN 978-81-935757-2-7.

[54] Souza, G.L. de; Moura, C.C.G.; Silva, A.C.A.; Marinho, J.Z.; Silva, T.R.; Dantas, N.O.; Bonvicini, J.F.S.; Turrioni, A.P. Effects of zinc oxide and calcium-doped zinc oxide nanocrystal on cytotoxicity and reactive oxygen species production in different cell culture models. *Restor. Dent. Endod.* **2020**, *45*, 54, doi:10.5395/rde.2020.45.e54.

[55] Duarte, C.A.; Goulart, L.R.; Filice, L. de S.C.; Lima, I.L. de; Campos-Fernández, E.; Dantas, N.O.; Silva, A.C.A.; Soares, M.B.P.; Santos, R.R. dos; Cardoso, C.M.A.; et al. Characterization of Crystalline Phase of TiO₂ Nanocrystals, Cytotoxicity and Cell Internalization Analysis on Human Adipose Tissue-Derived Mesenchymal

Stem Cells. *Materials (Basel)*. **2020**, *13*, 4071, doi:10.3390/ma13184071.

[56] Carvalho Naves, M.P.; de Moraes, C.R.; Silva, A.C.A.; Dantas, N.O.; Spanó, M.A.; de Rezende, A.A.A. Assessment of mutagenic, recombinogenic and carcinogenic potential of titanium dioxide nanocrystals in somatic cells of *Drosophila melanogaster*. *Food Chem. Toxicol.* **2018**, *112*, 273-228, doi:10.1016/j.fct.2017.12.040.

[57] Reis, É. de M.; de Rezende, A.A.A.; Santos, D.V.; de Oliveria, P.F.; Nicolella, H.D.; Tavares, D.C.; Silva, A.C.A.; Dantas, N.O.; Spanó, M.A. Assessment of the genotoxic potential of two zinc oxide sources (amorphous and nanoparticles) using the in vitro micronucleus test and the in vivo wing somatic mutation and recombination test. *Food Chem. Toxicol.* **2015**, *84*, 55-63, doi:10.1016/j.fct.2015.07.008.

[58] Reis, É. de M.; Rezende, A.A.A. de; Oliveira, P.F. de; Nicolella, H.D.; Tavares, D.C.; Silva, A.C.A.; Dantas, N.O.; Spanó, M.A. Evaluation of titanium dioxide nanocrystal-induced genotoxicity by the cytokinesis-block micronucleus assay and the *Drosophila* wing spot test. *Food Chem. Toxicol.* **2016**, *96*, 309-319, doi:10.1016/j.fct.2016.08.023.

[59] Silva, A.; Zóia, M.A.P.; Correia, L.I.V.; Azevedo, F.V.P.V.; Paula, A.T. de; Maia, L.P.; Carvalho, L.S. de; Carvalho, L.N.; Costa, M.P.C.; Giaretta, L.C.; et al. Biocompatibility of Doped Semiconductors Nanocrystals and Nanocomposites. In *Cytotoxicity*; InTech, 2018.

[60] Silva, A.C.A.; Dantas, N.O.; Silva, M.J.B.; Spanó, A.M.; Goulart, ; Luiz Ricardo Functional Nanocrystals : Towards Biocompatibility, Nontoxicity and. In *Advances in Biochemistry & Applications in Medicine*; 2017; pp. 1-27.

[61] Souza, G.L.; Silva, T.R.; Vieira, M.S.; Dantas, N.O.; Silva, A.C.A.; Moura, C.C.G. Development and study of cytotoxicity of calcium oxide nanocrystals - ScienceDirect. Dent. Mater. **2018**, *34*, e83.

Morais, P.C.; Dantas, N.O. Shell Thickness

[62] Silva, A.C.A.; Correia, L.I.V.; Silva, M.J.B.; Zóia, M.A.P.; Azevedo, F.V.P.V.; Rodrigues, Jéssica Peixoto Goulart, L.R.; Ávila, Veridiana de Melo Dantas, N.O. Biocompatible Magic Sized Quantum Dots: Luminescent Markers and Probes. In; Correia, L.I.V., Ed.; IntechOpen: Rijeka, 2018; p. Ch. 6 ISBN 978-1-78923-295-0.

[63] Silva, A.C.A.; Deus, S.L.V. De; Silva, M.J.B.; Dantas, N.O. Highly stable luminescence of CdSe magic-sized quantum dots in HeLa cells. Sensors Actuators, B Chem. **2014**, *191*, 108-114, doi:10.1016/j.snb.2013.09.063.

[64] Pilla, V.; De Lima, S.R.; Andrade, A.A.; Silva, A.C.A.; Dantas, N.O. Fluorescence quantum efficiency of CdSe/CdS magic-sized quantum dots functionalized with carboxyl or hydroxyl groups. Chem. Phys. Lett. **2013**, *580*, 130-134, doi:10.1016/j.cplett.2013.07.007.

[65] Almeida Silva, A.; Freitas Neto, E.; da Silva, S.W.; Morais, P.; Dantas, N. Modified Phonon Confinement Model and Its Application to CdSe/CdS Core–Shell Magic-Sized Quantum Dots Synthesized in Aqueous Solution by a New Route. J. Phys. Chem. C *117*, 1904-1914, doi:10.1021/jp308500r.

[66] Almeida Silva, A.; Silva, M.J.; da Luz, F.A.; Silva, D.; de Deus, S.; Dantas, N. Controlling the Cytotoxicity of CdSe Magic-Sized Quantum Dots as a Function of Surface Defect Density. *Nano Lett.* *14*, 5452-5457, doi:10.1021/nl5028028.

[67] Silva, A.C. a; da Silva, S.W.;

Sensor Surface Design with NanoMaterials: A New Platform in the Diagnosis of COVID-19
Modulation in Ultrasmall CdSe/
Cd_xSe_{1-x}/CdS Core/Shell Quantum
Dots via 1-Thioglycerol. *ACS Nano*
2014, *8*, 1913-1922,
doi:10.1021/nn406478f.

of electrochemical biosensors in the
COVID-19 pandemic: A perspective on

[68] Dias, E.H.V.; Pereira, D.F.C.;
de Sousa, B.B.; Matias, M.S.; de
Queiroz, M.R.; Santiago, F.M.; Silva,
A.C.A.; Dantas, N.O.; Santos-Filho,
N.A.; de Oliveira, F. In vitro tracking
of phospholipase A 2 from snake
venom conjugated with magic-sized
quantum dots. *Int. J. Biol. Macromol.*
2019, *122*, 461-468, doi:10.1016/j.
ijbiomac.2018.10.185.

[69] Sandino, J.; Pegg, G.; Gonzalez,
F.; Smith, G. Aerial Mapping of
Forests Affected by Pathogens Using
UAVs, Hyperspectral Sensors, and
Artificial Intelligence. *Sensors* **2018**,
18, 944, doi:10.3390/s18040944.

[70] Naudé, W. Artificial Intelligence
Against Covid-19: An Early Review.
IZA Discuss. Pap. No. 13110 **2020**, 1-
17.

[71] Silva, A.C.A.; Dantas, N.O.; Silva,
M.J.B.; Spanó, M.A.; Goulart,
L.R. Functional Nanocrystals :
Towards Biocompatibility,
Nontoxicity
and Biospecificity. In *Advances in
Biochemistry & Applications in
Medicine*; Rojeet Shrestha, Ed.; Open
Access eBooks: Wilmington, 2017; pp.
1-27
ISBN 978-81-935757-1-0.

[72] de Lima França, C.C.; da Silva
Terto, E.G.; Dias-Vermelho, M. V.;
Silva, A.C.A.; Dantas, N.O.; de
Abreu,
F.C. The electrochemical behavior
of core-shell CdSe/CdS magic-
sized
quantum dots linked to cyclodextrin
for studies of the encapsulation of
bioactive compounds. *J. Solid State
Electrochem.* **2016**, *20*, 2533-2540,
doi:10.1007/ s10008-016-3221-8.

[73] Mahshid, S.S.; Flynn, S.E.;
Mahshid, S. The potential application

Open

Open

the rapid diagnostics of SARS-CoV-2. *Biosens. Bioelectron.* **2021**, *176*, 112905, doi:10.1016/j.bios.2020.112905.

[74] Seo, G.; Lee, G.; Kim, M.J.; Baek, S.H.; Choi, M.; Ku, K.B.; Lee, C.S.; Jun, S.; Park, D.; Kim, H.G.; et al. Rapid Detection of COVID-19 Causative Virus (SARS-CoV-2) in Human Nasopharyngeal Swab Specimens Using Field-Effect Transistor-Based Biosensor. *ACS Nano* **2020**, *14*, 5135-5142, doi:10.1021/acsnano.0c02823.

[75] Rashed, M.Z.; Kopechek, J.A.; Priddy, M.C.; Hamorsky, K.T.; Palmer, K.E.; Mittal, N.; Valdez, J.; Flynn, J.; Williams, S.J. Rapid detection of SARS-CoV-2 antibodies using electrochemical impedance-based detector. *Biosens. Bioelectron.* **2021**, *171*, 112709, doi:10.1016/j.bios.2020.112709.

[76] Mojsoska, B.; Larsen, S.; Olsen, D.A.; Madsen, J.S.; Brandslund, I.; Alatraktchi, F.A. Rapid SARS-CoV-2 detection using electrochemical immunosensor. *Sensors (Switzerland)* **2021**, *21*, 1-11, doi:10.3390/s21020390.

[77] Yakoh, A.; Pimpitak, U.; Rengpipat, S.; Hirankarn, N.; Chailapakul, O.; Chaiyo, S. Paper-based electrochemical biosensor for diagnosing COVID-19: Detection of SARS-CoV-2 antibodies and antigen. *Biosens. Bioelectron.* **2021**, *176*, 112912, doi:10.1016/j.bios.2020.112912.

[78] Zhao, H.; Liu, F.; Xie, W.; Zhou, T.C.; OuYang, J.; Jin, L.; Li, H.; Zhao, C.Y.; Zhang, L.; Wei, J.; et al. Ultrasensitive supersandwich-type electrochemical sensor for SARS-CoV-2 from the infected COVID-19 patients using a smartphone. *Sensors Actuators, B Chem.* **2021**, *327*, doi:10.1016/j.snb.2020.128899.

[79] Eissa, S.; Zourob, M. Development of a Low-Cost Cotton-Tipped Electrochemical Immunosensor for the Detection of SARS-CoV-2.

Anal. Chem. **2021**, doi:10.1021/acs.analchem.0c04719.

[80] Fabiani, L.; Saroglia, M.; Galatà, G.; De Santis, R.; Fillo, S.; Luca, V.; Faggioni, G.; D'Amore, N.; Regalbuto, E.; Salvatori, P.; et al. Magnetic beads combined with carbon black-based screen-printed electrodes for COVID-19: A reliable and miniaturized electrochemical immunosensor for SARS-CoV-2 detection in saliva. *Biosens. Bioelectron.* **2021**, *171*, 112686, doi:10.1016/j.bios.2020.112686.

[81] Hashemi, S.A.; Golab Behbahan, N.G.; Bahrani, S.; Mousavi, S.M.; Gholami, A.; Ramakrishna, S.; Firoozsani, M.; Moghadami, M.; Lankarani, K.B.; Omidifar, N. Ultra-sensitive viral glycoprotein detection NanoSystem toward accurate tracing SARS-CoV-2 in biological/non-biological media. *Biosens. Bioelectron.* **2021**, *171*, 112731, doi:10.1016/j.bios.2020.112731.

[82] Li, X.; Qin, Z.; Fu, H.; Li, T.; Peng, R.; Li, Z.; Rini, J.M.; Liu, X. Enhancing the performance of paper-based electrochemical impedance spectroscopy nanobiosensors: An experimental approach. *Biosens. Bioelectron.* **2021**, *177*, 112672, doi:10.1016/j.bios.2020.112672.

[83] Vadlamani, B.S.; Uppal, T.; Verma, S.C.; Misra, M. Functionalized TiO₂ Nanotube-Based Electrochemical Biosensor for Rapid Detection of SARS-CoV-2. *Sensors* **2020**, *20*, 5871, doi:10.3390/s20205871.

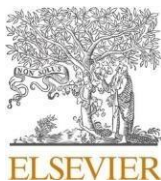
[84] Alafeef, M.; Dighe, K.; Moitra, P.; Pan, D. Rapid, Ultrasensitive, and Quantitative Detection of SARS-CoV-2 Using Antisense Oligonucleotides Directed Electrochemical Biosensor Chip. *ACS Nano* **2020**, *14*, 17028-17045, doi:10.1021/acsnano.0c06392.

[85] Torrente-Rodríguez, R.M.; Lukas, H.; Tu, J.; Min, J.; Yang, Y.; Xu, C.;

Rossiter, H.B.; Gao, W. SARS-CoV-2 RapidPlex: A Graphene-Based Multiplexed Telemedicine Platform for Rapid and Low-Cost COVID-19 Diagnosis and Monitoring. *Matter* **2020**, *3*, 1981-1998, doi:10.1016/j.matt.2020.09.027.

[86] Cui, F.; Zhou, H.S. Diagnostic methods and potential portable biosensors for coronavirus disease 2019. *Biosens. Bioelectron.* **2020**, *165*, 112349, doi:10.1016/j.bios.2020.112349.

IntechOpen



A comparative study of graphene-based electrodes for electrochemical detection of visceral leishmaniasis in symptomatic and asymptomatic patients

Beatriz R. Martins ^{a,c,1}, Cristhianne Molinero R. Andrade ^{a,c,1,*}, Guilherme F. Simão ^a, Rhéltheer de Paula Martins ^a, Luana Barbosa Severino ^a, Sarah Cristina Sato Vaz Tanaka ^a, Loren Q. Pereira ^a, Marcos Vinicius da Silva ^a, Fernanda Bernadelli de Vito ^a, Carlo José Freire de Oliveira ^a, Helio Moraes de Souza ^a, Anderson Barbosa Lima ^a, Virmondes Rodrigues Junior ^{a,c}, José Roberto Siqueira Junior ^a, Renata Pereira Alves ^{a,b}

^a Federal University of Triângulo Mineiro, MG, Uberaba, Brazil

^b Federal University of Triângulo Mineiro, Iturama, MG, Brazil

^c INCT-Neuroimmune Modulation, Uberaba 38025-350, Brazil

ARTICLE INFO

Keywords:

Electrochemical biosensor
Leishmaniasis
Point-of-care test
Asymptomatic infections
Portable analysis

ABSTRACT

Background: Visceral Leishmaniasis is a neglected tropical disease with a high rate of infection and mortality in affected areas. Around 50,000 to 90,000 new cases of visceral leishmaniasis (VL) are estimated every year. Individuals asymptomatic for the disease should also be considered in epidemiological surveillance of the disease, as they can help spread the parasite. Thus, the development of low-cost diagnosis methods that allow the identification of infected and asymptomatic individuals is required, especially in developing countries where this disease is endemic.

Results: In this work, we developed an immunosensor for recognizing anti-*Leishmania* antibodies in asymptomatic individuals and avoiding cross-reaction with Chagas disease (CD). For that, we used carbon-based screen-printed electrodes, modified with graphene oxide and gold. Reproducibility was assessed by calculating the relative standard deviation (RSD < 5 %) from cyclic voltammograms of [Fe(CN)₆]^{3-/4-} using three different electrodes, screen-printed carbon electrodes (DPR-110) and graphene modified screen-printed electrodes (DPR-110 GPH)

were purchased from DropSens (Oviedo, Asturias, Spain).

Significance: As an electrochemical methodology, we use cyclic voltammetry. After the tests were carried out, we considered that carbon electrodes adsorbed with reduced graphene oxide and modified with gold nanoparticles were the best platforms for detecting anti-*Leishmania* antibodies. In the study carried out, the limit of quantification (LOQ) for anti-*Leishmania* antibodies was established at 16.75 mg/mL, while the limit of detection (LOD) was 5.58 mg/mL. These limits indicate the minimum antibody concentration values that can be quantified and detected accurately and reliably in the analyzed sera.

1. Introduction

Visceral leishmaniasis (VL) is a neglected tropical disease that can be potentially mortal if left untreated. The causative parasite, *Leishmania infantum*, is transmitted by the bite of infected female phlebotomine sandflies. It is estimated that around 50,000 to 90,000 new cases of VL occur every year ([6]; WHO, 2023). According to the World Health

Organization (WHO, 2023), the disease is primarily prevalent in Brazil, India, and countries in East Africa [35].

Symptoms can vary, ranging from severe to mild, such as diarrhea, fever, hepatomegaly, and mild splenomegaly, among others. Some individuals may be infected and asymptomatic for long periods. Although they do not always develop symptoms, such individuals should be the focus of attention, as they can assist in the spread of the parasite; they

* Corresponding author.

E-mail address: cristhianne_m@hotmail.com (C.M.R. Andrade).

These authors contributed equally to this article.

<https://doi.org/10.1016/j.talo.2024.100339>

Received 10 April 2024; Received in revised form 3 June 2024; Accepted 17 June 2024

Available online 22 June 2024

2766-8319/© 2024 Published by Elsevier B.V. This is an open access article under the CC BY-NC-ND license (<http://creativecommons.org/licenses/by-nc-nd/4.0/>).

can serve as a possible reservoir or even contribute to the transmission through blood donations [2,25]. Studies have shown that parasites of the *Leishmania* genus can survive and remain infectious in stored blood bags. In Brazil, among healthy blood donors, some individuals exhibited immunoglobulin G (IgG) antibodies against *Leishmania*, suggesting prior contact with *Leishmania infantum*. This highlights the need for testing for leishmaniasis in asymptomatic individuals, especially blood donors in endemic areas [13,27].

Although there are some commercial tests available for the detection of the disease, such as Biolisa (BIOLISA LEISHMANIOSE VISCERAL®-Bioclin, Belo Horizonte, Brazil), rk39 protein (most present in *Leishmania donovani*), offer valuable diagnostic tools for leishmaniasis, in addition to recent academic studies involving the topic, they are sometimes insufficient in detecting asymptomatic infections and/or present a high financial cost [18,28]. Therefore, it is important to develop an efficient, low-cost, easily accessible test that guarantees sensitivity and specificity. In this context, electrochemical biosensors are platforms that possess these characteristics and could serve as an option for the diagnosis of asymptomatic patients.

There are some studies showing the development of biosensors aimed at detecting leishmaniasis, such as the study by Barraza and collaborators, who developed a paper platform for detecting anti-American cutaneous leishmaniasis antibodies [5] and the study by Park and collaborators, who made an electrochemical immunosensor for detecting antibodies against the surface protease (Gp63) of *Leishmania major* [29], both in human sera; and the study of an impedimetric immunosensor for the detection of *Leishmania infantum* [8], the latter in canine serum. However, there are still few biosensors currently reported in the literature focusing on the diagnosis of visceral Leishmaniasis in humans, mainly those that identify the detection of antibodies anti-*Leishmania infantum* in possibly asymptomatic and oligosymptomatic individuals.

Previously, our research group developed an immunosensor (graphite electrodes with the incorporation of gold nanoparticles) capable of detecting anti-*Leishmania* antibodies in sera from infected symptomatic individuals without showing significant cross-reactivity with Chagas Disease (CD) [22]. Leishmaniasis and Chagas Disease represent important public health problems, with high prevalence in several regions of the world. Accurate and early diagnosis of these diseases is crucial for successful treatment and control of transmission. However, the cross-occurrence between the disease-causing agents, *Trypanosoma cruzi* and *Leishmania spp.*, represents a significant challenge for traditional diagnostic methods, such as serological and molecular tests [4]. This cross-reactivity occurs due to the antigenic similarity between the parasites, which can lead to cross-recognition of antigens by the patient's immune system [21]. Consequently, diagnostic tests can present false-positive results, making it difficult to correctly identify the disease and appropriately direct treatment [23].

This problem is especially critical in areas endemic for both diseases, where the coexistence of cases of Chagas and leishmaniasis makes the diagnosis even more complex. Interpreting test results becomes a challenge and cross-reactivity can lead to delays in diagnosis, prescription of inappropriate treatment and, in serious cases, complications for the patient's health. The development of more specific and sensitive diagnostic methods is crucial to overcome these obstacles. New techniques, such as tests based on specific antigens and biomarkers, can offer greater diagnostic accuracy and help differentiate between Chagas and Leishmaniasis. Continuous studies and investments in research are essential to improve diagnostic tools and ensure accurate and timely diagnosis of these neglected diseases.

Despite advances in the diagnosis of human visceral leishmaniasis (HVL), there are still challenges to be overcome. Current tests, although effective, have limitations in detecting asymptomatic cases, which may represent an important reservoir of the disease and contribute to its spread, making early diagnosis and timely intervention difficult. Faced

with this gap, our research group set out to develop new diagnostic tests using electrochemical biosensors, based on research into efficient nanomaterials for this purpose, as early diagnosis is crucial for the successful treatment of HVL, reducing mortality and morbidity associated with the disease.

Graphene, one of the most explored carbon-based nanomaterials, has emerged as a promising tool for enhancing detection capabilities. Since its discovery in 2004, it has garnered significant interest from the research community, particularly for its potential applications in manufacturing electrochemical biosensors [11,24]. This study aims to evaluate a graphene-based immunosensor for the diagnosis of leishmaniasis. The developed immunosensor is capable of identifying asymptomatic individuals without cross-reaction with CD and allows the construction of analytical curve to evaluate the analytical performance of the modified electrodes.

2. Materials and methods

2.1. Sample acquisition

Serum samples from 4 patients diagnosed with VL (2 symptomatic and 2 asymptomatic patients), 2 patients diagnosed with cutaneous leishmaniasis, and 2 patients diagnosed with CD were obtained at the Immunology Research Laboratory and Hematology Research Laboratory of the Federal University of Triangulo Mineiro (Uberaba, State of Minas Gerais, Brazil).

The diagnosis of symptomatic individuals for VL was made through anamnesis, physical examination, and confirmation by laboratory tests, while the diagnosis of CD was made through laboratory tests. The collection and use of samples from patients who tested positive for infection by *Leishmania infantum* for these experiments were authorized by the Research Ethics Committee (CEP) under protocol number 1 846.584 (CAAE 58.301.516.8.0000.5154), while the collection and use of samples from patients infected with *Trypanosoma cruzi* were authorized by the CEP under protocol number 2 163 043 (CAAE 64,048,117.3.0000.5154).

Samples were collected from individuals who had received at least 4 blood transfusions and from individuals residing in the same households as the polytransfused patients in endemic areas for VL. Asymptomatic infection was determined by enzyme immunoassay to confirm the presence of anti-*Leishmania* spp. antibodies and Polymerase Chain Reaction (PCR) to detect parasitic DNA. These samples were authorized by CAAE number 29,950,120.4.0000.5154.

2.2. Techniques used to confirm positive samples for *Leishmania infantum*

2.2.1. qPCR protocol used for selection and confirmation of positive samples from asymptomatic individuals selected for standardization of tests in the developed immunosensor

For molecular biology analyses, DNA extraction from the blood samples was performed using Qiagen's DNA Mini Kit from Qiagen (Hilden, Germany), following the manufacturer's recommended method. The samples were subjected to qPCR to identify *Leishmania spp.* With primers described by Nicolas et al. [26]. The reaction consisted of 1XSYBR Green PCR Master Mix (Life Technologies, Carlsbad, CA, USA), 10pM of each primer, 50 ng of DNA, and ultrapure water for a final volume of 20 μ L. Amplification was performed at an initial holding temperature of 95 °C for 5 min, followed by 40 cycles at 95 °C for 1 min, 60 °C for 1 min, and melting curve analysis in 1 °C increments from 60

°C to 95 °C. Each assay included an internal control of human beta-actin in each sample. The database was analyzed using Applied Biosystems 7500 Real-Time PCR Software v2.3 (Thermo Fisher Scientific, USA). DNA from *Trypanosoma cruzi* was used to demonstrate the absence of cross-reactivity of the selected target, as described by Nicolas et al. [26].

2.2.2. Commercial enzyme-linked immunosorbent assay (ELISA) protocol used to evaluate the positivity of the selected sample from asymptomatic individuals for the standardization of immunosensor tests

The qualitative detection of IgG antibodies against *Leishmania infantum* was performed from the serum of the samples collected through an enzyme immunoassay (ELISA) with a commercially available kit (BIOLISA LEISHMANIOSE VISCERAL® - Bioclin, Belo Horizonte, Brazil) according to the manufacturer's recommendations. Samples whose Elisa Index (EI) was ≥ 1.2 were considered positive.

2.2.3. Indirect ELISA

The indirect ELISA for the detection of IgG antibodies was performed as described in Martins et al. [22] (Figure S1).

The indirect ELISA method was used to detect immunoglobulin G (IgG) antibodies against *Leishmania infantum*. High-affinity plates (Thermo Scientific™ Nunc™, Waltham, MA, USA) were sensitized with antigens (1 $\mu\text{g}/\text{mL}$) diluted in 0.06 mol/L carbonate-bicarbonate buffer (pH 9.6) and incubated for 18 h at 4 °C. The plates were then washed six times with PBS containing 0.05 % Tween 20 (PBS-T) and blocked with PBS containing 5 % skimmed milk powder (Molico®, Nestlé®, São Paulo, Brazil - PBS-M5 %) for 4 h at room temperature. After washing again, serum samples diluted 1:40 in PBS-M5 % were incubated for 2 h at room temperature. Six subsequent washes were performed before adding peroxidase-conjugated anti-human IgG antibody (IgG/horse-radish peroxidase (HRP), Dako), diluted 1:2000, for incubation for 2 h at room temperature.

After washing again, the reaction was revealed with the addition of the enzyme substrate 1,2-orthophenylenediamine (OPD, Dako) with 0.05 % H_2O_2 , subsequently stopped with H_3PO_4 . Positive and negative controls were included on each plate. Quantification of antibody levels was performed using the ratio between the optical absorbance (Abs) of the sample and the cut-off value. The cut-off was calculated as the mean Abs of the negative control serum plus three standard deviations. Samples with an enzyme index (IE) greater than 1.4 were considered positive.

2.3. Maintenance of *L. infantum* parasite cultures

The promastigote form of *Leishmania infantum* was cultured in the Schneider medium, supplemented with 10 % fetal bovine serum. When

the exponential phase was reached, the parasites were quickly centrifuged at 200x g for 10 min at 25 °C to eliminate the dead ones. Then, the supernatant containing the live parasites was centrifuged at 3500 rpm for 25 min at 25 °C and then washed twice at 3500 rpm for 20 min at 25

°C using incomplete Roswell Park Memorial 17 Institute (RPMI, Gibco, USA) medium. The supernatant was discarded, and the pellet containing the parasites was frozen at -80 °C until antigen extraction.

2.3.1. Production of promastigote antigens from parasites

For extraction of soluble crude antigens, the pellet was resuspended in phosphate-buffered saline (PBS) containing 0.05 % NP40 (Nonidet P-40 Substitute, Roche - Switzerland) with the COMPLETE protease inhibitor [COMPLETE™ ULTRA Tablets, Mini, EASYpack, Roche 2 Applied Science, Switzerland), and the antigen was obtained by the method of freezing in liquid nitrogen and thawing in a 37 °C water bath, followed by centrifugation at 10,000x g for 30 min at 4 °C. After that, the supernatant containing the crude soluble antigen was aliquoted and stored at -80 °C. The protein concentration of the antigen was determined by the NanoDrop™ 2000 spectrophotometers (Thermo Fisher Scientific, USA). The technique was performed and adapted based on Scott et al. [32]. A polyacrylamide gel electrophoresis was also performed to the presence of soluble proteins of *Leishmania infantum* (Figure S2).

2.4. Construction of Immunosensor

2.4.1. Electrode selection

For the construction of electrochemical immunosensors, the choice of specialist platforms for the target analytes is a crucial step. Thus, in this work, screen-printed carbon electrodes (DPR-110, Metrohm DropSens, Spain) modified with electrodeposited gold were used, a protocol previously developed by Martins et al. [22] [22]. Furthermore, printed graphene electrodes (DPR-110 GPH, Metrohm DropSens, Spain), printed carbon electrodes (DPR-110) modified with graphene oxide (DPR-110-GO), and printed carbon electrodes (DPR-110) modified with graphene oxide with electrodeposited gold (DPR110-GO-Au) were evaluated to obtain a diagnostic platform capable of detecting asymptomatic patients.

2.4.2. Equipment selection

The potentiostat Em Stat 1 (PalmSens BV, The Netherlands) connected to a notebook (Vaio, Intel Core i5 (3rd Gen) 3210 M / 2.5 GHz) was used to take the readings.

2.4.3. Electrochemical experiments

Electrochemical analyses were performed by cyclic voltammetry (CV). The changes in the electrochemical signals of Ferri-Ferro Potassium Cyanide $[\text{Fe}(\text{CN})_6]^{4-}/[\text{Fe}(\text{CN})_6]^{3-}$ (5×10^{-3} mol/L) containing KCl (0.10 mol/L) were evaluated (scan rate of 100 mV/s, at room

temperature (25 ± 1 °C)). All solutions used were prepared using ultrapure water (MilliQ, resistivity value greater than 18.2 M Ω , Millipore Corporation, Burlington, MA, USA).

2.4.3.1. Devices. For the experiments, carbon screen-printed electrodes (DRP-110) and screen-printed electrodes modified with graphene (DRP-110 GPH) were used both purchased from DropSens (Oviedo, Asturias, Spain). These electrodes consist of a ceramic strip with a three-electrode system: working, reference and counter-reference, ideal for analyzing single drops. The reference is made of silver ink (known as silver pseudoreference electrode), while the counter reference and working electrode are made of carbon ink (DRP-110) or graphene ink (DRP-110 GPH), respectively.

In addition to the commercial electrodes mentioned, in this work we compared tests with carbon electrodes modified with graphene oxide. In graphene oxide-modified electrodes (DRP-110-GO), functionalized graphene oxide was added (15 μL) by adsorption onto carbon electrodes (DRP-110) at a concentration of 0.5 mg/dL and then electrochemically reduced.

Subsequently, in another group of carbon electrodes (DPR-110), in addition to the adsorption of graphene oxide, there was also performed the deposition of a gold film through CV in a gold chloride solution (HAuCl_3 , 1 g/L) prepared in 1 mol/L H_2SO_4 [22].

2.4.4. Immunosensor

For the construction of the immunosensor, 4 μL of the solution containing the total soluble antigens of *Leishmania infantum* was pipetted onto the working electrode and immobilized by adsorption. After drying the solution, blocking was performed to prevent non-specific binding by pipetting 4 μL of 1 % bovine serum albumin (BSA). Then, 4 μL of the patient's serum was pipetted. After all these steps, the electrodes were washed and dried. For the electrochemical evaluation of the antigen-antibody interaction, a solution of $[\text{Fe}(\text{CN})_6]^{4-}/[\text{Fe}(\text{CN})_6]^{3-}$ (5 mM) was used, and the reading was performed using the CV technique (Fig. 1). All readings were performed at room temperature ($25^\circ\text{C} \pm 1^\circ\text{C}$), and all tests were performed in triplicate.

2.4.5. Raman spectrophotometry

Electrode surface analyses were performed using the LabRAM HR Evolution, HORIBA equipment with HORIBA Scientific's LabSpec

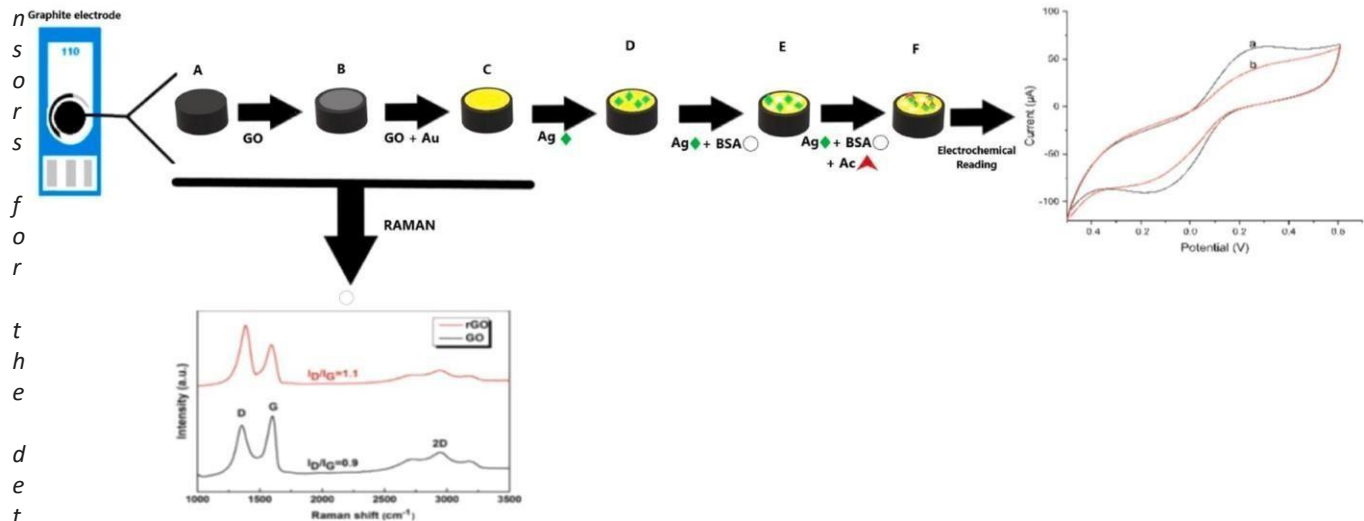


Fig. 1. Representative image of the electrochemical immunosensor developed using commercial carbon electrodes modified with graphene oxide and gold nanoparticles (DPR-110-GO-Au). The preparation steps of the immunosensors are as follows: (a) the commercial carbon electrode was used as the base platform; (B) carbon was modified with graphene oxide nanoparticles; (C) the electrodes already modified with graphene oxide were electroplated with gold nanoparticles; (D) after material modifications, the gross antigen of *Leishmania infantum* was immobilized in modified surface of the electrodes; (E) for blocking nonspecific interactions, a 1 % bovine serum albumin (BSA) blocking solution was coupled to the platform; (F) after preparations, the antibodies were coupled (real sample/serum); and (G) finally, the electroanalytic solution was inserted, and the process of transduction was started; thus, the surface with the antigen probe was automatized as presented in a cyclic voltammetry (CV). For the evaluation of chemical modifications performed on the surface of the electrodes, Raman spectrophotometry was used as a means of verification.

software (LabSpec 6 Spectroscopy Suite) and optical microscope (Olympus BX41) in x10Vis, x40UV, and x100Vis objectives. The 10x (x10Vis) and 100x (x100Vis) objectives are used for wavelengths in the visible region (vis), and the 40x (x40UV) objective is used for the ultraviolet region. The images were generated at the Laboratory of New Insulating and Semiconductor Materials as well as the Multiuser Microscopy Laboratory at the Federal University of Uberlândia, Minas Gerais (MG), Brazil.

2.4.6. Specificity and selectivity

Sera containing anti-*Trypanosoma cruzi* antibodies from individuals with CD were also tested to confirm that the immunosensor would be able to eliminate possible cross-reactions.

2.4.7. Statistical analysis

With the aim of ensuring uniformity and clarity in the analyses, and following protocols described by [22], we constructed column charts using peak current data obtained using cyclic voltammetry (CV). The current percentages, which represent the oxidation and reduction currents of the redox probe, were calculated in relation to the initial CV (without biomolecule), considered as a reference value (100 %). Consequently, a low percentage of current indicates a high coverage of the electrode surface by biomolecules, either through proportional immobilization or specific molecular recognition. In summary, column plots and analysis of current percentages provide valuable information about the interaction between the biomolecules and the redox probe. The decrease in current reflects the extent of electrode surface coverage, revealing details about the efficiency of immobilization and the specificity of molecular recognition. The analyses are descriptive and are based on the comparative study of the voltammograms and their interpretations in bar charts and linear graphs (calibration).

3. Results and discussion

3.1. Samples

The asymptomatic individuals used in our tests come from an endemic area for VL, and the confirmation of positivity in these patients was confirmed through positive qPCR for the detection of parasitic DNA or positive commercial ELISA tests for the detection of antibodies. Table 1 shows that the samples of selected asymptomatic individuals were identified as follows: SBP-14 and FO 01P Patients diagnosed with leishmaniasis were identified as follows: VAL and LV1. Those diagnosed with CD were denoted as CH1 and CH2.

3.2. Graphene and modification

Fig. 2 shows the activation of screen-printed electrodes sold with graphene (110-GPH) and screen-printed graphite electrodes with graphene oxide adsorbed (before and after the reduction). The choice of KCl as electrolyte and the use of cyclic voltammetry were based on the ionic properties of the KCl electrolyte, as it dissociates into K^+ and Cl^- ions, improving the transfer of electrons between the electrode surface and the biochemical material, optimizing the biosensor performance. Furthermore, its ionic strength and neutrality are responsible for improvements in the adsorption of graphene oxide, promoting a stable and

Table 1
Identification of selected samples and description of confirmatory tests used.

	Identification	Bioclin ELISA	Indirect ELISA	qPCR
Asymptomatic	SBP 14	7.45	2.78	Negative
	FO 01P	2.14	1.98	Positive
Symptomatic	VAL	NP	4.53	NP
	LV1	NP	4.24	NP
Chagas disease	CH1	NP	5.94	NP
	CH2	NP	8.89	NP
Cutaneous	LA 01	NP	2.48	NP
	LA 05	NP	2.64	NP

*NP = Test not performed. Bioclin ELISA (EI > 1.2); Indirect ELISA (EI > 1.4).

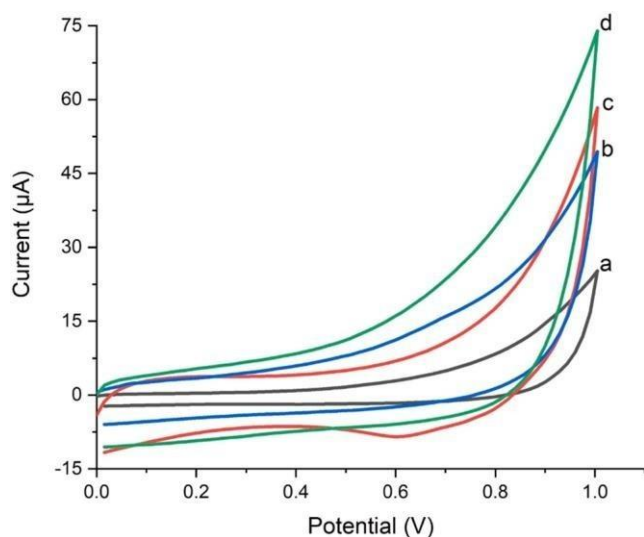


Fig. 2. Cross-platform comparison cyclic voltammogram in electroanalytical substance KCl 0,1 mol/L; a: commercial graphene electrode, area in value 4.9780; b: commercial graphene electrode after reduction, area in value 13.0393; c: graphite electrode with adsorbed graphene oxide, area in value 14.7234; d: graphite electrode with graphene oxide adsorbed after reduction, area in value 21.8200.

efficient interface for the immobilization of the biomaterial, and not influencing undesirable electrostatic effects, contributing to the reproducibility of the process.

In this work, the OriginLab Corporation 2019 software, a widely used tool for scientific data analysis, was used to study cyclic voltammograms (VCs). The area under the VC curve, a crucial parameter for understanding the electrochemical system, was calculated using the specific function for area analysis. Through this analysis, we obtained valuable information about the electrochemical behavior of the system under study. The type (Area Type) parameter was used to be based on results described in Fig. 2 determine the absolute area of the VC, considering all current values, both positive and negative. This area under the curve represents the quantification of charge transferred during the redox process, providing information about the efficiency of electrode modification and the interactions between the analyte and the electrochemical surface. The joint analysis of the area under the VC curve with the physicochemical characterization of the analyte and the developed electrochemical system is fundamental for a complete understanding of the redox process and the efficiency of electrode modification. This approach allows optimization of the electrochemical system for specific applications, such as electrochemical sensors and biosensors.

The results show a higher current in graphite with adsorbed graphene oxide. On comparing the percentage areas in value, we observed the following: A-B: 161.936349 % gain; C-D: 48.199199 % gain; A-C: 195.7666787 % graphite gain with graphene adsorbed on initial activation; and B-D: 67.339893 % graphite gain with adsorbed graphene in the final activation.

Previous research has reported that the use of graphene oxide compared to graphene is more advantageous in aqueous solutions due to the ability to increase the surface area of the electrodes, improve electron transfer, and increase the conductivity [7,30].

Graphene-based electrochemical detection platforms are responsible for increasing the surface area, electron transfer, sensitivity, and specificity of these devices [3].

Graphene oxide interacts well with biomolecules, showing good biocompatibility. It has several applications in the health sector and can be used both in diagnoses and disease treatments. It has antimicrobial, antitumor, antioxidant, and antiparasitic actions; it can also be used to identify various biomolecules [17,20,34]. However, graphene oxide

presents better results when it is reduced [1,14].

Based on results described in Fig. 2, we initially proceeded to develop an immunosensor, comparing the performance of commercial graphene (DPR-110 GPH) and graphite with adsorbed graphene oxide (DPR-110-GO). The results showed that graphene was able to increase the surface area, but graphene oxide provided a better reading area, enabling improved detection of anti-*Leishmania* antibodies in sera from asymptomatic individuals (Fig. 3).

The graphene oxide (GO) modified electrode showed a higher percentage current response compared to the commercial graphene electrode. This difference can be attributed to the structural characteristics of the GO-modified electrode, such as its larger surface area, which facilitates the adsorption of the analyte and, consequently, increases the sensitivity of the platform for the detection of anti-*Leishmania* antibodies. In summary, the search for a greater percentage difference in the current response aims to optimize the detection of anti-*Leishmania* antibodies, allowing a more precise differentiation between patients with the disease and those with other conditions that may present crossover results. The structural characteristics of the GO-modified electrode, such as its greater surface area, contribute to this optimization of the platform.

Based on these results (Fig. 3), we chose to follow the tests with graphite electrodes with adsorbed graphene oxide since this modification presented a better potential for the construction of this electrochemical immunosensor. This platform makes it possible to enhance the properties of graphene oxide and provides a better financial cost-benefit compared to the diagnostic proposal presented. Furthermore, in electrochemical tests evaluated by CV, the results can follow the analysis based on oxidation or reduction; in this work, we chose to follow our analysis evaluating the oxidation peaks, as these exhibited better performance on the target platform.

The article by Martins et al. [22] [22] showed the need to incorporate gold electrodeposition to improve the surface area and consequent increase in the detection window. Thus, we tested whether gold electrodeposition would be the best option for the graphite electrode adsorbed with graphene oxide as well. We also decided to test if the graphite electrode deposited with gold platform developed by Martins et al. [22] could detect antibodies anti-*Leishmania infantum* in asymptomatic as well as symptomatic individuals (fig. 4a-b).

In fact, the electrodeposition of gold nanoparticles is necessary to increase the surface area of electrochemical platforms since it is capable of generating a decisive current gain to increase the electrochemical precision. In addition, VL antigens have specificities that favor the electrodeposition of gold [8,22].

The graphite electrode modified with gold demonstrated recognition of anti-*Leishmania* antibodies in the serum of the asymptomatic individual (Fig. 4a), but the detection process was less efficient than the graphite electrode adsorbed with graphene oxide and gold, which showed a significant drop in current (Fig. 4b).

Finally, in addition to demonstrating the ability to detect both symptomatic and asymptomatic individuals, we tested serum samples from chagasic individuals to prove that the differentiation between anti-*Leishmania infantum* and anti-*Trypanosoma cruzi* antibodies also occurred in this electroanalytical platform. As shown in Fig. 5 and the correlation chart in Fig. 6, the detection of individuals positive for CD showed only a slight drop in current, which was considered negative. Fig. 6 also shows an advanced analysis of the performance of the developed electrochemical biosensor, demonstrating its ability to detect anti-*Leishmania* antibodies with precision and efficiency, while in the ELISA method the anti-*Trypanosoma cruzi* antibodies present in samples from chagasic patients were "confused" with antibodies anti-*Leishmania infantum*. This is important because the parasites of the *Leishmania* present structures and proteins similar to *Trypanosoma cruzi*, which causes CD, as both are trypanosomatids. Thus, serological tests for the detection of anti-*Leishmania* antibodies may present false-positive results in individuals with CD and even other diseases [23,36].

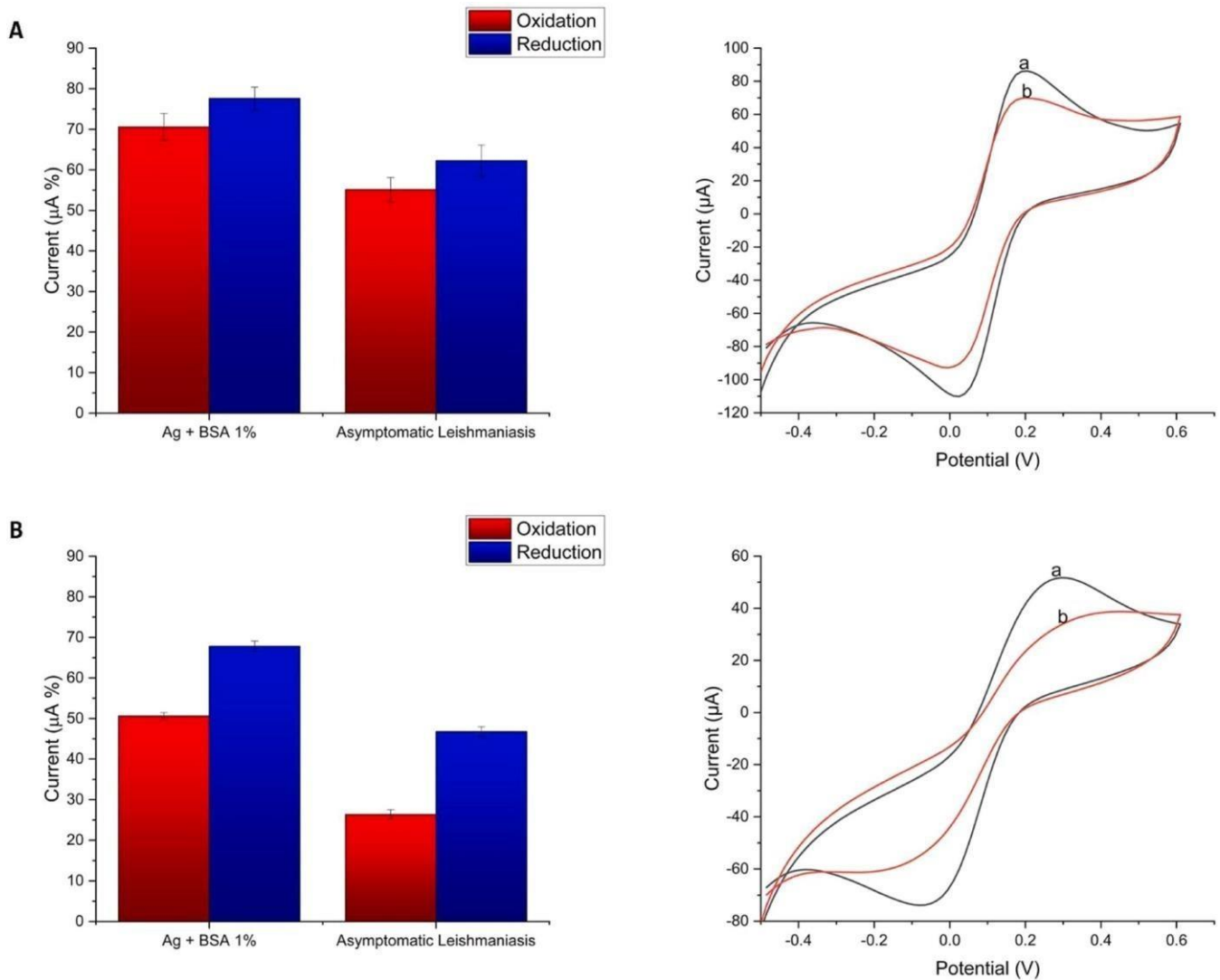


Fig. 3. Cyclic voltammograms for the redox probe and bar plots representing data referring to the detection of anti-*Leishmania* antibodies in an asymptomatic individual for leishmaniasis infection from an endemic area on a commercial graphene platform (A) and adsorbed graphene oxide (B). We emphasize that in "a" we represent the electrochemical platform consisting of a surface modified with biomolecules, such as BSA (bovine serum albumin) and specific antigen, in this case BSA acts as a blocking layer, while the antigen serves as a recognition site for the analyte. In "b" we represent the analyte, in this case, the antibody, which binds to the antigen on the surface of the electrochemical platform, triggering a measurable electrochemical response, this response is used to detect and quantify the presence of the antibody in the tested sample. Error bars represent the mean and standard deviation (SD) of triplicate measurements for each experimental condition.

Sera from individuals positive for cutaneous leishmaniasis were also tested. Although the antigen used is from *Leishmania infantum*, it was expected that there would be some recognition of cutaneous anti-*Leishmania* antibodies since both parasites belong to the same genus and therefore have very similar structures (antigens). A study by Viana et al. [33] even showed that the immunotherapeutic treatment of dogs naturally infected with *Leishmania infantum*, using *Leishmania amazonensis* antigens (etiological agent of cutaneous leishmaniasis) as a basis, resulted in clinical improvement in the animals, with a reduction in the parasite burden, at least initially [33]. Leal et al. (2015) also observed partial protection in mice challenged with *Leishmania infantum* and immunized with a *Leishmania amazonensis* antigen vaccine associated with an adjuvant [16].

The identification of *Leishmania* proteins using bioinformatics tools showed the existence of proteins shared between species as well as the existence of exclusive proteins [19]. The immunosensor developed here was able to differentiate the antibody detection of patients with visceral and cutaneous leishmaniasis, although not as well as the exclusion of patients with CD. However, a form of future improvement would be the

purification of antigens from both species to further increase the specificity [10].

In our study, we also performed an immunoenzymatic assay on the same samples used in the immunosensor, and as expected, there was a cross-reaction with CD (Figure S1). These results corroborate data in the literature that indicate high phylogenetic compatibility between the parasites *Leishmania* sp. and *T. cruzi*, which influences the creation of effective diagnoses for the detection and differentiation of diseases caused by these pathogens. In line with this ELISA finding, currently, there are tests available that may have low sensitivity and/or specificity [31]. When analyzing the literature in search of devices aimed at detecting VL (Table 2), it is possible to observe a better rate of sensitivity and specificity of electrochemical techniques compared to the other techniques studied.

Fig. 7 shows the analytical curve of anti-*Leishmania* antibodies. In this redox probe, the current value is inversely proportional to the consumption of antibodies. Sera at different dilutions were analyzed to validate sensor sensitivity analyses. The sera were diluted in the following ratios: 1, 1:3.5, 1:50, 1:1,000, and 1:100,000. This plot shows

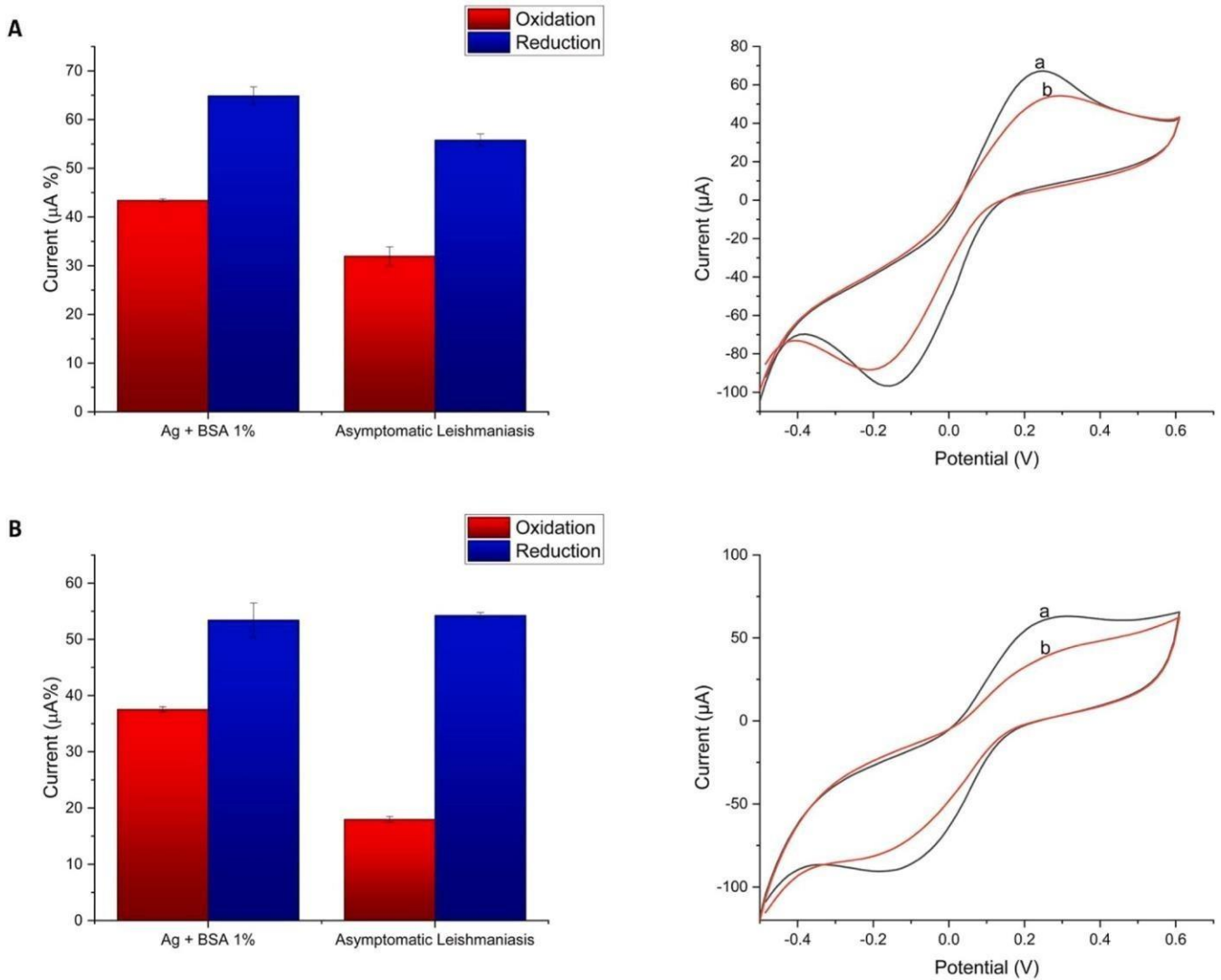


Fig. 4. - Cyclic voltammograms for the redox probe and bar plots representing data referring to the detection of anti-*Leishmania* antibodies in an asymptomatic individual for leishmaniasis infection from an endemic area on a commercial graphite electrode modified with gold (A) and commercial graphite adsorbed with graphene oxide and modified with gold (B). We emphasize that in "a" we represent the electrochemical platform consisting of a surface modified with biomolecules, such as BSA (bovine serum albumin) and specific antigen, in this case BSA acts as a blocking layer, while the antigen serves as a recognition site for the analyte. In "b" we represent the analyte, in this case, the antibody, which binds to the antigen on the surface of the electrochemical platform, triggering a measurable electrochemical response, this response is used to detect and quantify the presence of the antibody in the tested sample. Error bars represent the mean and standard deviation (SD) of triplicate measurements for each experimental condition.

the correlation coefficient of 0.99889 (for the equation: $i(\%)$

$= 49.6972 \times 7.69631[\text{serum dilution ratio}]$), revealing a quantification limit of 17.25 % and detection limit 5.75 % (in current percentage data)

or revealing a quantification limit of 16.75 mg/mL and detection limit 5.58 mg/mL (SBP-14). Inset shows tolerance from linear regression of a peak current (%) vs. concentration of antibodies of leishmaniasis.

Thus, given our results, we carried out an analysis of the surface of the electrodes using the Raman spectrophotometry technique. This tool is very useful in the characterization of carbonaceous materials, such as graphene and its derivatives. These materials have about 3 absorption bands and vibrational modes that are active in Raman spectroscopy, giving rise to the D and G bands. The D band (appearing around 1330 cm^{-1}) is the result of the breathing mode of the six-membered ring formed by sp^2 carbon.

In a perfect crystalline lattice, the vibrational mode is prohibited. So in graphene, this band appears with low intensity. However, if there are defects in the crystalline lattice — the result of oxidation, for example, in

the preparation of graphene oxide (GO) — the intensity of this band

increases. The G band, on the other hand, arises from two vibrational modes (also in the plane, originating from E_{2g} and E_{1u}) around 1590 cm⁻¹ [12]. These bands can be used as an indication of material change. Generally, in GO, the intensities of these bands are very close, with the G band exhibiting slightly higher intensity. The ratio of the intensities between these bands, known as ID/IG bands, is typically below 1.

The production of reduced graphene oxide (rGO) via GO reduction results in a small shift in the number of waves (cm⁻¹) of absorption in the D, G, and 2D bands, with a more significant increase in the intensity of the D band resulting in a larger ID/IG than the GO [9,15]. In the region of approximately 2700 cm⁻¹, the 2D band appears. This band is a D harmonic band, which occurs in a vibrational spectrum of a molecule

when the molecule makes a transition from the ground state ($=\nu 0$) to the second excited state ($\nu=2$) [12].

When analyzing the results, we observed that the Raman spectrum of the commercial graphene electrode (Fig. 8a-1) presents a characteristic profile of a material composed of graphene, as the D band presents low intensity, as mentioned before. The spectra of the initial samples of the

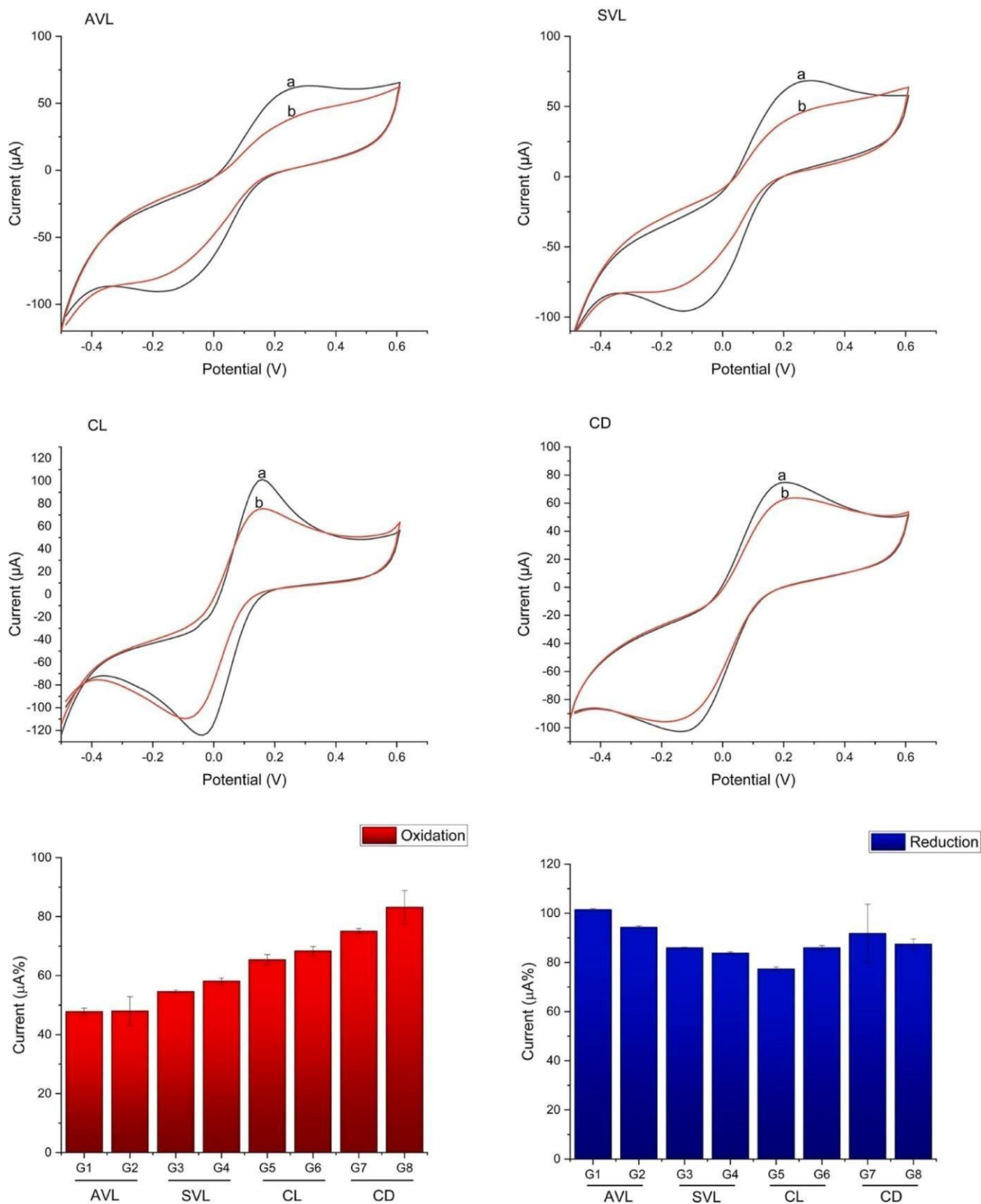


Fig. 5. Graphite electrode with adsorbed graphene and electrodeposited gold, where we can observe asymptomatic visceral leishmaniasis (AVL), symptomatic visceral leishmaniasis (SVL), cutaneous leishmaniasis (CL), and Chagas disease (CD). We emphasize that in "a" we represent the electrochemical platform consisting of a surface modified with biomolecules, such as BSA (bovine serum albumin) and specific antigen, in this case BSA acts as a blocking layer, while the antigen serves as a recognition site for the analyte. In "b" we represent the analyte, in this case, the antibody, which binds to the antigen on the surface of the electrochemical platform, triggering a measurable electrochemical response, this response is used to detect and quantify the presence of the antibody in the tested sample. Error bars represent the mean and standard deviation (SD) of triplicate measurements for each experimental condition.

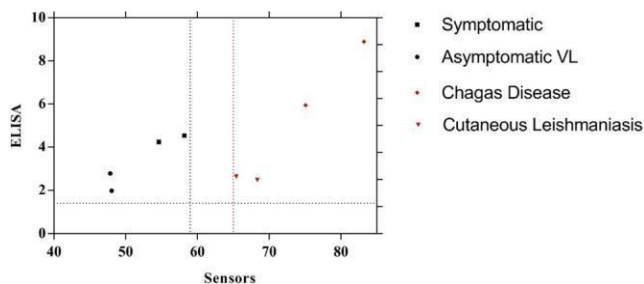


Fig. 6. Correlation graph between results from electrochemical sensors (x-axis) and ELISA results (y-axis), where we can observe asymptomatic visceral leishmaniasis, symptomatic visceral leishmaniasis, cutaneous leishmaniasis, and Chagas disease.

Table 2
Comparison of Visceral Leishmaniasis detection methods.

Method	Material	Sensitivity/ Specificity	References
ELISA	DNA/blood	91.47–97.5 %/100 %	[1,6]
PCR	Urine	93.8 %–95 %/100 %	[1,4]
PCR	Serum	80.7–93.9 %/95.7–100 %	[7]
Electrochemical	Serum	100 %/100 %	[2,5]
Immunochromatographic	Serum/total blood*	92.7–96.3 %/100 %	[3*,6]

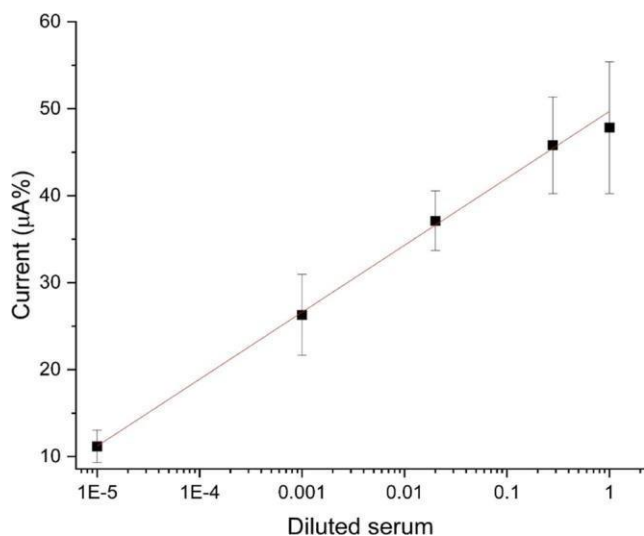


Fig. 7. Analytical curve obtained from current peak percentages for measurements of the biosensors in the presence of diluted serum (1; 1:3.5; 1:50; 1:1000; and 1:100,000) containing antibodies. The percentages were calculated from the initial CV (without biomolecule), totalling 100 %. Error bars represent the mean and standard deviation (SD) of triplicate measurements for each experimental condition. To carry out these tests, graphite modified with graphene oxide and gold was used. The analytical curve of the device developed for leishmaniasis has the “Y” axis representing the current in micro Ampere (%) and the “X” axis representing the dilution of the serum from the positive asymptomatic patient, this provides valuable information about the sensitivity and specificity of the biosensor for disease detection. Thus, the analytical curve shows a gradual increase in current as serum dilution decreases.

pre-treatment graphene electrode (Fig. 8a- 4); 1 cycle between 0.0 and 1.0 V), post-treatment graphene electrode (Fig. 8a- 3); 1 cycle between 0.0 and 1.0 V), graphene electrode in electrochemical reduction treatment with KCl (Fig. 8A- 2); 10 cycles between 0.015 and –1.5 V) showed a small increase in I_D/I_G ratio, as shown in Fig. 8, due to the increase in

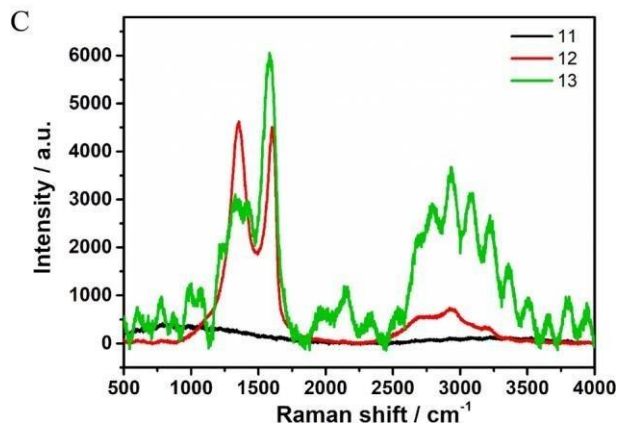
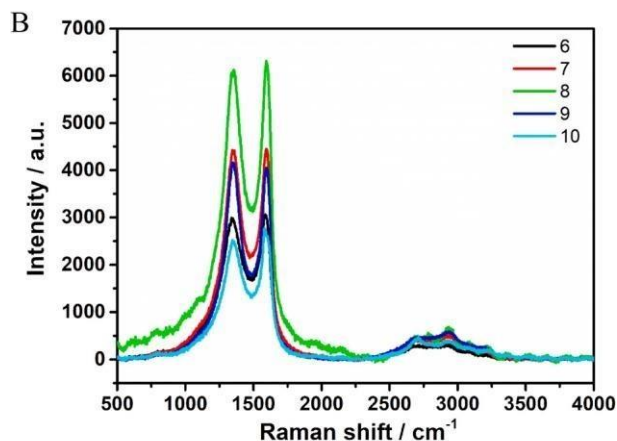
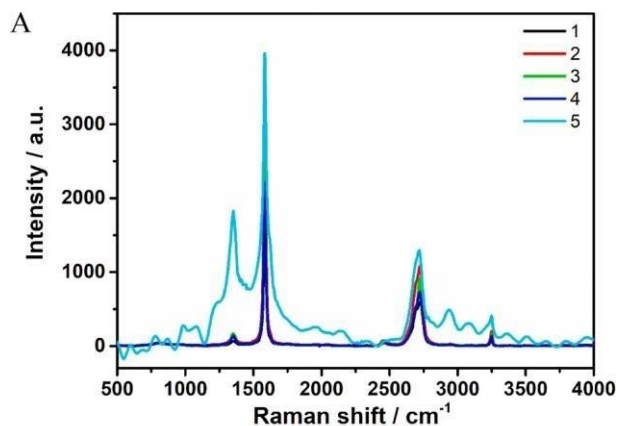


Fig. 8. In (A), representative figure of analysis by Raman spectrophotometry of commercial graphene electrodes. In (1), the commercial graphene data - laser 532 BL-SD are represented, in (2) the reduced commercial graphene data - laser 532 BL-SD are represented, in (3) the pre-reduced activated commercial graphene data - laser 532 BL-SD are represented, in (4) the post-reduced activated commercial graphene data - laser 532 BL-SD are represented, in (5) the gold-modified commercial graphene data - laser 532 BL-SD are represented. In (B) representative figure of analysis of commercial carbon electrodes modified with graphene oxide by Raman spectrophotometry. In (6), we observe the graphite electrode laser 532 BL-SD, in (7) we observe the graphite electrode the reduced graphene data - laser 532 BL-SD are represented, in (8) we observe the gold-modified graphite electrode the reduced graphene data - laser 532 BL-SD are represented, in (9) the post-reduced activated commercial graphite electrode data - laser 532 BL-SD are represented, in (10) the pre-reduced activated commercial graphite electrode data - laser 532 BL-SD are represented. In (C) representative figure of analysis by Raman spectrophotometry of the chemical elements used. In (11) are represented the KCL, in (12) the Grafeno and in (13) the gold - laser 532 BL.

the defect in the crystalline graphene network resulting from oxidation caused by the electrochemical treatment. On the other hand, the Au deposition (20 cycles between—0.4 and 1.2 V and sulfuric acid H₂SO₄), sample commercial graphene electrode and Au, resulted in a greater introduction of defects in the graphene crystal lattice ($I_D/I_G=0.46$) given the greater potential and greater number of electrochemical cycles in H₂SO₄ used in the preparation of this sample.

The addition of GO to the graphite electrode produced samples with a Raman spectrum characteristic of GO i.e., the intensity of the D and G bands was very close, as can be seen in Fig. 8. The samples commercial graphite electrode and graphene (Fig. 8b– 10) (1 cycle between 0.0 and 1.0 V) resulted in similar I_D/I_G ratios, showing that this type of treatment did not significantly change the material. On the other hand, the samples commercial graphite electrode and graphene (Fig. 8b– 9) (1 cycle between 0.0 and 1.0 V after the electrochemical reduction of GO) and commercial graphite electrode and reduced graphene (Fig. 8B– 7) (10 cycles between 0.015 and—1 0.5 V) resulted in an increase in the I_D/I_G ratio, indicating the conversion of GO to rGO via electroreduction.

Fig. 8 show the spectra of the graphene and gold samples, respectively, while the I_D/I_G ratios for these samples are shown. The difference between is that a baseline correction was performed in Fig. 8a. Upon analyzing Fig. 8b, it is observed that in the region around 1300 cm⁻¹, there does not seem to be an absorption band but only noise. Therefore, even after correcting the baseline, as shown in Fig. 8a, it is not possible to determine the true intensity of the D band for these samples, which in turn affects the obtained I_D/I_G value.

4. Conclusion

The research developed in this work expands the diagnosis of human visceral leishmaniasis, here we highlight the early detection of asymptomatic patients. Through the electrodeposition of gold nanoparticles on carbon electrodes, we developed electrochemical immunosensors with high sensitivity and specificity, overcoming the challenges of traditional methods.

The results demonstrated that the graphite electrode modified with graphene oxide and gold was efficient in detecting anti-*Leishmania* antibodies in symptomatic and asymptomatic individuals, without risk of cross-reactivity with CD. Gold electrodeposition on carbon electrodes modified with graphene oxide provided an ideal platform for the immobilization of specific antigens, allowing the precise recognition of epitopes present in the serum of patients with visceral leishmaniasis.

This innovative approach solves a crucial problem with commercially available screening tests, which often fail to identify asymptomatic patients. Due to the test's high sensitivity and specificity and low cost, it can be a valuable diagnostic tool, especially in regions with limited infrastructure. The results showed that surfaces functionalized with GO and electrodeposited with gold are interesting platforms for the development of an immunosensor.

The biosensor produced presents interesting properties, such as good selectivity and sensitivity. This is a promising technique for molecular analysis of a VL-specific biomarker. Future studies will expand the system to determine VL in plasma and saliva samples, in addition to adding stability and repeatability tests. Our research is not limited to sensor development. We intend to improve and adapt them for public health applications, enabling large-scale, high-performance tests. Future studies will focus on the selection of purified antigens for the diagnosis of asymptomatic patients and the development of sensors with long stability periods.

We believe that electrochemical immunosensors modified with graphene oxide and gold electrodeposition represent a promising tool for the specific and selective diagnosis of visceral leishmaniasis. With a reduced cost compared to Western blot and superior performance to ELISA, this technology paves the way for more effective detection of the disease, especially in its early stages, when treatment is most crucial and the chances of a cure are greater.

Our research contributes significantly to the advancement of the area of biosensors and the fight against visceral leishmaniasis, with a main focus on the early detection of asymptomatic patients. Through the optimization and validation of electrochemical immunosensors, we hope to contribute to future research that aims to transform this technology into a practical and accessible tool for the accurate and effective diagnosis of disease, saving lives and promoting public health.

5. Funding

This work was supported by the Research Foundation of the State of Minas Gerais (FAPEMIG, APQ – 01083-16), the National Council for Scientific and Technological Development (CNPq, 465389/2014-7 INCTBio), the Coordination for the Improvement of Higher Education Personnel (CAPES, financial code 001), and the Pro-Rectorcy for Research and Post-Graduation of Federal University of Triângulo Mineiro (UFTM).

CRedit authorship contribution statement

Beatriz R. Martins: Writing – review & editing, Writing – original draft, Visualization, Validation, Methodology, Investigation, Formal analysis, Data curation, Conceptualization. **Cristhianne Molinero R. Andrade:** Writing – review & editing, Writing – original draft, Visualization, Validation, Methodology, Investigation, Formal analysis, Data curation, Conceptualization. **Guilherme F. Simão:** Writing – review & editing, Software, Methodology, Investigation, Formal analysis. **Rhéltheer de Paula Martins:** Writing – review & editing, Investigation. **Luana Barbosa Severino:** Writing – review & editing, Investigation. **Sarah Cristina Sato Vaz Tanaka:** Writing – review & editing. **Loren Q. Pereira:** Writing – review & editing. **Marcos Vinicius da Silva:** Writing – review & editing. **Fernanda Bernadelli de Vito:** Writing – review & editing. **Carlo José Freire de Oliveira:** Writing – review & editing. **Helio Moraes de Souza:** Writing – review & editing. **Anderson Barbosa Lima:** Writing – review & editing, Software, Methodology, Investigation, Formal analysis. **Virmondes Rodrigues Júnior:** Writing – review & editing, Visualization, Validation, Investigation, Formal analysis, Data curation. **Jose Roberto Siqueira Junior:** Writing – review & editing, Visualization, Validation, Investigation, Formal analysis, Data curation. **Renata Pereira Alves:** Writing – review & editing, Writing – original draft, Visualization, Validation, Supervision, Resources, Project administration, Methodology, Investigation, Funding acquisition, Formal analysis, Data curation, Conceptualization.

Declaration of competing interest

The authors declare no conflict of interest.

Data availability

The data that has been used is confidential.

Acknowledgments

We thank the funding agencies Research Foundation of the State of Minas Gerais (FAPEMIG), the National Council for Scientific and Technological Development (CNPq), the Coordination for the Improvement of Higher Education Personnel (CAPES), and the Pro-Rectorcy for Research and Post-Graduation of Federal University of Triângulo Mineiro (UFTM).

References

- [1] S. Azizighannad, S. Mitra, Stepwise reduction of Graphene Oxide (GO) and its effects on chemical and colloidal properties, *Sci. Rep.* 8 (2018) 1–8, <https://doi.org/10.1038/s41598-018-28353-6>.
- [2] R. Badaro, T.C. Jones, E.M. Carvalho, D. Sampaio, S.G. Reed, A. Barral, R. Teixeira, W.D. Johnson, New perspectives on a subclinical form of visceral leishmaniasis, *J. Infect. Dis.* 154 (1986) 1003–1011, <https://doi.org/10.1093/infdis/154.6.1003>.
- [3] Y. Bai, T. Xu, X. Zhang, Graphene-based biosensors for detection of biomarkers, *Micromachines (Basel)* 11 (2020), <https://doi.org/10.3390/mi11010060>.
- [4] L.S. Barcelos, A.A.S.de Aguiar, F.N.G. Boni, L.E.P. Carneiro, T.B.de Carvalho, E. Peresi-Lordelo, Diagnóstico da doença de Chagas: avaliação da reação cruzada em pacientes com Leishmaniose visceral, *Res. Soc. Dev.* 10 (2021) e55910414597, <https://doi.org/10.33448/rsd-v10i4.14597>.
- [5] D.E. Barraza, P.I. Nanni, M.E. Bracamonte, R.E. Chaile, C.B. Goy, L. Acuña, J. D. Marco, R.E. Madrid, Simple and promising paper-based electrochemical platform for serological detection of American tegumentary leishmaniasis, *Mem. Inst. Oswaldo Cruz* 119 (2024) 1–10, <https://doi.org/10.1590/0074-02760230149>.
- [6] P.A. Bates, Transmission of Leishmania metacyclic promastigotes by phlebotomine sand flies, *Int. J. Parasitol.* 37 (2007) 1097–1106, <https://doi.org/10.1016/j.ijpara.2007.04.003>.
- [7] J.S.F. Camargos, A.D.O. Semmer, S.N. Silva, Características E Aplicações Do Grafeno E Do Óxido De Grafeno E As Principais Rotas Para Síntese, *J. Eng. Exact Sci.* 3 (2017) 1118–1130, <https://doi.org/10.18540/jcecvl3iss8pp1118-1130>.
- [8] T.A.R. Cordeiro, M.V.C. Gonçalves, D.L. Franco, A.B. Reis, H.R. Martins, L. F. Ferreira, Label-free electrochemical impedance immunosensor based on modified screen-printed gold electrodes for the diagnosis of canine visceral leishmaniasis, *Talanta* 195 (2019) 327–332, <https://doi.org/10.1016/j.talanta.2018.11.087>.
- [9] X.Y. Cui, R.K. Zheng, Z.W. Liu, L. Li, B. Delley, C. Stampfl, S.P. Ringer, Magic numbers of nanoholes in graphene: tunable magnetism and semiconductivity, *Phys. Rev. B - Condens. Matter Mater. Phys.* 84 (2011) 1–7, <https://doi.org/10.1103/PhysRevB.84.125410>.
- [10] R.T. Daltro, L.M. Leony, N.E.M. Freitas, A.A.O. Silva, E.F. Santos, R.P. Del-Rei, M.E. F. Brito, S.P. Brandão-Filho, Y.M. Gomes, M.S. Silva, Cross-Reactivity using chimeric trypanosoma cruzi antigens: diagnostic performance in settings where chagas disease and American cutaneous or visceral leishmaniasis are Coendemic, *Ramona* 57 (2019) 1–10, <https://doi.org/10.1128/JCM.00762-19>.
- [11] A.M. Díez-Pascual, Graphene-based polymer nanocomposites: recent advances, *Polymers (Basel)* 14 (2022) 10–13, <https://doi.org/10.3390/polym14102102>.
- [12] A.C. Ferrari, D.M. Basko, Raman spectroscopy as a versatile tool for studying the properties of graphene, *Nat. Nanotechnol.* 8 (2013) 235–246, <https://doi.org/10.1038/nnano.2013.46>.
- [13] K.F. Fukutani, V. Figueiredo, F.S. Celes, J.R. Cristal, A. Barral, M. Barral-Netto, C. I. de Oliveira, Serological survey of Leishmania infection in blood donors in Salvador, northeastern Brazil, *BMC Infect. Dis.* 14 (2014) 1–8, <https://doi.org/10.1186/1471-2334-14-422>.
- [14] B.J. Hong, O.C. Compton, Z. An, I. Eryazici, S.T. Nguyen, Successful stabilization of graphene oxide in electrolyte solutions: enhancement of biofunctionalization and cellular uptake, *ACS Nano* 6 (2012) 63–73, <https://doi.org/10.1021/nn202355p>.
- [15] D. Konios, M.M. Stylianakis, E. Stratakis, E. Kymakis, Dispersion behaviour of graphene oxide and reduced graphene oxide, *J. Colloid Interface Sci.* 430 (2014) 108–112, <https://doi.org/10.1016/j.jcis.2014.05.033>.
- [16] J.M. Leal, M. Mosquini, L.P. Covre, N.P. Staggmiller, R.R. Rodrigues, D. Christensen, H.L.D.M. Guedes, B. Rossi-Bergmann, D.C.D.O. Gomes, Intranasal vaccination with killed Leishmania amazonensis promastigotes antigen (LaAg) associated with CAF01 adjuvant induces partial protection in BALB/c mice challenged with Leishmania (infantum) chagasi, *Parasitology* 142 (2015) 1646, <https://doi.org/10.1017/S0031182015001584>.
- [17] J.-S. Lee, J. Kim, H. Shin, D.-H. Min, Graphene oxide-based molecular diagnostic biosensor for simultaneous detection of Zika and dengue viruses, *2D Mater* 7 (2020) 1–12, <https://doi.org/10.1088/2053-1583/ab9a64>.
- [18] M.F. L'èveque, E. Battery, P. Delaunay, B.E. Lmimouni, K. Aoun, C. L'ollivier, P. Bastien, C. Mary, C. Pomares, J. Filliaux, L. Lachaud, Evaluation of six commercial kits for the serological diagnosis of mediterranean visceral leishmaniasis, *PLoS Negl. Trop. Dis.* 14 (2020) 1–12, <https://doi.org/10.1371/journal.pntd.0008139>.
- [19] B.S.S. Lima, L.C. Fialho, S.F. Pires, W.L. Tafuri, H.M. Andrade, Immunoproteomic and bioinformatic approaches to identify secreted Leishmania amazonensis, L. braziliensis, and L. infantum proteins with specific reactivity using canine serum, *Vet. Parasitol.* 223 (2016) 115–119, <https://doi.org/10.1016/j.vetpar.2016.04.019>.
- [20] R.K. Maech, A.I. Jaafar, B.A.A.H. Hasoon, N.N. Hussein, Preparation and characterization of graphene oxide for biological application, *Drug Invent. Today* 14 (2020) 2020, <https://doi.org/10.13140/RG.2.2.23987.86562>.
- [21] E.L. Malchiodi, M.G. Chiaramontb, N.W. Taranto, R.A. Margni, Cross-reactivity studies and differential serodiagnosis of human infections caused by Trypanosoma cruzi and Leishmania spp; use of immunoblotting and ELISA with a purified antigen (Agl63B6), *Clin. Exp. Immunol.* 97 (1994) 417–423, <https://doi.org/10.1111/j.1365-2249.1994.tb06104.x>.
- [22] B.R. Martins, Y.O. Barbosa, C.M.R. Andrade, L.Q. Pereira, G.F. Simão, C.J. de Oliveira, D. Correia, R.T.S. Oliveira, M.V. da Silva, A.C.A. Silva, N.O. Dantas, V. Rodrigues, R.A.A. Munoz, R.P. Alves-Balvedi, Development of an electrochemical immunosensor for specific detection of visceral leishmaniasis using gold-modified screen-printed carbon electrodes, *Biosensors* 10 (2020) 1–15, <https://doi.org/10.3390/BIOS10080081>.
- [23] H.J.de Matos, A.Y.das N. Pinto, A.M.M. Miranda, F.L.C. Silva, F.L.de P. Ramos, Cross-reactivity in serological tests between Chagas disease and visceral leishmaniasis in endemic regions for both diseases, *Rev. Pan-Amazônica Saude* 6 (2015) 51–54, <https://doi.org/10.5123/s2176-62232015000100007>.
- [24] J. Meneses, T. van de Kemp, R. Costa-Almeida, R. Pereira, F.D. Magalhães, M. Castilho, A.M. Pinto, Fabrication of polymer/graphene biocomposites for tissue engineering, *Polymers (Basel)* 14 (2022) 1–25, <https://doi.org/10.3390/polym14051038>.
- [25] G. Michel, C. Pomares, B. Ferrua, P. Marty, Importance of worldwide asymptomatic carriers of Leishmania infantum (L. chagasi) in human, *Acta Trop* 119 (2011)69–75, <https://doi.org/10.1016/j.actatropica.2011.05.012>.
- [26] L. Nicolas, E. Prina, T. Lang, G. Milon, Real-time PCR for detection and quantitation of Leishmania in mouse tissues, *J. Clin. Microbiol.* 40 (2002) 1666–1669, <https://doi.org/10.1128/JCM.40.5.1666-1669.2002>.
- [27] M. Ortalli, A.M. De Pascali, S. Longo, N. Pascarelli, A. Porcellini, D. Ruggeri, V. Randi, A. Procopio, M.C. Re, S. Varani, Asymptomatic Leishmania infantum infection in blood donors living in an endemic area, northeastern Italy, *J. Infect.* 80 (2020) 116–120, <https://doi.org/10.1016/j.jinf.2019.09.019>.
- [28] L.Q. Pereira, S. Tanaka, M.M. Ferreira-Silva, M.P. Santana, F. Gomes, P.R. Aguiar, V.R. Junior, A. Fernandes, F.B. Vito, H. Moraes-Souza, Identificação de infecção assintomática de Leishmania L. infantum por sorologia em pacientes politransfundidos e controles de área endêmica para Leishmaniose visceral, *Hematol. Transfus. Cell Ther.* 43 (2021) S356–S357, <https://doi.org/10.1016/j.htct.2021.10.605>.
- [29] B. Perk, Y. Tepeli Buyuksunetçi, S. Bachraoui Bouzaïen, M.F. Diouani, U. Anik, Fabrication of metal-organic framework based electrochemical Leishmania immunosensor, *Microchem. J.* 192 (2023) 108958, <https://doi.org/10.1016/j.microc.2023.108958>.
- [30] J.T. Robinson, F.K. Perkins, E.S. Snow, Z. Wei, P.E. Sheehan, Reduced graphene oxide molecular sensors, *Nano Lett* 8 (2008) 3137–3140, <https://doi.org/10.1021/nl8013007>.
- [31] M.C.A. Sanchez, B.J. Celeste, J.A.L. Lindoso, M. Fujimori, R.P. De Almeida, C.M.C. B. Fortalez, A.F. Druzian, A.P.F. Lemos, V.C.A. De Melo, A.M.M. Paniago, I. T. Queiroz, H. Goto, Performance of rK39-based immunochromatographic rapid diagnostic test for serodiagnosis of visceral leishmaniasis using whole blood, serum and oral fluid, *PLoS ONE* 15 (2020) 1–19, <https://doi.org/10.1371/journal.pone.0230610>.
- [32] P. Scott, E. Pearce, P. Natovitz, A. Sher, Vaccination against cutaneous leishmaniasis in a murine model. I. Induction of protective immunity with a soluble extract of promastigotes, *J. Immunol.* 139 (1987) 221–227.
- [33] K.F. Viana, G. Lacerda, N.S. Teixeira, A.S. Rodrigues Cangussu, R.W. Sousa Aguiar, R.C. Giunchetti, Therapeutic vaccine of killed Leishmania amazonensis plus saponin reduced parasite burden in dogs naturally infected with Leishmania infantum, *Vet. Parasitol.* 254 (2018) 98–104, <https://doi.org/10.1016/j.vetpar.2018.03.010>.
- [34] L.S. Vitorino, T.C. dos Santos, I.A.A. Bessa, E.C.S. Santos, B.R.F. Verçoza, L.A.S. de Oliveira, J.C.F. Rodrigues, C.M. Ronconi, Amphoterin-B-loaded polymer-functionalized reduced graphene oxides for Leishmania amazonensis chemophotothermal therapy, *Colloids Surfaces B Biointerfaces* 209 (2022), <https://doi.org/10.1016/j.colsurfb.2021.112169>.
- [35] WHO, Leishmaniasis [WWW Document], World Heal. Organ, 2023. URL, <https://www.who.int/news-room/fact-sheets/detail/leishmaniasis> (accessed 3.23.22).
- [36] M.F. Zanette, V.M.F. de Lima, M.D. Laurenti, C.N. Rossi, J.P. Vides, R.F. Vieira, C. da, A.W. Biondo, M. Marcondes, Serological cross-reactivity of Trypanosoma cruzi, Ehrlichia canis, Toxoplasma gondii, Neospora caninum and Babesia canis to Leishmania infantum chagasi tests in dogs, *Rev. Soc. Bras. Med. Trop.* 47 (2013) 105–107, <https://doi.org/10.1590/0037-8682-1723-2013>.